Bearing Grease

In-line Assessment of Lubrication Contamination in Slew Bearings Using Active Ultrasound Spectroscopy

ME-MME54035: Master Thesis
Report Number: 2024.MME.8906

C.E. van Eijk

Delft University of Technology

TU Delft

Bearing Grease

In-line Assessment of Lubrication Contamination in Slew Bearings Using Active Ultrasound Spectroscopy

by

C.E. van Eijk

In partial fulfilment of the requirements for the degree of

Master of Science
in Mechanical Engineering

At the Department of Maritime and Transport Technology of the Mechanical Engineering Faculty of the Delft University of Technology
To be publicly defended on March 20, 2024 at 14:00.

Student Number:	4599756	
MSc Track:	Multi-Machine Engineering	
Report Number:	2024.MME.8906	
Chair:	Dr. J. Jovanova	TU Delft
Supervisor:	Dr. L. Pahlavan	TU Delft
Supervisor:	Dr. B. Scheeren	TU Delft
Date:	March 20, 2024	

Cover: Romeijn, E. (2023). *Bokalift 2.* (Modified) [Photograph].

TU Delft

Preface

”The broader one’s understanding of the human experience, the better design we will have.” This quote by Steve Jobs, expresses a sentiment that I have followed throughout my time at the TU Delft, and even before that. I have many interests and hobbies, and have often been told that I am quite impulsive in pursuing these. One week I’ll be fully invested in rock-climbing, and the next I’ll be working on improving my skill on some new musical instrument. But one passion that has never wavered is engineering. Therefore, no one was surprised when I went on to pursue this passion at university. The decision to study Mechanical Engineering is again motivated by the sentiment expressed in the quote by Steve Jobs. Why choose other engineering disciplines, when you can choose the comprehensive and all-encompassing Mechanical Engineering. After graduating from the ME Bachelor, I once again found myself at a crossroad; which master would best fit my impulsive and broad interests? Multi Machine Engineering, with its huge, mechanical machines, logistical problems and granular materials seemed to have it all. So, together with Jouke, Quincy and Ben, I embarked on a journey; first-year weekend, countless projects, late night exam study sessions, presentations and much, much more. Naturally, I was not fully satisfied with everything that Multi Machine Engineering had to offer, resulting in me taking extra courses like Turning Technology into Business, and Nuclear Reactor Physics (this last one was driven by watching the Chernobyl documentary one too many times). All this, eventually led me to the world of bearing condition monitoring.

In this thesis, I shine a light on on the various aspects that are of importance when designing and evaluating a novel condition monitoring setup for offshore bearing grease. Chapter one will highlight the various steps that have been followed during this research. Chapter two will dive into the background information that substantiated the development of the condition monitoring setup. Chapter three will present the process and results of numerous laboratory experiments to investigate various effects that influence ultrasound spectroscopy. Chapter four will highlight the process of designing and experimentally evaluating an in-line bearing grease condition monitoring setup. Chapter five encompasses the design of a comprehensive bearing condition monitoring strategy and Chapter six lists the various conclusions that have been drawn from this research.

This work would not have been possible, if it were not for Bart, Pooria and Jovana. Bart, I would like to thank you for your weekly input and your troubleshooting skills in the lab. Were it not for your insights and out of the box thinking, the fickle nature of the ultrasound wave would have crushed me long before completing this thesis. Pooria, I would like to thank you for your numerous technical insights, presentation pointers and project-altering questions during our weekly coffee runs. And Jovana, I would like to thank you for your guidance during many previous projects, as well as for introducing me to this subject. Additionally, I would like to thank Rachid from Huisman, and the other HiTeAM contributors for their valued feedback and help during the real world experiments.

To end this preface, I would like to thank my friends, my sister Renée, my parents Vincent and Nicolette, and my girlfriend Suzanne, for always believing in me, pushing me to achieve my full potential, and helping me when help was needed. I hope you all enjoy reading this thesis!

C.E. van Eijk
Delft, March 2024

Abstract

This thesis presents the design and experimental evaluation of an in-line, active ultrasound, condition monitoring setup for the detection of contamination in offshore bearing grease. This process is divided into three distinct research steps. First of all, the influences that affect ultrasound propagation through a bearing grease sample have been investigated through various laboratory experiments. Next, a practical, real-world experiment using a linear bearing has been designed and conducted with the aim of determining the applicability of such an in-line condition monitoring setup. Lastly, the performance of the in-line active ultrasound setup has been evaluated, improvements have been proposed and an overall condition monitoring strategy has been devised.

During the laboratory experiments, various influences on ultrasound wave propagation have been investigated. First of all, design-specific parameters, such as the distance between the sensors, the test-setup material, and the scalability of the measured output voltage have been investigated. Next, the effects of temperature fluctuations, air bubble fluctuations, water contamination and iron particle contamination on the attenuation and velocity of waves for active ultrasound spectroscopy were investigated. It has been shown that air bubble concentration and temperature fluctuations influence the attenuation of the ultrasound in the grease sample. Therefore, the temperature should be kept constant throughout the other experiments. Additionally, the air bubble concentration should be managed through a constant resting time throughout the other experiments. Moreover, it has been shown that a condition monitoring setup employing active ultrasound spectroscopy is able to determine water contamination and iron particle contamination. The highest sensitivity of this contamination detection is located in the first percentage of contamination concentration, showing an amplitude drop of about 0.5dB/mm to 1dB/mm and a change in speed of sound of about 5% to 15%. It is however, difficult to differentiate between the different types of contamination using only the attenuation and velocity spectroscopy methods.

The practical, real-world experiment using an operational Huisman linear bearing has illustrated the applicability of using an in-line grease condition monitoring setup in such an environment, by evaluating obstacles such as spatial constraints, location constraints, flowability of the grease and surrounding noise. It has been shown that these obstacles pose minimal challenges for the successful implementation of an in-line grease monitoring setup for effective condition monitoring of offshore bearing grease.

The evaluation of the improved in-line active ultrasound condition monitoring setup has highlighted the strengths and weaknesses of implementing such a setup for offshore applications. A possible combination of the proposed grease condition monitoring method with Acoustic Emission monitoring offers

Contents

List of Figures

List of Tables

Nomenclature

Abbreviations

Abbreviation	Definition
AE	Acoustic Emission
AUS	Active Ultrasound Spectroscopy
CM	Condition Monitoring
DAQ	Data Acquisition System
HiTeAM	High-Tech Acoustic Monitoring
HTL	High Temperature Limit
HTPL	High Temperature Performance Limit
ISO	International Organisation for Standardisation
JIP	Joint Industry Project
LGT	Linear Guideway Type (recirculating linear ball bearings)
LTL	Low Temperature Limit
LTPL	Low Temperature Performance Limit
ME	Faculty of Mechanical Engineering
MTT	Maritime and Transportation Technology
NLGI	National Lubricating Grease Institute
RTDs	Resistance Temperature Detectors
SAOS	Ship and Offshore Structures
TU Delft	Delft University of Technology

Symbols

Symbol	Definition	Unit
A	Amplitude	[dB]
B	Bulk modulus	[Pa] or [N/m^2]
c	Speed of sound	[m/s]
E	Young's modulus	[Pa] or [N/m^2]
f	Frequency	[Hz] or [s$^-1$]
m	Mass	[kg]
M	Molecular mass	[u]
P	Change in sound pressure	dB
R	Gas constant	8.31 [J/mol*K]
t	Time	[s]
T	Temperature	[K]
V	Volume	[m^3]
x	propagation distance	[m]
α	Attenuation coefficient	[-]
γ	Adiabatic index	[-]
λ	Wavelength	[m]
ρ	Density	[kg/m^3]
σ	tensile stress	[Pa] or [N/m^2]
τ	tensile strain	[-]

1

Introduction

Global warming and climate change are pressing issues, and solving these problems becomes more important every day. The energy consumption caused by humans is at the heart of this challenge. To avoid a climate catastrophe, it is of great importance to diminish the reliance on fossil fuels and replace this with clean, sustainable sources of energy [1]. One of the ways to generate sustainable energy is by using offshore wind farms, which can occupy vast areas of otherwise unused oceans. Additionally, there is a lot of wind activity over the oceans and therefore the offshore wind farms can run at full power almost continuously [2]. According to research conducted by WindEurope, the contribution of European offshore wind farms to the generation of renewable energy shall grow from 1.2 GW in 2022 to 22.4 GW in 2030 [3]. However, a vast majority of these wind farms still need to be built and highly specialized equipment on board of highly specialized vessels is needed to do so. Bearing failure aboard such a supporting vessel can cause the installation or maintenance processes to be halted, causing high repair costs and unforeseen equipment downtime. This problem highlights the need for apt bearing condition monitoring systems [4].

In order to tackle this problem, a High-Tech Acoustic Monitoring collaboration (HiTeAM) has been set up. This multiple-phase Joint Industry Project (JIP) is a collaboration between the Ship and Offshore Structures section (SAOS) of the Maritime and Transportation Technology department (MTT) of the Mechanical Engineering faculty (ME) of the Delft University of Technology (TU Delft), and various companies specializing in products with offshore applications. It aims to develop and validate a reliable, quantitative method for condition monitoring of highly-loaded, low-speed roller bearings, which are often used in offshore applications. More specifically, this JIP project is focussed on the development of such a condition monitoring system using Acoustic Emission (AE) of active defects of the roller bearings [5].

One of the topics that will be addressed in stage four of this JIP, and also the purpose of this research, is determining the feasibility of using active ultrasound spectroscopy as a condition monitoring setup in an in-line grease assessment system (HiTeAM Phase 4 Project Proposal, personal communication, January 01, 2023).

1.1. Purpose of Research

The purpose of this research is to design and experimentally evaluate a novel way of conducting in-line grease assessments through condition monitoring (CM) using Active Ultrasound Spectroscopy (AUS) to determine the presence of contamination in bearing grease of offshore roller bearings. The principle behind this method is based on the interaction between the ultrasonic waves and the contamination in the grease and this interaction is governed by the properties of the grease and the contamination, the wavelength of the ultrasound and the environmental factors present in an offshore environment. On top of the design and the experimental evaluation of the novel in-line condition monitoring set, an assessment of its applicability on offshore settings has been conducted. A selection of complementary condition monitoring systems has been conducted in order to design an overall condition monitoring strategy for offshore roller bearings.

1.2. Research Questions

In order to successfully accomplish the goal of this research, the following research question will have to be answered:

> *How can active ultrasound spectroscopy support in-line condition monitoring of offshore bearings, by assessing the contamination of the grease?*

This research question has been divided into the following sub-questions:

1. How can **active ultrasound spectroscopy** be used to monitor the condition of bearing grease?
2. How can the condition of bearing grease be monitored using an **in-line monitoring setup**?
3. What are the **limitations** of using an in-line active ultrasound spectroscopy monitoring setup for bearing condition monitoring?

The first sub-question deals with the assessment of the applicability of active ultrasound spectroscopy to the condition monitoring of bearing grease by evaluating the different effects that influence the propagation of ultrasound through a grease sample. The second sub-question deals with the design of the in-line monitoring setup and its practical application into a offshore linear roller bearing. The third sub-question deals with the assessment of the developed in-line, active ultrasound, grease monitoring setup, as well as the recommendations of possible improvements, the selection of complementary condition monitoring techniques and the preliminary design of an overall condition monitoring strategy.

1.3. Methodology and Scope of Research

To address these sub-questions and, consequently, the main research question, the following approach has been employed. An exploration of the relevant literature has been undertaken to gain insight into the diverse array of roller bearings used in offshore applications. Additionally, an analysis of the different grease types, bearing failure mechanisms and resultant grease contamination sources within these bearings has been conducted.

Addressing the first sub-question entailed an exploration of the relevant literature concerning the working principles of active ultrasound spectroscopy. Additionally, influences on ultrasound propagation including but not limited to temperature and air bubble concentration, as well as tap water contamination and iron particle contamination have been evaluated through an array of laboratory experiments.

The literature exploration also served as a foundational step in addressing the second sub-question, in which an in-line grease monitoring setup has been conceptualized. To extend the investigation, a practical real-world experiment was devised, involving the application of the in-line monitoring configuration to an offshore linear roller bearing.

The third sub-question is addressed through a review of the relevant literature, focusing on the various condition monitoring techniques in offshore bearing applications, along with their associated trade-offs. Additionally, the performance of the developed in-line, active ultrasound condition monitoring setup is evaluated, and an analysis of the empirical data obtained from the practical linear bearing experiment is carried out. This leads to the identification of valuable supplementary assessment methods, which subsequently leads to the preliminary design of an overall condition monitoring strategy.

1.4. Outline of Research

The outlined sub-questions provide the foundation for this research, consequently shaping the structure of the subsequent chapters.

- **Chapter 1:** the purpose, research questions, methodology, scope, and outline of this research.
- **Chapter 2:** a review of the relevant background information, consisting of an exploration of the relevant literature concerning the roller bearings in offshore applications, as well as the grease types, failure mechanisms and contamination sources. Additionally, various bearing condition monitoring methods and active ultrasound spectroscopy have been explored.
- **Chapter 3:** the design and execution of laboratory experiments to investigate the various influences on ultrasound propagation in a grease sample.
- **Chapter 4:** the design and execution of a practical real-world experiment using the designed in-line grease monitoring setup.
- **Chapter 5:** an assessment of the limitations and possible improvements of the developed in-line grease monitoring setup, as well as a selection of useful complementary condition monitoring techniques and the preliminary design of an overall condition monitoring strategy.
- **Chapter 6:** a summary of the conclusions of this report, and recommendations for further research and future design steps.

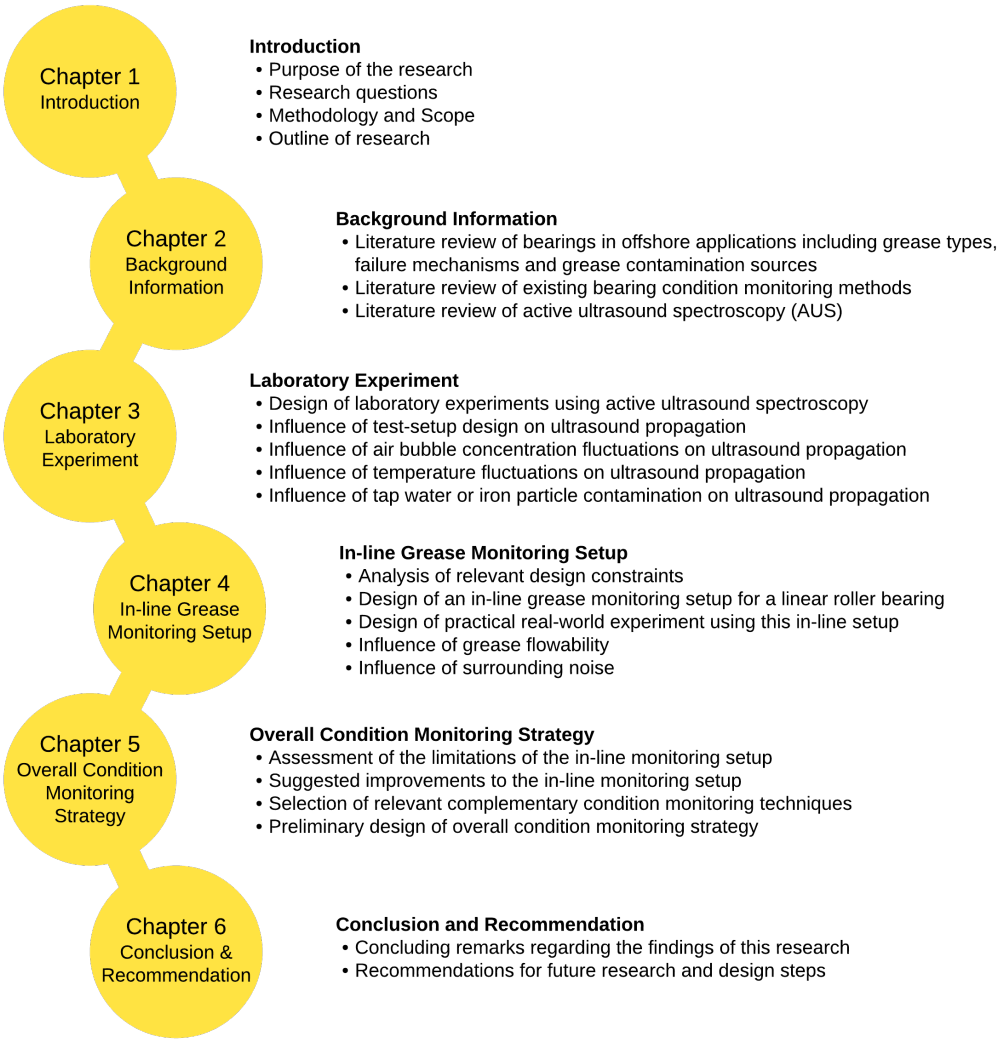

Figure 1.1: Outline of this report.

2

Background Information

Within this chapter, a summary of the relevant background information has been provided. This summary encompasses an exploration of the relevant literature, delving into intricate aspects concerning roller bearings in offshore applications. Moreover, a thorough investigation into various grease types, failure mechanisms, and sources of contamination has been conducted. This summary is complemented by an examination of diverse bearing condition monitoring techniques, and followed by a focused exploration of the principles and applications of active ultrasound spectroscopy.

2.1. Roller Bearings in Offshore Applications

Roller bearings, also referred to as rolling-element bearings, are used to support loads while minimizing friction [6]. The rolling elements support and guide rotating or oscillating movements and due to their high precision and low internal friction, roller bearings are often used in machine elements such as shafts, axles, or wheels to transmit axial loads, radial loads and overturning moments [7].

2.1.1. Classification of Bearing Types

A roller bearing typically consists of four main components: the inner ring with raceway, the outer ring with raceway, the rolling elements and the cage, as can be seen in Figure 2.1. The inner ring, the outer ring and the rolling elements are primarily responsible for the transmission of movements and loads and these are generally made using a chrome alloy steel with the necessary hardness. The role of the cage involves maintaining separation among the rolling elements and providing guidance during movement. Cages are frequently crafted from materials such as steel, brass, or plastic [8].

It's important to differentiate between cylindrical roller bearings and ball bearings. The primary distinction becomes evident when examining the contact points of the respective rolling elements. Roller bearings feature cylindrical rollers with a comparatively larger contact surface, enabling them to bear heavier loads. Conversely, their rotational speeds are reduced due to heightened friction between the rollers and raceways, resulting from the increased contact area. In contrast, ball bearings possess a lower load-carrying capacity due to the minute point of contact between the raceway and the rolling element. Nonetheless, they can achieve higher rotational speeds owing to their reduced rolling friction [10].

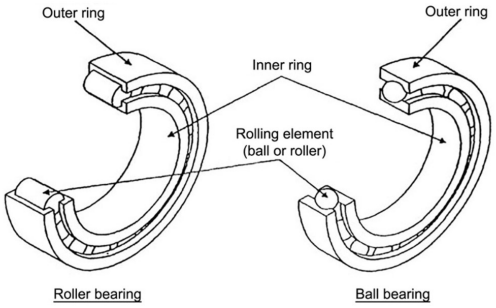

Figure 2.1: Main components of roller and ball bearings [9]

Based on the type of support that the bearing provides during rotation and motion, a distinction can be made between radial bearings, thrust bearings and linear bearings [11].

Radial Bearings

Radial bearings stand out as one of the most frequently employed types of bearings, excelling in their ability to bear radial loads while minimizing friction during rotations. This makes them particularly adept at facilitating the rotational motion of wheels and sheaves in offshore applications. Varieties of radial bearings include deep groove ball bearings, cylindrical roller bearings, and needle bearings. Deep groove ball bearings are typically used for wheel axles and transmissions, as well as electric machines and household appliances due to their wider speed range as compared to other bearing types. Cylindrical bearings find their niche in applications that demand high radial stiffness, precision, and elevated speeds. Meanwhile, needle bearings come into play when radial space is constrained [11]. A schematic of cylindrical roller bearings and ball bearing can be seen in Figure 2.1. In addition to the bearings that consist of one row of rollers, bearings also exist with two or more rows of rollers, in order to increase the load bearing capacity of the bearing.

Thrust Bearings

Thrust bearings, alternatively referred to as axial bearings, demonstrate exceptional proficiency in supporting axial loads. This characteristic renders them especially valuable for offshore applications involving slewing or turret motions. Varieties of thrust bearings, classified by the shape of their individual rollers, encompass thrust ball bearings, thrust cylindrical roller bearings, thrust needle bearings, thrust tapered roller bearings, and thrust spherical roller bearings [11]. A thrust ball bearing can be seen in Figure 2.2a. Within the class of thrust bearings, a clear distinction emerges between standard thrust bearings capable of bearing axial loads exclusively, and slewing bearings engineered to tolerate a certain degree of radial load and overturning moment [12]. In the case of slewing bearings, they inherently feature two sets of raceways: the *capacity row*, tasked with withstanding the combined axial force and tilting moment, and the *support row*. An exception to this pattern is the three-row roller bearing, which introduces a third set of rollers responsible for accommodating the radial load of the bearing [13]. Less frequently encountered slewing bearings include variations such as the double-row ball or cylindrical roller bearings, as well as wire raceway ball or cylindrical roller bearings [14].

(a) A thrust ball bearing [15].

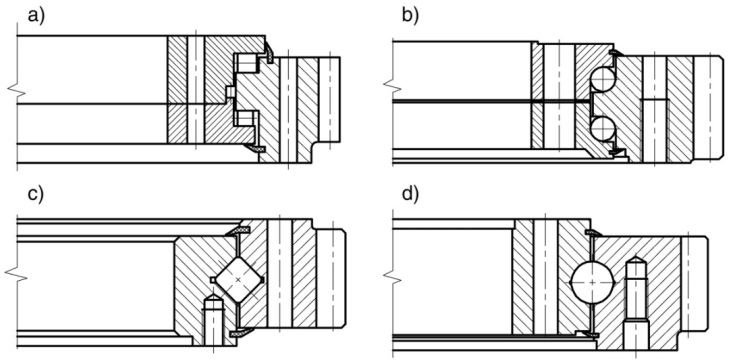

(b) Four types of slewing bearings: a) Three-row roller bearing, b) double-row ball bearing, c) single-row roller bearing (cross-roller), d) single-row ball bearing [13].

Figure 2.2: Typical thrust bearings.

Linear Bearings

Linear bearings, also referred to as linear motion rolling bearings, linear guideway type (LGT) recirculating linear ball bearings [16] or linear rolling guides [17], facilitate linear movements along a rail by utilizing rollers or balls that move in a recirculating manner. The working principle of a linear bearing is illustrated in Figure 2.3a. In comparison to conventional sliding guides, linear bearings offer several advantages such as reduced friction and prevention of stick-slip, rendering them particularly suitable for applications demanding precision and smooth motion [16]. Similar to radial and thrust bearings, the linear bearings can accommodate the linear motion, either by using balls or rollers [18]. The configuration of a Hiwin EG Series linear bearing is depicted in Figure 2.3b.

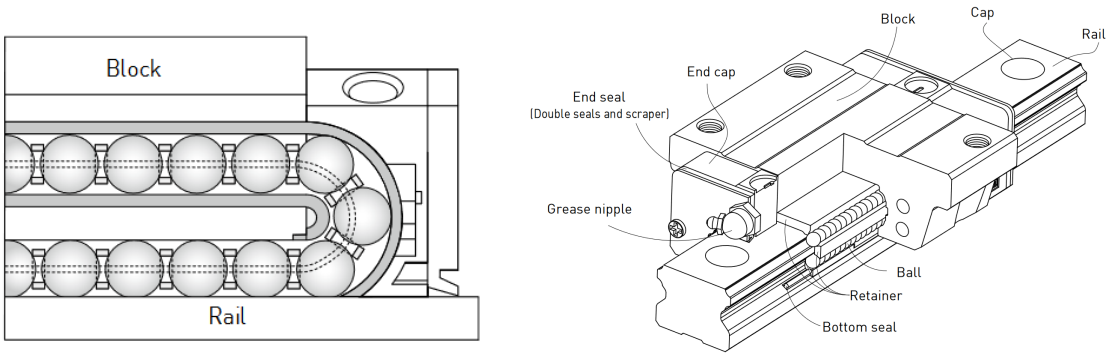

(a) The working principle of a linear bearing [18].

(b) The layout of a Hiwin EG Series linear bearing [18].

Figure 2.3: Typical linear bearings.

2.1.2. Classification of Lubrication Types

Lubrication plays a critical role in maintaining optimal bearing functionality, by preventing metal-on-metal contact and the subsequent wear [19]. However, a distinction must be made between oil and grease lubrication. In all bearing applications, including small scale roller bearings as well as large offshore roller bearings, $80 - 90\%$ of the bearings are lubricated with grease instead of oil [20]. This preference often stems from the cost-effectiveness of grease, as well as the fact that grease is more easily retained within the bearings. In contrast, oil lubrication demands a more intricate sealing arrangement. Only in specific applications, oil is chosen as a lubricant. This is done when the re-lubrication interval is too short for the application of grease lubrication or when extracting used grease is too expensive. Additionally, oil is used when the bearing lubricant serves other processes, or when it serves to dissipate excess heat from within the bearing [21].

Grease Composition

The composition of lubricating grease for bearings consists of three components: the base oil, a thickener, and potentially a range of additives. The base oil typically consists of mineral oils, synthetic oils or a mixture thereof, while the thickener can take the form of either an organic or inorganic variety. The type of thickener in lubricating grease is often dictated by the operating temperatures of the bearing [22]. Occasionally, chemical additives are introduced to the grease to enhance its resistance to oxidation, rust, and wear. Additives are particularly employed in bearings exposed to water and salt, and specific additives find use in high-pressure situations. It is worth noting that the inclusion of additives can reduce the grease oxidation life [11].

Grease Properties

The classification of grease often happens according to the thickener type that has been used [23]. However, more selection criteria are of importance when choosing the right grease type for a specific application.

- *Consistency,* sometimes referred to as grease stiffness, is assessed by determining the depth to which a standard cone sinks into the grease at a temperature of $25°C$ [11]. The National Lubricating Grease Institute (NLGI) has devised a scale wherein lower numbers correspond to softer greases. The significance of selecting the right grease consistency is highlighted by its role in ensuring that the grease remains within the bearing, striking a balance to minimize excessive friction. Greases with a NLGI 1, 2 or 3 grade are often used for bearing applications [24].
- *Kinematic viscosity,* describes the resistance of the grease to flow. According to standards from the International Organisation for Standardisation (ISO), the viscosity is measured at $40°C$. Often, the viscosity is also determined at $100°C$ to determine the viscosity index: a measure of the decrease in viscosity when subjected to an increase in temperature [24].
- *Temperature range,* signifies the spectrum of temperatures over which grease effectively lubricates the bearing according to its designed function. This range is typically characterized by four distinct temperature points: the Low Temperature Limit (LTL), the Low Temperature Performance Limit (LTPL), the High Temperature Performance Limit (HTPL), and the High Temperature Limit

(HTL). The LTL signifies the lowest temperature at which the bearing can be initiated without encountering difficulties due to the characteristics of the grease. Within the span between the LTPL and the HTPL, the grease adequately supplies lubrication to the raceways and operates as intended.When the HTL is exceeded, the grease undergoes irreversible structural changes and loses its effectiveness. The LTL and HTPL serve as lower and upper bounds, respectively, for determining the suitability of grease in specific applications [24].

- *Dropping point,* characterizes the temperature at which heated grease initiates flow through a standardized opening. This temperature is always much higher than the HTPL [24].
- *Oil separation,* signifies the release of oil as a function of temperature and time. The selection of grease for a particular application needs to consider the appropriate level of oil bleeding. Inadequately low oil separation values may lead to grease starvation, while excessively high values can result in leakages. [24].
- *Other properties,* include the corrosion protection, the water resistance and the mechanical stability; the degree in which the consistency of the grease changes over time [24]. Additionally, it's crucial to consider the miscibility with other greases when transitioning from one grease to another. Similarly, when lubricating a new bearing, one must be mindful of the miscibility with the preservation oils used to protect new bearings [7].

2.1.3. Classification of Failure Mechanisms

Rolling bearings are indispensable in the construction and operation of rotating machinery and other rotating components. Nevertheless, the failure of rolling bearings constitutes more than half of all failures in rotating machinery, leading to shutdowns, downtime, and subsequent economic losses. [25]. Annually, approximately 10 billion bearings are produced. Out of this total, 90% are expected to surpass the lifespan of the equipment in which they are installed. About 9.5% of these bearings will undergo premature replacement as a preventive measure, while 0.5% will be replaced due to damage or complete failure [26]. While the percentage of broken bearings might appear modest, 0.5% of the total bearing production equates to approximately 50 million bearings breaking annually. This underscores the need for predictive maintenance and condition monitoring. Furthermore, effective condition monitoring can significantly enhance the management of the remaining 99.5% of bearings. If the quality of bearings surpassing the lifespan of their equipment is ascertainable, they could be repurposed or refurbished. Improved condition monitoring could also lead to a reduction in the number of prematurely replaced bearings.

The causes of roller bearing failures can be categorized into four main groups. Among the failed bearings, a third experience failure due to insufficient lubrication, a third fail as a result of fatigue, a sixth is caused by inadequate seals, and the remaining sixth is attributed to other reasons like improper mounting or handling [26]. This division can be seen in Figure 2.4.

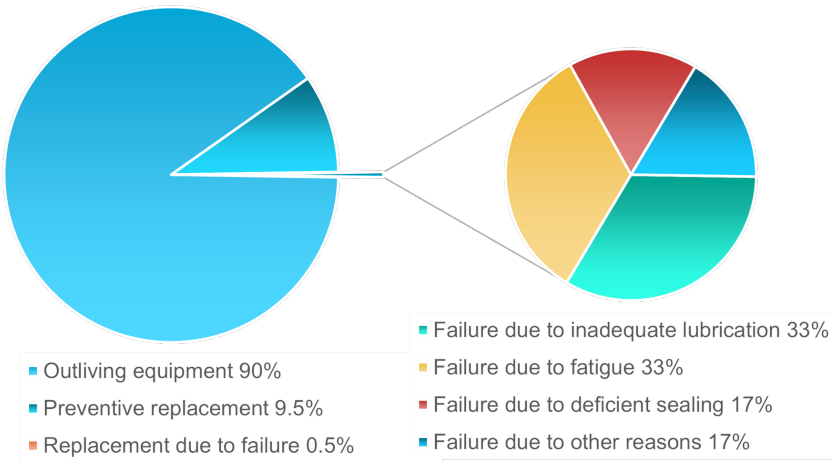

Figure 2.4: Bearing failure distribution of all bearings worldwide [26].

2.1.4. Classification of Damage Mechanisms

The failure mechanisms outlined in subsection 2.1.3 manifest in or on the bearing material as one or more of the following damage mechanisms: plastic deformation, rolling contact fatigue, mechanical wear or chemical wear.

Plastic Deformation

Plastic deformation occurs when a permanent indentation forms on the surface due to a static or impact load surpassing the yield limit. This damage mechanism can result from improper assembly, mounting, or handling, or from the introduction of contamination due to deficient sealing or inadequate lubrication [11, 26]. Types of plastic deformation damage include:

- *Brinelling,* which is defined as surface indentations in the bearing surface in the shape of the rolling elements, generally caused by overload due to vibrations. Bearings that suffer from brinelling may eventually fail due to spalling or flaking [11, 27].
- *Nicks,* are surface injuries caused by the interaction of hard or sharp objects with the bearing surface due to improper handling or installation. Nicks may eventually cause more severe damage, such as pitting or spalling [11, 26].
- *Debris bruises,* consists of surface indentations, which are caused by contamination particles that are introduced either by a failure of the seals, or by damage to parts of the bearing. These particles are crushed between the rolling elements and the raceways, and subsequently cause indentations. Eventually, debris bruises can lead to pitting or spalling damage [11].
- *Cage breakage,* is caused by an abnormal loading of the cage bridges by the rolling elements, either due to improper assembling and handling, or by excessive roller skewing and loss of internal geometry [11, 28]

Rolling Contact Fatigue

Rolling contact fatigue is induced by the contact stress between the rolling element and the raceways [25]. It constitutes a progressive and localized damage mechanism, implying that it can manifest in a variety of appearances [11]. This damage mechanism is initiated by local surface and subsurface stress regions, plastic deformation of the material, or dislocations within the material structure. This triggers the initiation and growth of rolling contact fatigue cracks. At the intersection of multiple fatigue cracks, pit formation can occur [29]. This damage mechanism translates directly into the fatigue failure mechanism. Types of rolling contact fatigue include:

- *Pitting,* is associated with small surface cavities caused by local stress concentrations [11, 26].
- *Peeling,* is caused by cracks that form at a shallow angle and propagate parallel to the surface of the bearing. It appears as if a thin slice of the bearing material has been peeled away [11, 26].
- *Spalling,* is characterized by the removal of large volumes of material from the bearing surface and the formation of large and deep cavities on the raceways [11].
- *Flaking,* is considered to be the progressive state of spalling, and is characterized by material break-off in a ripple pattern [11].
- *Fracture,* is considered the most severe type of rolling contact fatigue and occurs when the local stresses cause a crack to propagate through the material to eventually cause complete separation of the bearing material [11, 25].

Mechanical Wear

Mechanical wear is a result of abnormal friction between the rolling elements and the raceways [25]. This friction leads to the gradual removal of material from the surfaces [11]. Deficient sealing, allowing contamination to enter the bearing, or improper lubrication can cause this damage mechanism. Improper lubrication may arise from using the wrong lubricant or quantity, or adhering to an incorrect lubrication interval [25, 26]. Types of mechanical wear include:

- *Adhesive wear,* is characterized by the transfer of material from one surface to another. Adhesive wear occurs in inadequately lubricated bearings. The poor lubrication causes metal-on-metal contact, and strong bonds between the two surfaces may be formed due to frictional heat. Four severity levels can be distinguished; scoring, scuffing, smearing and seizing [11, 26, 29].

- *Abrasive wear,* is signified by the removal of bearing material and the generation of wear debris material, either caused by the introduction of hard, foreign particles, or the contact of multiple rough surfaces [11, 29].
- *Fretting wear,* can be identified as grooves worn into bearing surfaces. These grooves are caused by micro-movements between surfaces, often during transportation or in machine handling processes [11].

Chemical Wear

Chemical wear, also referred to as corrosion, corrosive wear or tribochemical wear, occurs when chemical or electrochemic reactions take place on and interact with the bearing surface [11, 25, 29]. Types of chemical wear include:

- *Hydrolysis,* the most prevalent version of chemical wear, is caused by the hydrolysis reaction between moisture and the bearing surface. This moisture can either originate from the water that is present in the lubrication, or, when dealing with deficient sealing, from the environment surrounding the bearing [11, 25].
- *Acid etching,* is a second type of chemical wear, in which acid substances react with and dissolve the bearing surface to form salts, creating dark-bottomed pits in the process. Eventually, these pits may lead to spalling [11].

2.1.5. Classification of Grease Contamination Sources

Bearing grease contamination can stem from several sources. Firstly, the grease contamination can originate in the bearing itself, due to any of the highlighted damage mechanisms. Secondly, inadequate sealing or improper handling of the bearing can cause foreign particles or water to contaminate the grease. Additionally, certain damage mechanisms can elevate local temperatures due to friction, leading to overheating and the breakdown of the grease itself.

Bearing-Originated Particle Contamination

As was discussed in section 2.1, a bearing typically consists of four main parts; the inner ring, the outer ring, the rolling elements and the cage. The first three components are typically made using a chrome alloy steel with a particular hardness, whereas the cages are often created using steel, brass, or plastics [8]. When subjected to one or more of the above-mentioned damage mechanisms, particles may break off of these bearing components and contaminate the grease. Various papers have discussed or investigated the effect of particle contamination using pre-contaminated grease samples with known contamination levels, with the aim of recreating real contamination sources. Different types of metals such as aluminium oxide, iron oxide or steel have been used to imitate particle contamination from damaged bearing components. An overview of these can be found in Table 2.1.

Environment-Originated Particle Contamination

When a bearing has an inadequate sealing arrangement, or is subjected to improper handling, particle contamination originating from the surrounding environment may occur. Airborne dirt and dust may enter the bearing grease [30]. This type of particle contamination has in previous research been imitated using silica particles, as can be observed in Table 2.1.

Environment-Originated Water Contamination

Similar to environment-originated particle contamination, environment-originated water contamination of bearing grease can be caused by an inadequate sealing arrangement or improper handling. Especially, bearings that operate in offshore environments are often exposed to moisture, which may get into the bearing grease. Additionally, water contamination of grease can also be caused by substances used to manufacture or preserve the bearing, such as cutting fluids and anti-rust oils. Water contamination has in previous research been imitated using regular tap water, rain water, or tap water with a specified amount of salt, as can be observed in Table 2.1.

Decomposition of Grease

For the sake of completeness, decomposition of the grease due to the overheating of the grease caused by frictional heat has been listed here, however, this shall not be further investigated within the scope of this work.

Material	Average Particle Sizes [μm]	Concentration in Grease	Source
Aluminium oxide	68, 80, 91, 141	0.75cm^3 per 50g	[31]
Aluminium oxide	18	0, 0.01, 0.02, 0.04, 0.08 wt%	[32]
Iron (flaky powder)	42	0.2, 2 wt%	[33]
Iron oxide	5	0.2 wt%	[33]
Iron oxide	10, 20, 30, 40, 53, 63, 75, 90, 106	25 wt%	[34]
Iron oxide	53	5 - 45 wt% (5wt% steps)	[34]
Silica	90, 150, 300	10, 20, 30 wt%	[35]
Silica (quartz, dust)	9	0.02, 0.2, 2 wt%	[33]
Silica	10, 20, 30, 40, 53, 63, 75, 90, 106	25 wt%	[34]
Silica	53	5 - 45 wt% (5wt% steps)	[34]
Steel	68, 80, 91, 141	0.75cm^3 per 50g	[31]
Steel (powder)	20	0.075, 0.75, 7.5 wt%	[33]
Anti-rust oil		0, 0.45, 0.9, 1.8, 3.0, 6.0 wt%	[36]
Cutting fluid		0, 0.45, 0.9, 1.8, 3.0, 6.0 wt%	[36]
Rainwater		10	[37]
Water		0.31, 0.58, 1.07, 1.71 3.34, 6.6 wt%	[38]
Water		0, 0.45, 0.9, 1.8, 3.0, 6.0 wt%	[36]
Water		10	[37]
Water(5% salt)		10	[37]
Water(10% salt)		10	[37]
Water(15% salt)		10	[37]

Table 2.1: Types and concentrations of particle and water contamination that have been used in other research.

2.2. Bearing Condition Monitoring Methods

In order to predict and possibly prevent the failure mechanisms discussed in subsection 2.1.3 condition monitoring (CM) techniques are applied. Condition monitoring is a process or tool that revolves around the early detection of faults or damage mechanisms. This is done with the aim of minimizing the bearing downtime, but also to optimize the maintenance regime [4]. The different types of condition monitoring, as well as their applicability to offshore roller bearings, has been highlighted in this section.

2.2.1. Classification of Condition Monitoring Methods

The various condition monitoring methods that are being implemented or researched can be divided into a number of categories according to their working principles. These categories are; temperature monitoring, visual inspection, vibration inspection, electric inspection, acoustic inspection and particle contamination inspection.

Temperature Monitoring

Temperature monitoring is the most common monitoring technique applied to measure a bearing's health [4, 11]. An increase in temperature may signify imminent bearing damage if the operation conditions have not been altered [26]. As a bearing is damaged, the torque of the bearing increases, which in turn generates heat [11]. Types of sensors that are typically used to monitor the temperature of bearings include resistance temperature detectors (RTDs), optical or infrared pyrometers or thermocouples. Temperature monitoring is often applied because of its relatively low costs and easy applicability, however, it develops slower when compared to other condition monitoring methods and may therefore be too late to give a warning of damage [4, 11, 39].

Visual Inspection

Another condition monitoring method that is often applied is that of visual inspection through a machine vision detection system [40], which can be done either by disassembling the full bearing, or by visual inspection through inspection hatches.

- *Disassembly of the bearing,* includes the removal of the bearing from its operational location and the disassembly of that bearing in order to inspect all the separate components. For large, offshore bearings, this will occur every five years, coinciding with the ship's maintenance in order to

minimize equipment downtime. Because this condition monitoring method is so thorough, seeing as all the individual components can be inspected separately, it has a high probability of detecting the damage mechanisms present in the bearing. A downside to this method is that it is an extremely time-consuming and expensive technique. Additionally, the disassembly and subsequent reassembly of a bearing may in turn introduce damage or contamination to the bearing (Eric Romeijn, personal communication, June 20, 2023).

- *Inspection hatches,* are used to locally inspect certain parts of the bearing. Comparable to the disassembly, this method provides the possibility to visually inspect parts of the bearing, however, the person inspecting the bearing is limited in his access by the location of the inspection hatches. Additionally, while the inspection hatches are open, it is possible to introduce contamination to the bearing (Eric Romeijn, personal communication, June 20, 2023).

Mechanical Inspection

The mechanical inspection method is based on knowledge about the axial and radial play of a bearing. When implementing this method, a known load is applied in alternating direction, causing a deflection within the bearing. From this deflection, the play of the bearing can be determined, which can be compared to the play tolerances of the bearing (Eric Romeijn, personal communication, June 20, 2023). Excessive axial or radial play can lead to misalignment and vibrations, and subsequently to wear or failure. Insufficient axial or radial play may however lead to excessive wear, frictional losses and elevated temperatures [41]. This method specializes in the condition monitoring for bearings as a whole, and is therefore capable of indicating overall wear, however, it is not able to locate cracks or inspect individual bearing components (Eric Romeijn, personal communication, June 20, 2023).

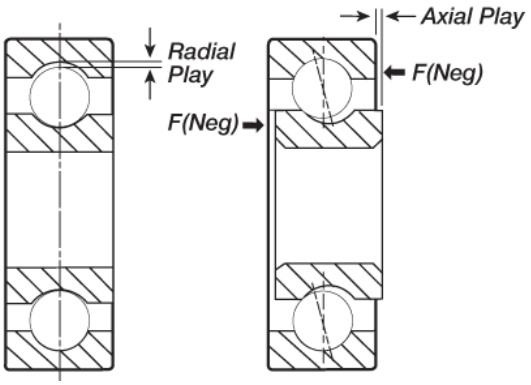

Figure 2.5: Difference between axial and radial play [41]

Vibration Analysis

Another method that is often used to monitor the condition of bearings is vibration analysis. Bearings, when in rotary motion, generate characteristic vibrations, which can be captured using a type of accelerometer sensor such as a seismic or piezoelectric accelerometer or an eddy current transducer [4, 11, 42]. The vibrations, or accelerations, that are measured can be compared to previous records in order to detect possible damages of the bearing. A major downside to this technique, is that it is less successful in detecting bearing damage on low-speed bearings due to the limited change in response associated with defects in these bearings and therefore, vibration analysis is mainly applicable to monitor bearings that have a fast motion and constant load [39, 43].

Acoustic Monitoring

Acoustic monitoring is essentially quite similar to vibration analysis since both techniques record and interpret vibrations, however, these two techniques are generally accepted as two different techniques, mainly because vibration sensors measure the local motion, and acoustic sensors measure the component's sounds levels. Additionally, vibration sensors are mounted rigidly to the bearing, whereas acoustic emission sensors are fixed to the bearing using some sort of low-attenuation glue or gel [4]. Two main acoustic monitoring methods can be distinguished.

- *Acoustic emission monitoring,* is a monitoring technique that measures the acoustic signals that are emitted from the bearing material as a sudden release of energy, when the microstructure of that bearing material is plastically deformed [39]. The acoustic emission sensors measure stress waves with significantly higher frequencies as compared to regular vibration analysis methods. [42]. An advantage of acoustic emission monitoring is its ability to identify surface and sub-surface micro damage [4].

- *Guided wave phased array ultrasonic testing,* is a monitoring method in which an ultrasound wave is actively transmitted through the bearing material in order to 'scan' the material for defects. The echo of this ultrasound wave can then be processed and compared to previous scans. An advantage of this method is that ultrasonic measurement techniques are directly sensitive to mechanical changes, and can directly assess the condition of the bearing [44]. Downsides to this method are that it requires a skilled operator and the technique is limited by bearing accessibility (Eric Romeijn, personal communication, June 20, 2023).

Electrostatic Monitoring

Electrostatic monitoring is a term to describe monitoring techniques that detect electric charge differences [39]. The stiffness of the bearing material influences the electrical resistance of the material, and therefore electrostatic monitoring can be used to detect changes caused by bearing damages or defects [4]. One type of electrostatic monitoring that attracts a lot of interest is eddy current inspection. In eddy current inspection, an excitation signal is fed into a primary coil which is placed close to the conduction bearing material. This signal induces transient eddy currents and subsequent magnetic fields in the conducting bearing material, which are received by a secondary coil. The received signal contains information about the conductivity and permeability of the bearing material, which can be compared to the results of previous measurements [40, 45]. Unfortunately, the electrostatic monitoring of bearings is not applied often due to difficulties in the detection of bearing defects (Eric Romeijn, personal communication, June 20, 2023).

Lubrication Analysis

Lastly, lubrication analysis is employed as a bearing condition monitoring method, aiming to quantify the composition of the bearing lubricant. Within this method, it is important to differentiate between oil lubricated bearings and grease lubricated bearings and between online lubrication analysis and offline lubrication analysis [4, 39].

- *Oil lubricated bearings,* are often equipped with online oil debris monitoring systems. The high flow-rate of the lubrication oil, causes a homogeneous distribution of the contaminants throughout the oil, and by placing an inline sensor on the exit drain of the bearing, the oil, and debris passing through the sensor can be measured before the oil is being filtered [11, 39].
- *Grease lubricated bearings,* are often monitored using an offline lubrication analysis. This entails taking a periodic sample of the grease and spectrographically analysing the sample in a laboratory [4]. However, due to the higher viscosity and partially stagnant portions of the grease, the distribution of contaminants within the grease is less even, which in turn causes the success of this monitoring technique to be dependent on the sampling quality and location. Additionally, the offline method ensures a delay between the cause of the degradation and the detection of the degradation [39].

2.2.2. Applicability of Condition Monitoring Methods

For this research, it is important to determine the applicability of the various above-mentioned condition monitoring methods to grease-lubricated, low-speed, offshore roller bearings, and to determine their ability to track down bearing defects. Based on the failure mechanisms discussed in subsection 2.1.3, the damage mechanisms discussed in subsection 2.1.4, and personal communication with bearing condition monitoring specialists, the subjects that the various condition monitoring methods will be graded on are as follows:

- The ability to detect defects of the roller elements.
- The ability to detect defects of the bearing raceways.
- The ability to detect defects of the sealing arrangement.
- The ability to locate wear damage.
- The ability to locate fatigue damage.

Based on their respective strengths and weaknesses, the various condition monitoring techniques have been graded. An overview of the ability to detect defects of the various condition monitoring methods can be observed in Table 2.2. Additionally, an explanation as to why these scores have been appointed is provided.

Method	Rollers	Raceway	Seals	Wear	Fatigue
Temperature	No	No	No	Yes	No
Disassembly	Yes	Yes	Yes	Yes	Yes
Hatches	Maybe	Maybe	Maybe	Maybe	No
Mechanical	No	No	No	Yes	No
Vibration	No	No	No	No	No
Acoustic Emission	Yes	Yes	No	Yes	Yes
Guided Wave	No	Maybe	No	No	Yes
Electrostatic	No	Yes	No	Yes	Yes
Online Oil	No	No	No	No	No
Offline Grease	Yes	Yes	Yes	Maybe	No

Table 2.2: Detection of defects by condition monitoring methods.

- *Temperature:* Although the temperature monitoring techniques are cheap, easy to implement, and do not introduce any additional problems such as contamination or damage, they are not the ideal condition monitoring method since they are only able to provide insights into the temperature behaviour of the bearing, and therefore only provide insights into the frictional heat that is generated with wear damage.
- *Disassembly:* The disassembly of the bearing seems like the ideal condition monitoring method, because after disassembly, it is possible to detect and locate all five of the defect types, however, it is noteworthy that the disassembly of large offshore bearings often results in a downtime of the equipment of several months. Additionally, the disassembly of the bearing can introduce damage and contamination to the bearing.
- *Hatches:* Inspection of the bearing by using the inspection hatches seems to considerably reduce the downtime of the equipment when compared to disassembling the bearing, however, the location of the inspection hatches greatly influences the ability of this method to successfully detect and locate the bearing damage. Additionally, it is not possible to sufficiently detect fatigue damage, and the employment of inspection hatches may introduce contamination into the bearing.
- *Mechanical:* The mechanical inspection method only provides insights into the radial and axial play of the bearing as a whole. When compared to previous measurements and catalogue values of the radial and axial play, some notion of the ongoing wear damage within the bearing can be deduced. However, the axial and radial play information can not be translated into separate damage mechanisms.
- *Vibration:* Due to the low speed of these offshore bearings, vibration analysis is unlikely to provide a successful condition assessment.
- *Acoustic Emission:* Acoustic emission monitoring requires further research to establish itself as a commonly employed method. Nevertheless, it holds significant potential for detecting defects and damage in offshore roller bearings. Although it can effectively identify particle contamination during overrolling, the acoustic emission monitoring method has limitations in determining the origin of these particles. As a result, it is unable to differentiate between particles originating from inside or outside the bearing, rendering it unsuitable for detecting seal defects.
- *Guided Wave:* Because this method is based on the propagation and the echo of an ultrasound beam through the bearing material, it is very sensitive to the placement and direction of this ultrasound beam. Because not all parts of a bearing are easily accessible, it is often difficult to successfully implement this method. Additionally, this method is mainly meant to determine fatigue damage.
- *Electrostatic:* The electrostatic monitoring techniques are able to determine defects due to fatigue and wear, because these defects change the electrical footprint of the overall bearing material. Additionally, given that the method is applied close to the raceway, it is able to determine defects of the raceway, however, in order to determine defects of the rollers, the individual rollers must be examined and for that to happen, the bearing must be disassembled. Therefore, this method, when applied individually, is not able to determine defects of the rollers.
- *Online Oil:* Due to dealing with grease lubricated bearings, online oil analysis is not applicable.

- *Offline Grease:* Through grease assessment, and subsequent particle analysis, it is possible to determine the types of contamination within the grease, and thus determine the origin of this contamination. Because of this, grease assessment is able to determine defects of the rollers or the raceways, as well as wear damage to the bearing, and the presence of contamination or water in the grease may signify a seal defect. However, grease assessment is not capable of detecting fatigue damage. Additionally, the location at which the grease sample has been taken influences the particle contamination levels of that sample. Lastly, letting the sample be evaluated in a laboratory causes a delay on the detection of faults.

Based on the findings presented in Table 2.2, it can be concluded that the disassembly method is the only stand-alone method capable to evaluate all of the possible bearing faults. Additionally, it is possible to apply a combination of various condition monitoring techniques to fully cover all bearing monitoring aspects.

2.3. Active Ultrasound Spectroscopy

An additional condition monitoring method that is receiving more and more attention is that of active ultrasound spectroscopy, in which the analysis of changes in ultrasonic parameters provides insights into the material characteristics of the sample that is being examined. Ultrasound poses a good alternative to other condition monitoring methods as an online, contact free, continuous monitoring method [46]. In this section, the basic principles of ultrasound and ultrasound spectroscopy shall be further highlighted. Additionally, an overview of the various ways of implementing ultrasound to monitor the condition of materials has been provided.

2.3.1. Ultrasound

Sound waves are manifestations of mechanical waves, as opposed to light waves, which are electromagnetic waves [47]. These mechanical disturbances can present themselves in solid, liquid or gas mediums, but not in a vacuum, because the particle interactions facilitate energy transfer which makes it possible for the sound to travel. When a mechanical disturbance occurs, the bonds between the particles cause the particle to oscillate around their equilibrium positions. Consequently, the elastic forces maintaining particle cohesion transmit the oscillatory motion to adjacent stationary particles or those in the next plane. Therefore, a sound wave represents the propagation of mechanical energy through a medium, achieved by transferring oscillatory and vibratory motions to neighbouring particles through elastic bonds [48].

The width of the oscillation is also referred to as the amplitude of the wave, which can be interpreted as the strength of the oscillation, and is often expressed in Decibels [dB]. The number of oscillations per second is referred to as the frequency of the wave and is often expressed in Hertz [Hz]. The distance between two peaks of the wave is referred to as the wavelength of the wave and is often expressed in metres [m]. The speed of a sound wave, c, expressed in metres per second [m/s] is subsequently defined as the product of the frequency at the source and the wavelength of this wave:

$$c = f\lambda_{wave} \tag{2.1}$$

As can be seen in Figure 2.6, the frequencies that form the audible range for humans exist between 20Hz and 20kHz. Ultrasound refers to sound waves that occur beyond that audible range [48]. At frequencies above 10MHz, the sound waves are referred to as microwaves [49].

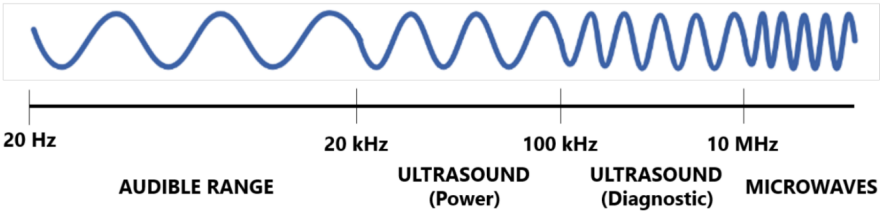

Figure 2.6: The sound spectrum [49].

Propagation of Ultrasound

Various types of wave propagation modes can be classified for sound waves, and they are differentiated by the direction of their particle vibrations. Four main categories can be identified. These are longitudinal waves, transverse waves, surface waves and plate waves [48, 50].

- *Longitudinal Waves,* are also referred to as pressure waves, compression waves, or density waves. These are waves in which the particles oscillate parallel to the direction of the wave propagation. Longitudinal waves can be generated in solids, liquids, and gasses. Common speech is an example of longitudinal waves [47, 48, 50].
- *Transverse Waves,* are also referred to as shear waves. These are waves in which the particles oscillate perpendicular to the direction of the wave propagation. Transverse waves require an acoustically solid material for effective propagation, and therefore these waves do not propagate in liquids or gasses [47, 48, 50].
- *Surface Waves,* are also referred to as Rayleigh waves. These waves combine the longitudinal and transverse motion to form an elliptical motion. Surface waves travel the surface of relatively thick solid material and, similar to transverse waves, they can not propagate through liquids or gasses [50].
- *Plate Waves,* are similar to surface waves in that they combine transverse and longitudinal waves, however, plate waves can only be generated in thin materials. Examples of plate waves are Lamb waves and Love waves. Again, these waves can only propagate in solid materials, and therefore will not propagate in liquids or gasses [50].

The stiffness between the bonds of a material, which can be a solid, liquid or gas, determines the speed at which the sound wave propagates through the material. A material with stiffer particle bonds has a more efficient energy transfer and therefore a faster bulk speed of sound [48]. The theoretical speed of sound of longitudinal waves in a medium depends on the square root of the elastic property of the medium, divided by the inertial property of the medium:

$$c = \sqrt{\frac{\text{elastic property}}{\text{inertial property}}} \tag{2.2}$$

For a solid, this means that the speed of sound of longitudinal waves is dependent on the Young's modulus [E] and the density [ρ] of the solid. For a liquid, the speed of sound depends on the bulk modulus [B] and the density [ρ]. For an ideal gas, the speed of sound depends on the adiabatic index [γ], the gas constant [R], the absolute temperature [T] and the molecular mass [M] [51].

$$c_{sol,l} = \sqrt{\frac{E}{\rho}}, \qquad c_{liq} = \sqrt{\frac{B}{\rho}}, \qquad c_{gas} = \sqrt{\frac{\gamma RT}{M}} \tag{2.3}$$

The Young's modulus describes the tendency of a solid material to deform along its long axis and is defined as the ratio of the tensile stress [σ] to the tensile strain [τ]. The bulk modulus at constant entropy represents the resistance of a solid or fluid material to compression and is defined as the ratio of pressure [P] increase to the relative decrease of the material volume [V] [52, 53].

$$E = \frac{\sigma}{\tau} \qquad B = -V\frac{\delta P}{\delta V} = \rho\frac{\delta P}{\delta \rho} = \rho c_{liq}^2 \tag{2.4}$$

Attenuation of Ultrasound

Attenuation of a sound wave is defined as the loss of strength or the decreasing energy of that wave as it travels through a medium. Causes of signal attenuation are absorption, scattering, reflection, refraction, and diffraction [46, 48].

- *Absorption,* occurs when the sound waves lose energy due to the interaction with the molecules of the medium. The sound energy is converted into other forms of energy, such as heat, which is subsequently absorbed by the material that the sound is travelling through. The degree of absorption depends on the frequency of the wave and the properties of the medium [48].

- *Scattering,* occurs when the sound waves encounter contaminants in the medium that have a much smaller particle diameter compared to the wavelength of the wave. Most of the wave travels through the particle, whereas only a small part of the energy is radiated in all directions. When the sound wave encounters such inhomogeneity, the scattering causes a reduction in the amplitude of the transmitted waves [46, 48].
- *Diffraction,* occurs when dealing with somewhat larger particles, obstacles, or edges. During diffraction, the wave can bypass these obstacles by 'bending' around them instead of passing through them. The reflected echo is very small. The diffraction does not cause a reduction in the amplitude of the transmitted waves [46].
- *Reflection,* happens when a wave comes upon an interface between two mediums, given that the acoustic impedances of the mediums differ, and the boundary between the interfaces is much larger than the wavelength. Upon encountering the boundary, a part of the wave energy is returned into the first medium and is said to be reflected. This reflection reduces the energy available for further transmission through the medium [46].
- *Refraction,* is in some ways the opposite of reflection, since it encompasses the portion of the wave energy that passes through the interface and goes into the second medium. The change in acoustic velocities between the first and the second medium can lead to changes in the direction of the propagation of the wave [46].

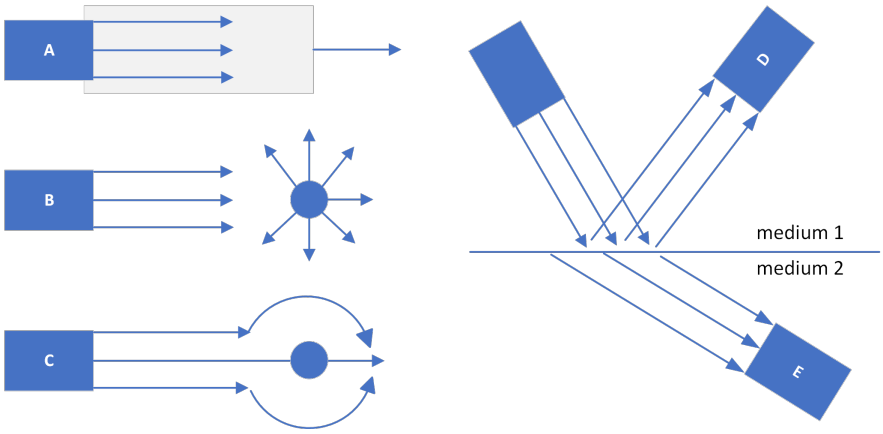

Figure 2.7: The five wave attenuation principles; a) absorption, b) scattering, c) diffraction, d) reflection and e) refraction.

2.3.2. Active Ultrasound Spectroscopy Techniques

Based on the attenuation principles discussed above, a range of ultrasound spectroscopy techniques have been developed. These include ultrasonic attenuation spectroscopy, ultrasonic velocity spectroscopy, ultrasonic reflectometry, the backscattering method, the ultrasonic Doppler method and the ultrasonic process tomography [46, 47, 54]. An overview of the layout of the ultrasonic transducers for the various methods can be found in Figure 2.8.

Ultrasonic Attenuation Spectroscopy

Ultrasound attenuation spectroscopy, also referred to as the shadow method, the intensity measurement or as ultrasound extinction spectroscopy, has found its main application in particle sizing [46, 47, 54]. This method is mainly based on the transmission of the ultrasound through the medium, and therefore, a transmitting transducer and a receiving transducer are placed opposite of each other, as can be seen in Figure 2.8. During this method, the attenuation coefficient α is obtained from the difference between the amplitude of the transmitted wave and the received wave. The phase information is obtained through data inversion. The attenuation of the signal is caused by the interaction of the wave with the medium, causing the amplitude of the signal to drop. The change in sound pressure [P] with the propagation distance [x] can be characterized using the following equation [46].

$$P = P_0 e^{-\alpha} \tag{2.5}$$

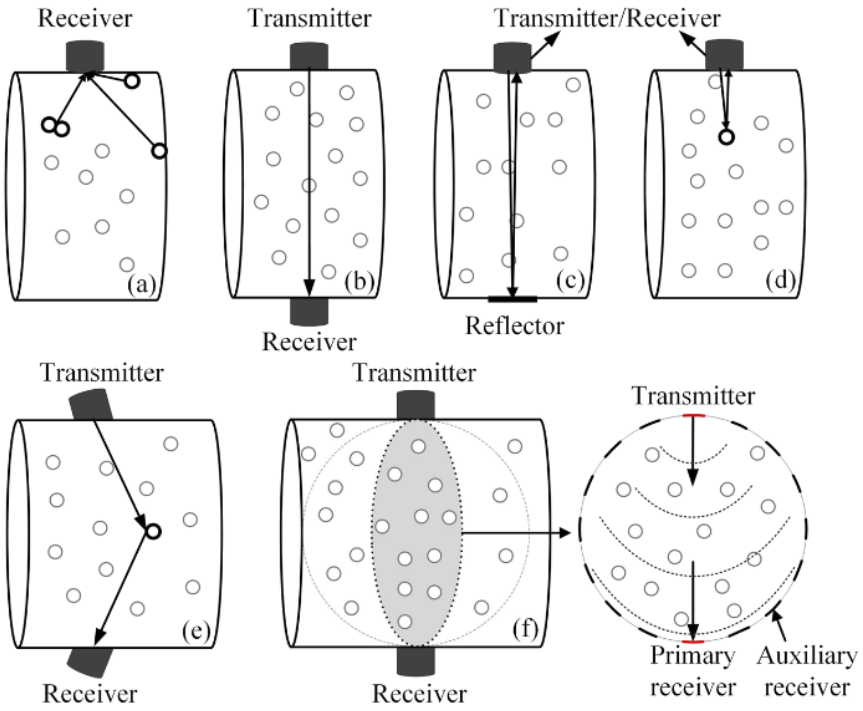

Figure 2.8: The layout of the ultrasonic transducers in the various methods; a) acoustic emission, b) attenuation spectroscopy and velocity spectroscopy, c) Reflectometry, d) backscattering, e) Doppler and f) process tomography [46].

After the selection of a theoretical model, the theoretical attenuation spectrum can be compared to the practical attenuation spectrum obtained through measurements, and, using an error function, the correctness of the hypothesised situation can be calculated using the following Root-Mean-Square Error equation [46].

$$E_{RMSE} = \sqrt{\frac{\sum_{j=1}^{N} (\alpha_{sim} - \alpha_{meas})^2}{N}} \tag{2.6}$$

The ultrasound attenuation spectroscopy method is mainly applied to the localisation and sizing of particles within a medium, and its basic working principle can be seen in Figure 2.9. The main advantages of ultrasound attenuation spectroscopy include its capability to characterize intact, concentrated dispersed systems, as well as the fact that attenuation measurements do not need an excessively stable temperature and can therefore be performed on large samples. Additionally, information on the compressibility of the medium can be obtained [54].

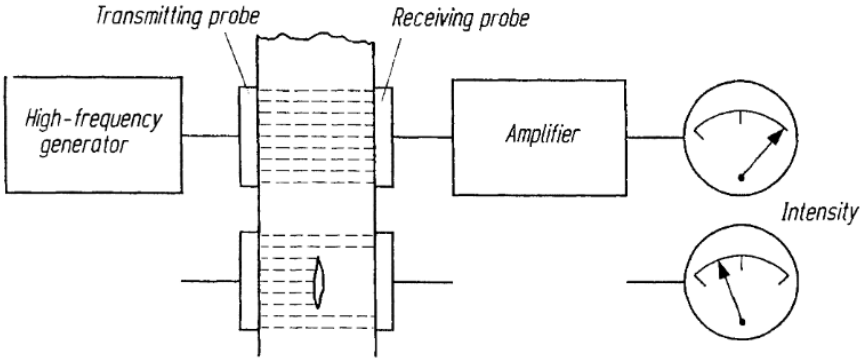

Figure 2.9: Principle of ultrasound attenuation spectroscopy [47].

Ultrasonic Velocity Spectroscopy

Ultrasonic velocity spectroscopy, otherwise referred to as the transit time method, revolves around the fact that ultrasound velocity, and subsequently the transit time through a medium, is determined by the density and the elasticity of said medium [47, 54, 55]. The sensor layout used for velocity spectroscopy is similar to that of attenuation spectroscopy, using both a transmitting and a receiving sensor facing each other [46]. As with the attenuation spectroscopy, the velocity spectroscopy consists of two steps, determining the ultrasound velocity and comparing this to some model or reference [56].

$$c = \frac{x}{t} \tag{2.7}$$

The ultrasound velocity is extremely sensitive to the molecular organization and the interactions between the molecules, and can therefore be used to monitor a broad range of processes. However, it needs high measurement resolution and cannot be carried out in large samples due to the need for sufficient temperature control. The ultrasonic velocity spectroscopy has been used both in combination with the attenuation technique, and as a stand-alone method [46, 54, 55].

Ultrasonic Reflectometry

Ultrasonic reflectometry, also referred to as the pulse-echo method or the echo reflection method, is based on the comparison between the original pulse and the reflected echo. Contrary to the attenuation and velocity spectroscopy, This method uses only one transducer that both radiates an ultrasound pulse, as well as 'listens' for pulse echoes returned from the back wall [46–48, 57]. Similar to the attenuation and velocity methods, is that also in reflectometry, the differences in amplitude or time domain between the generated pulse and the received echo are analysed to deduce the relevant information [46].

Although the ultrasonic reflectometry can be used for many applications including flow pattern recognition or liquid concentration measurements, it is difficult to implement under actual factory conditions. This is due to the fact that this method is based on the reflections of the back wall, which might change due to corrosion or other damage. Additionally, the ultrasound has to travel back and forth through the sample, which may impose to much attenuation to be received at all [46].

Backscattering Method

The backscattering method has a similar working principle to the ultrasonic reflectometry in the sense that it only utilizes one transducer that both transmits the signal, as well as receives it. But whereas the reflectometry method receives and analyses the reflections of the back wall, the backscattering method receives and analyses the soundwaves that radiate of off particle contamination due to scattering. A comparison between reflectometry and backscattering can be seen in Figure 2.10. Backward scattering occurs when the scattering angle is between 90° and 180° [46, 47, 57]. However, for most single particle scattering, the scattering angle is somewhere around 0°, which results in a weak backscattered signal [46]. Additional difficulties arise for this method, due to the fact that it is difficult to distinguish between particles, entrained air and water [57].

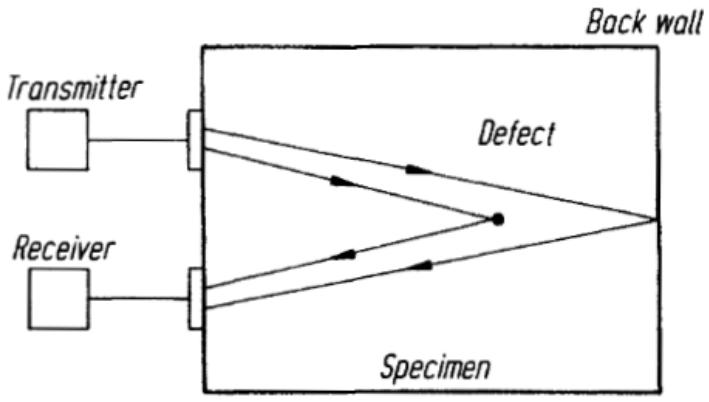

Figure 2.10: Principle of ultrasound reflectometry and backscattering [47].

Ultrasonic Doppler Method

This method is based on the Doppler effect, or Doppler shift, which occurs when the wave source and the receiver are in relative motion with respect to the examined medium. This causes the frequency and wavelength of the received wave to differ from the source wave. It is generally used to determine flow velocity and flow rate. Difficulties arise when large particles or high flow velocities are present. Additionally, it can only be used for liquids containing a specific number of particles and bubbles, and its accuracy is low [46].

Ultrasonic Process Tomography

Tomography focusses on the evaluation of a flow by providing cross-sectional images of that flow, which can be used for flow pattern recognition. The composition of the flow can be obtained through image processing of these cross-sections. Limitations to this method include difficulty with providing real-time measurements due to long time interval between transmissions, difficulty with distinguishing between particles, gas and liquid bubbles, and difficulty with resolution and quality of the constructed cross-sectional images [46].

2.3.3. Piezoelectric Transducers

A transducer is a component that converts electrical currents into mechanical vibrations or the other way around. They can therefore be used to detect sound, like a microphone, but also to generate sound, like a speaker. Piezoelectric-element-based transducers are most commonly employed within ultrasonic spectroscopy settings [47, 53].

The Piezoelectric Effect

The piezoelectric effect, first discovered in 1880 by the brothers Curie, exists of two inversely related principles. Firstly, the direct piezoelectric effect, encompasses the generation of an electric charge, when external mechanical pressure deforms the piezoelectric material. This effect is used for measuring practices, and can be compared with a microphone. Secondly, the inverse piezoelectric effect, encompasses the deformation of the piezoelectric material due to an applied potential difference. This effect is used to produce mechanical pressures, deformations, and oscillations, and can be compared with a speaker [47, 48, 53].

The piezoelectric effect can occur in a crystal when the unit cell of that crystal lacks a centre of symmetry. The formation of dipoles is caused by the distance between the positively and negatively charged particles in the crystal. Closely packed dipoles tend to align themselves along the same direction. When such a material undergoes deformations, the charge distribution is disturbed, causing a potential difference across the surface of the crystal. This process can also be reversed, By applying a potential difference across the surface of the crystal, the crystal deforms and generates mechanical vibrations. Due to their ability to convert electrical current into mechanical vibration, as well as mechanical vibration into electrical current, they provide the ideal connection between an acoustic and an electric system [47, 53].

The Piezoelectric Transducer

The piezoelectric transducer, is a transducer that incorporates a piezoelectric crystal in order to detect or transmit ultrasonic waves, and convert them to or from an electrical signal. These types of transducers come in a range of sizes, shapes, and frequency ranges, and can be either implemented as a bare piezoelectric element, or as a commercial transducer. The piezoelectric crystal is either circularly, squarely or rectangularly shaped. A wear plate separates the piezoelectric crystal from the testing material. Damping is provided through the backing material [48, 53].

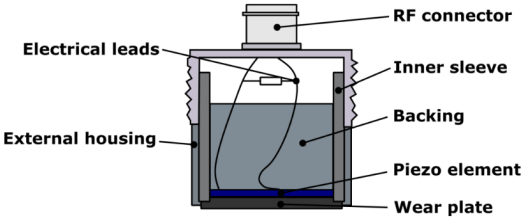

Figure 2.11: Schematic of a piezoelectric transducer [48].

3

Laboratory Experiments

This chapter delves into the comprehensive process of conceptualizing, planning, and executing laboratory experiments, concerning the application of active ultrasound spectroscopy for the detection of particle contamination of grease samples. It encompasses a thorough examination of the purpose and the hypotheses guiding the investigation. The design of the experimental setup is expounded upon, shedding light on the selection and utilization of materials and equipment. The methodology of the experiments is intricately discussed, encompassing the procedural aspects during the experiments, along with a meticulous overview of data collection and analysis. The subsequent section delves into a detailed discussion of the obtained results, followed by the formulation of conclusive insights drawn from the experimentation process.

3.1. Purpose and Hypotheses of Experiments

The main purpose of these experimental investigations is to probe the efficacy of active ultrasound spectroscopy in discerning and detecting contamination within grease samples sourced from roller bearings, by the deliberate transmission of active ultrasound pulses characterized by specific frequencies and amplitudes through a diverse array of grease samples, each preassigned with predetermined contamination levels. These experiments seek to achieve two objectives. Firstly, it aims to establish the practicality and reliability of ultrasound spectroscopy as a tool for pinpointing and characterizing grease contamination in roller bearings. Secondly, it delves into a comprehensive exploration of how various factors, including distinct test setups, laboratory conditions, diverse grease types, and different types of contamination, might influence the overall quality of condition monitoring with ultrasound spectroscopy. By meticulously examining these variables, the experiments strive to contribute valuable insights into the potential applications and nuances of active ultrasound spectroscopy in the realm of grease contamination detection and condition monitoring.

Based on review of the relevant literature, it is expected that the propagation of the ultrasound, and therefore the applicability of ultrasound spectroscopy, is affected by the following factors; signal type, sensor type, grease type, distance between the sensors, design of the test-setup, air bubble concentration fluctuations, temperature fluctuations and contamination of the grease sample.

Influence of Signal Type

The transmitted signals used to conduct the experiments, have a predetermined frequency and amplitude. Fluctuations in these wave properties may influence the propagation of the ultrasound wave, and the attenuation of the ultrasound wave, while moving through the grease sample. To account for this, a range or frequencies and amplitudes must be used for the transmitted signal for all measurements.

Influence of Sensor Type

Not every sensor or transmitter is capable of producing or receiving the same frequency range or amplitude range. Additionally, the transmitter or receiver might not be able to process every frequency at the same amplitude. Because of this, the sensors must be selected upon the need for a certain

type of signal, and the frequency distribution of the selected sensors must be taken into account when processing the received data. Lastly, to ensure sensor reciprocity, all experiments must be repeated after flipping the transmitting and receiving sensors around, and the results of both the forward and the backward measurements should be relatively close.

Influence of Grease Type

The composition and properties of the grease, including the type of base oil, thickener, and additives, contribute to how ultrasound waves interact with the medium. As can be observed in Equation 2.3, the speed of sound in a liquid medium is dependent on the density and the elasticity of that medium. Therefore, the grease type must be kept constant for all experiments, while alternating the other influences, in order to exclude the grease type effects on the propagation of ultrasound.

Influence of Distance Between Sensors

The distance between the transmitting sensor ant the receiving sensor is expected to have an effect on the amount of signal that propagates through the medium. Based on Equation 2.5, the change in sound pressure over distance is constant for a constant medium. This means that an increase in propagation distance causes a decrease in received signal amplitude. Therefore, an ideal sensor distance must be determined, and throughout the experiments, this distance should remain constant.

Influence of Noise

Noise can be introduced to the received signal in various ways. The most obvious source of noise is background noise, originating from the surroundings of the laboratory and the measurements. These can easily be identified and excluded by recording the surrounding noise levels at a low threshold and subsequently setting the measurement threshold above this amplitude. Additionally, filters can be applied to filter out unwanted noise, this however may also alter the desired signals. Another source of noise, may be the propagation of the transmitted ultrasound wave through other mediums than the grease. An example of this might be the propagation of the wave through the enclosure or test-setup that holds the grease sample and the sensors. To exclude this noise source, the propagation of the ultrasound through the test-setup material must be investigated.

Influence of Air Bubble Concentration Fluctuations

Air bubbles are introduced into the grease sample during procedures such as the churning of the grease inside the bearing, extraction of grease from the bearing, or the loading of the grease into the test setup. It is expected that the introduction of air bubbles, will increase the amount of boundaries, and therefore increase the amount of attenuation and subsequently decrease the received signal amplitude. Additionally, it is assumed that the air bubbles will dissipate out of the grease sample over time, which would result in a decrease of boundaries, a decrease in attenuation and an increase in received signal amplitude. Additionally, it is expected that the introduction of air bubbles into the grease sample, will decrease the overall bulk speed of sound of the grease sample. The dissipation of air bubbles over time would therefore cause an increase in bulk speed of sound of the grease sample over time. To investigate this effect, dissipation time experiments have been conducted to reveal the ultrasound behaviour when subjected to air bubble concentration fluctuations. Additionally, the dissipation time has been kept constant for all other measurements in order to maintain a relatively constant grease sample homogeneity. It should however be noted, that the air bubble concentration is also influenced by the test-setup loading procedure, and even though great care has been invested in maintaining this process as constant as possible, small air bubble concentration fluctuations may be caused by this procedure.

Influence of Temperature Fluctuations

Temperature fluctuations are introduced into the grease sample when the laboratory temperature fluctuates. An increase in temperature is expected to increase the particle energy of the grease sample, and subsequently increase the overall wave energy and therefore the amplitude of the received signal. Additionally, it is known that the speed of sound in a medium increases with an increase in temperature [58]. This has to do with the fact that for most materials, an increase in temperature, will cause an increase in relative movement of the particles in the medium and a subsequent decrease in density of the medium. Based on Equation 2.3, a decrease of the density will cause an increase in the speed

of sound. It is therefore expected that an increase in temperature will cause an increase in speed of sound. To investigate this effect, temperature fluctuation experiments have been conducted to reveal the effect of ultrasound propagation when subjected to various grease temperatures. Additionally, the grease temperature has been kept constant for all other measurements.

Influence of Contamination

As was discussed in subsection 2.1.5, bearing grease can be contaminated by particles either from the bearing itself or from the environment, or by water. These contamination sources impact the propagation of the ultrasound through the contaminated grease sample. In order to detect these types of contamination, techniques such as ultrasonic attenuation spectroscopy and ultrasonic velocity spectroscopy are applied.

As was discussed in subsection 2.3.2 ultrasonic attenuation spectroscopy employs the difference between the baseline attenuation behaviour, recorded when ultrasound is transmitted through a clean grease sample, and the measured attenuation behaviour from a possibly contaminated grease sample. For the experiments conducted in this research, these two measurements can be related using the following formulas, which are inspired by the approach of Scheeren et al. [59] and Berkhout [60].

$$P_{base} = D_r W_{base} D_t S + N_{base} \qquad N_{base} << P_{base} \tag{3.1}$$

$$P_{cont} = D_r W_{cont} D_t S + N_{cont} \qquad N_{cont} << P_{cont} \tag{3.2}$$

Herein, P_{base} represents the recorded response of the baseline measurement and P_{cont} the recorded response of the contaminated measurement. D_r is the transfer function of the receiving sensor, whereas D_t is the transfer function of the transmitting sensor. W_{base} is the propagation function of the baseline measurement, whereas W_{cont} is the propagation function of the contaminated measurement. S is the source function, and N_{base} and N_{cont} represent the noise, all of which are presented in the frequency domain. If the noise functions are neglected, this results in the following ratios:

$$\frac{P_{cont}}{P_{base}} = \frac{W_{cont}}{W_{base}} \tag{3.3}$$

From this, it can be concluded that the ratio of the recorded responses is a suitable measure for the attenuation behaviour, and can therefore be used to determine disturbances of the ultrasound propagation in the grease sample possibly caused by contamination or air bubbles.

Ultrasonic velocity spectroscopy on the other hand, employs the change in speed of sound between the contaminated medium and the clean baseline medium, as was discussed in subsection 2.3.2. The speed of sound of the medium is determined by the density and the elasticity of said medium.

Using these two spectroscopy techniques, the influence of various concentrations of tap water contamination and iron particle contamination on the ultrasound propagation through a contaminated grease sample can be investigated. The introduction of water contamination to a grease sample is expected to introduce more medium boundaries and therefore more attenuation to the ultrasound wave. Therefore, it is expected that an increase in water content will cause a decrease in received signal amplitude. Additionally, it is expected that the introduction of water into the grease will increase the density of the bulk. An increase in density causes a decrease in speed of sound. The introduction of iron particle contamination to a grease sample is expected to increase the amount of attenuation caused by scattering and diffraction. An increase in scattering attenuation especially, is expected to decrease the received signal amplitude. Additionally, this scattering is expected to lengthen the overall distance that the wave has to travel in order to travel from the transmitting to the receiving sensor, and therefore the bulk speed of sound will decrease with an increase in iron particles.

The conducted experiments aim to validate and identify these effects while also working towards alleviating the adverse impact they exert on the transmitted signals. The selection of the signal type used in these experiments shall be discussed in section 3.2. The selection of sensor type and grease type shall be discussed in section 3.3. The influence of distance, test-setup material, air bubble concentration fluctuations, temperature fluctuations and various types of contamination have been investigated and discussed in the matching methodology subsections.

3.2. Design of Experimental Setup

Throughout the various laboratory experiments, the aim was to identify and validate the influences that have been listed in the previous section. In order to do so, an experimental setup has been designed to methodically investigate the impact of these influences on the applicability of active ultrasound spectroscopy as a condition monitoring method for bearing grease.

3.2.1. Experimental Setup

A waveform generator is employed to generate the desired waveform. This waveform is then sent both through a power amplifier to the transmitting sensor, and directly to the Data Acquisition System (DAQ). The transmitting sensor converts the electrical signal to an ultrasound waveform, which propagates through the grease sample and is captured by the receiving sensor. The receiving sensor converts the received ultrasound waveform back into an electrical signal, which is sent through a pre-amplifier to the DAQ. The DAQ converts the electrical signal into a format suitable for processing using specific software. All the collected data is then stored on a laptop, where it can undergo processing. The processed data can be interpreted to give insights into the condition of the grease and, consequently, the condition of the bearing. An illustration of the experimental setup can be found in Figure 3.1.

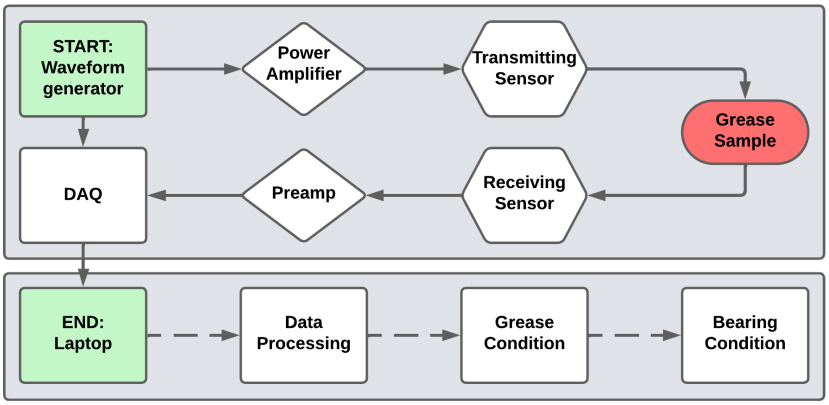

Figure 3.1: Design of the experimental setup used for the various experiments.

3.2.2. Signal Type

The ultrasound spectrum, as can be observed in Figure 2.6, stretches from waveforms with a 20kHz frequency to a 10MHz frequency. Ultrasonic inspection is usually done at frequencies higher than 100kHz [61]. For the various laboratory experiments, it has been decided to use frequencies ranging from 200kHz to 900kHz, with steps of 100kHz. This is done to create a broad spectrum of frequencies in order to determine the behaviour of the grease when subjected to various frequencies. The transmitting and receiving sensors have been selected according to this frequency range demand.

Additionally, it has been decided to specify a wave period instead of using a continuous wave. By doing so, it is possible to transmit a separate pulse, with a clear begin and end. This pulse can then be transmitted multiple times, and the multiple recorded responses can then be averaged to get rid of noise. With this in mind, it has been decided to keep the wave period constant at six periods for every frequency. Additionally, it has been decided to transmit this six-period waveform every one second for ten seconds, resulting in a total of ten transmitted waveforms and ten received waveforms. In Figure 3.2 an example of such a waveform has been depicted. Shown in this figure, is the average of ten individual 200kHz pulses with six periods.

3.2.3. Data Processing

As can be observed from Figure 3.1, both the originally generated waveform, as well as the received waveform are both collected by the DAQ and sent to a laptop. For the data acquisition, the Vallen Acquisition and Vallen VisualAE software is used. Subsequently, a couple of processing steps and corrections are applied to the data in order to make the data interpretable. For this, MATLAB is used.

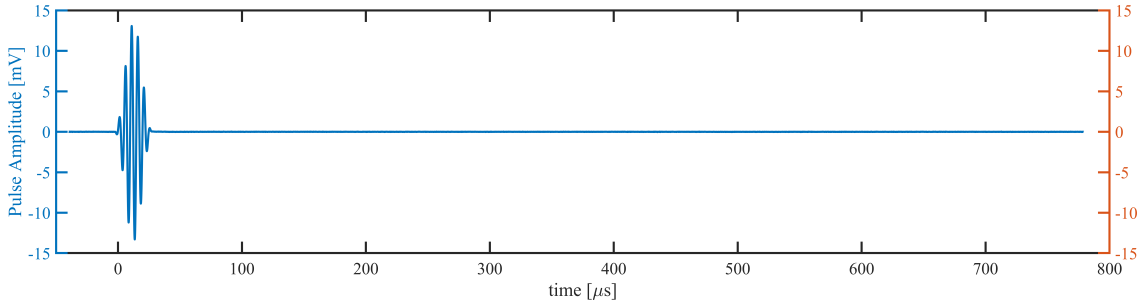

Figure 3.2: Example of a full signal range, showing an average of ten transmitted 200kHz pulses with six periods.

For the data collection, it is first important to note that the data acquisition software only registers signals of which the amplitude exceeds a certain user-defined threshold. Secondly, it is important to understand that the Vallen software treats every first threshold crossing as a single waveform. This means that when this threshold is set too high, no signals will be recorded, and when this threshold is set too low, a lot of noise waveforms will be recorded alongside the desired waveforms. It is therefore important to select a threshold somewhere between the noise level and the received signal level. Thirdly, each waveform includes a specific pre-trigger length, which is a user-defined amount of data points preceding the moment of threshold crossing, and a distinct total signal length, which is the total amount of data points that is being recorded for every threshold crossing.

For the experiments discussed in this thesis, the sample rate was set to 5MHz, or one sample every $0.2\mu s$. The total signal length is 4096 samples, or $819.2\mu s$ for all signals. For the transmitted signals, generated by the waveform generator, the pre-trigger length is 200 samples, or $40\mu s$, and for the received signals, the pre-trigger length is 500 samples, or $100\mu s$. In Figure 3.2, the data points from $t = -40\mu s$ to $t = 0\mu s$ represent the pre-trigger length of this specific transmitted signal. At $t = 0\mu s$, the threshold crossing takes place and the waveform is recorded. The total signal length is $40\mu s + 779.2\mu s = 819.2\mu s$.

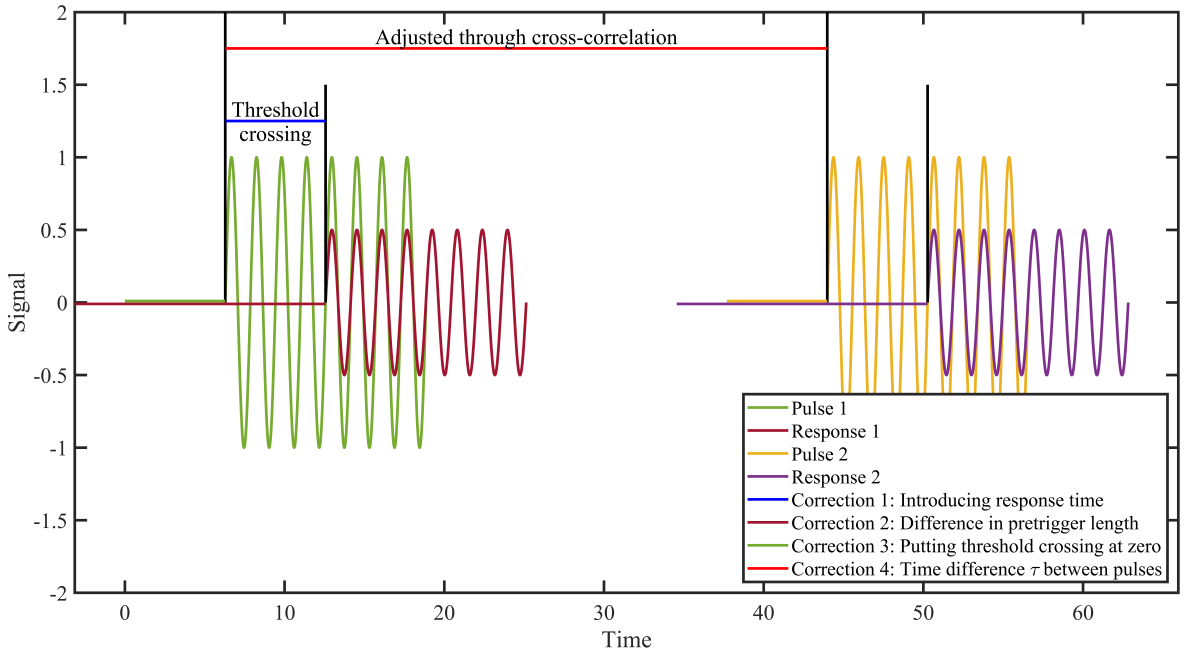

Figure 3.3: Illustration showing the corrections that have been applied to improve the raw data.

Upon importation into MATLAB, the full signal length is perceived as the desired signal, and because of that, the start of the pre-trigger is plotted at $t = 0$, rather than the more pertinent moment of threshold crossing. Additionally, as was named before, the transmitted signals do not share the same pre-trigger length as the received signals. To make the signals that are collected by the DAQ interpretable, a number of corrections have been applied. An illustration of these corrections can be seen in Figure 3.3. In this illustration, the pulses signify the signals that have been transmitted by the waveform generator and subsequently the transmitting sensor, whereas the responses signify the received signals.

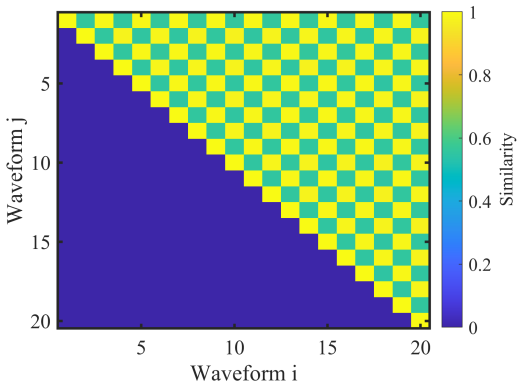

Figure 3.4: Cross-correlation pattern showing 10 transmitted waveforms (odd) and 10 received waveforms (even).

1. **Correction 1: Introducing the response time:** Given that every signal is plotted at $t = 0$, the inherently significant response time (the duration it takes for the signal to travel from the transmitter to the receiver) is obscured and requires restoration. Fortunately, the precise time of threshold crossing for all signals is preserved. As a result, the disparity between the exact times of threshold crossings can be computed for each pair of transmitted and received signals.
2. **Correction 2: Difference in pre-trigger length:** As mentioned earlier, not every signal shares the same pre-trigger length. The transmitted waveforms have a pre-trigger length of 200 data points, whereas the received waveforms have a pre-trigger length of 500 data points. Since the initiation of the pre-trigger is initially plotted at $t = 0$ for all signals, the variation in pre-trigger length needs correction. Given that the pre-trigger lengths are known for all waveforms, a straightforward adjustment can be made to shift the received waveforms backwards by 300 data points to ensure that the received waveforms align with their paired transmitted waveforms.
3. **Correction 3: Putting the threshold crossing at $t = 0$:** Initially, the initiation of the pre-trigger is set at $t = 0$. However, for a more meaningful interpretation of the data, it is more advantageous to position the threshold crossing of the generated signals at $t = 0$. With the pre-trigger lengths known, it is once again a straightforward adjustment to shift the waveforms in a manner that places the threshold crossing at $t = 0$.
4. **Correction 4: Time difference τ between the pulses:** Due to various subtle discrepancies in the signals, minor time differences between the generated pulses can arise. On top of that, between every pulse, one second elapses. Employing cross-correlation of the generated pulses enables the precise determination of the time difference τ between the various pulses. Shifting the generated pulses and their corresponding responses by this time difference τ in relation to the first generated pulse, enhances the visualization of the various pulses and responses and places the pulses on top of each other, with their threshold crossings around $t = 0$. In Figure 3.4, an example of such a cross correlation pattern has been shown. The transmitted signals are signified by the odd waveforms i and j, and the received signals are signified by the even waveforms i and j. High similarity can be observed when odd waveforms are compared to odd waveforms, and when even waveforms are compared to even waveforms.
5. **Correction 5: Averaging:** As was discussed in subsection 3.2.2, ten pulses are transmitted, and ten responses are received. After the fourth correction step, the ten pulses have been placed on top of each other, with their threshold crossings around $t = 0$ and their respective responses have been modified accordingly. The last correction applied to the signals is to average them. The transmitted waveforms are averaged with respect to one another, and the received responses are averaged with respect to one another too.

3.3. Materials and Equipment

In this section, a comprehensive overview of all the materials and equipment used in conducting these laboratory experiments has been provided. It serves to shed light on the resources necessary for the accurate data collection and analysis. It also serves to facilitate a list of the necessary resources for the reproducibility of the experimental results.

3.3.1. Materials

An overview of the grease types and contamination samples used to execute the various experiments has been provided below. An extensive overview of the various greases that have been researched can be found in Appendix B. An extensive overview of the various contamination sources that have been researched can be found in Table 2.1.

Grease

- *Shell Gadus S2 V220 2:* New, clean samples of this grease were used.
- *Mobilux EP2:* New, clean samples of this grease were used.
- *Mobilux EP2:* Pre-contaminated grease samples with unknown contamination were used. These samples originated from a Huisman linear bearing. The bearing was in a 100% lifetime condition, meaning that the bearing had outlived its calculated lifetime.

Contamination

- *Tap water:* samples of regular tap water were used.
- *Iron particles:* for analysis reduced, particle size $10\mu m$, EMSURE 1.03819.0100.

3.3.2. Equipment

An overview of all the equipment used to execute the various laboratory experiments has been provided below. An extensive overview of the various available sensors can be found in Appendix B. An overview of the experimental setup is depicted in Figure 3.1.

Electrical Components

- *Waveform generator:* RS PRO RSDG 1032X 30MHz 150MSa/s [62].
- *Data Acquisition System:* Vallen Systeme AMSY-6 [63].
- *Laptop:* any laptop with Vallen Acquisition, Vallen VisualAE and MATLAB installed.

Amplification Components

- *Power Amplifier:* Falco Systems WMA-300 [64].
- *Pre-Amplifier:* Vallen Systeme AEP5H - 40dB [65].

Ultrasonic Sensors

The sensors used in the various experiments were selected keeping the desired frequency range in mind. As discussed in section 3.2, a broad frequency range is desired to determine the behaviour of the grease when subjected to a broad range of frequencies.

- *Transmitting Sensor:* Mistras WSα Sensor, frequency range: 100kHz to 1MHz [66].
- *Receiving Sensor:* Mistras WSα Sensor, frequency range: 100kHz to 1MHz [66].

Cables

- *BNC to BNC:* RG58 Coaxial Cable
- *BNC to SMA:* RG316 Coaxial Cable
- *BNC to BNC splitter:* RS PRO Tee, three-way splitter

Measuring Devices

- *Scale:* Digital scale, precision 0.1 grams
- *Thermometer:* Digital thermometer, precision 0.1 °C

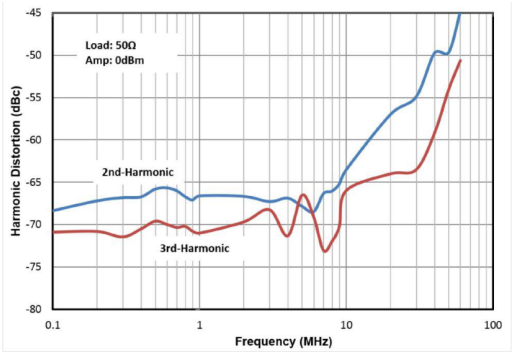

(a) Harmonic distortion of the waveform generator [62].

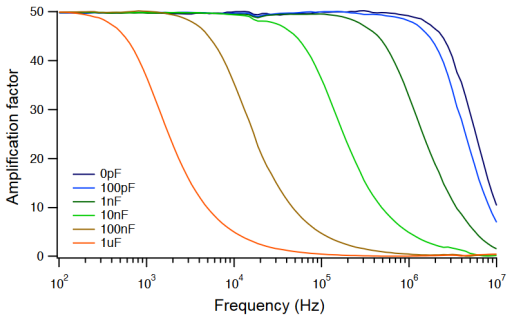

(b) Frequency response of the power amplifier [64].

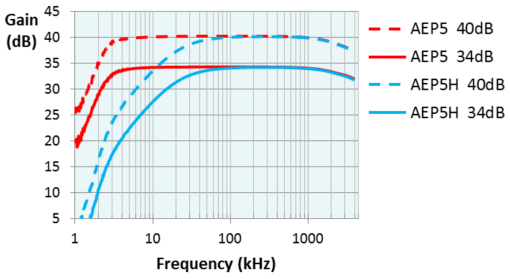

(c) Frequency response of the Vallen Systeme AEP5H - 40dB [65].

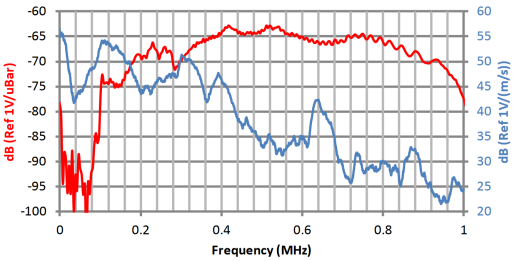

(d) Frequency response of the Mistras WSα sensor [66].

Figure 3.5: Frequency responses of various pieces of equipment.

Physical Grease Setup

In order to secure the ultrasonic sensors, and create a compartment to contain the to be examined grease, a couple of sensor holders were designed.

- *PVC setup:* a modular setup with emphasis on ensuring the simplicity of adjusting the distance between the sensors, while maintaining the sensors at a 180 °angle to one another. This modular approach allows for the efficient exploration of diverse distances but also ensures the stability and consistency of the sensor arrangement throughout the experiments. It can be seen in Figure 3.6a.
- *3D-printed setup 1:* this second setup was designed with emphasis on enhancing the ease of experimentation. The primary configuration of the setup features a square cross-section, transitioning gradually into a circular cross-section on both sides. Furthermore, the incorporation of two sensor holders on either side of the square section adds versatility to the setup. The distance between the two sensor surface plates is precisely maintained at 22 mm, secured by the screw cap affixed to the sensor holders. This design ensures a standardized and controlled environment for conducting experiments with precision. It can be seen in Figure 3.6b.

(a) The PVC setup.

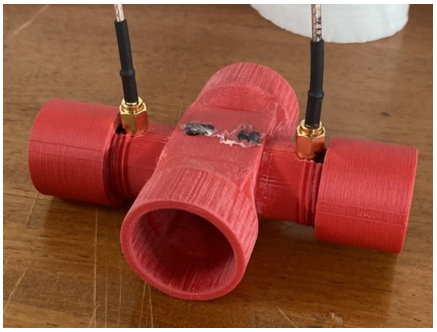

(b) 3D printed setup 1.

Figure 3.6: The physical grease setups that were used in the laboratory experiments.

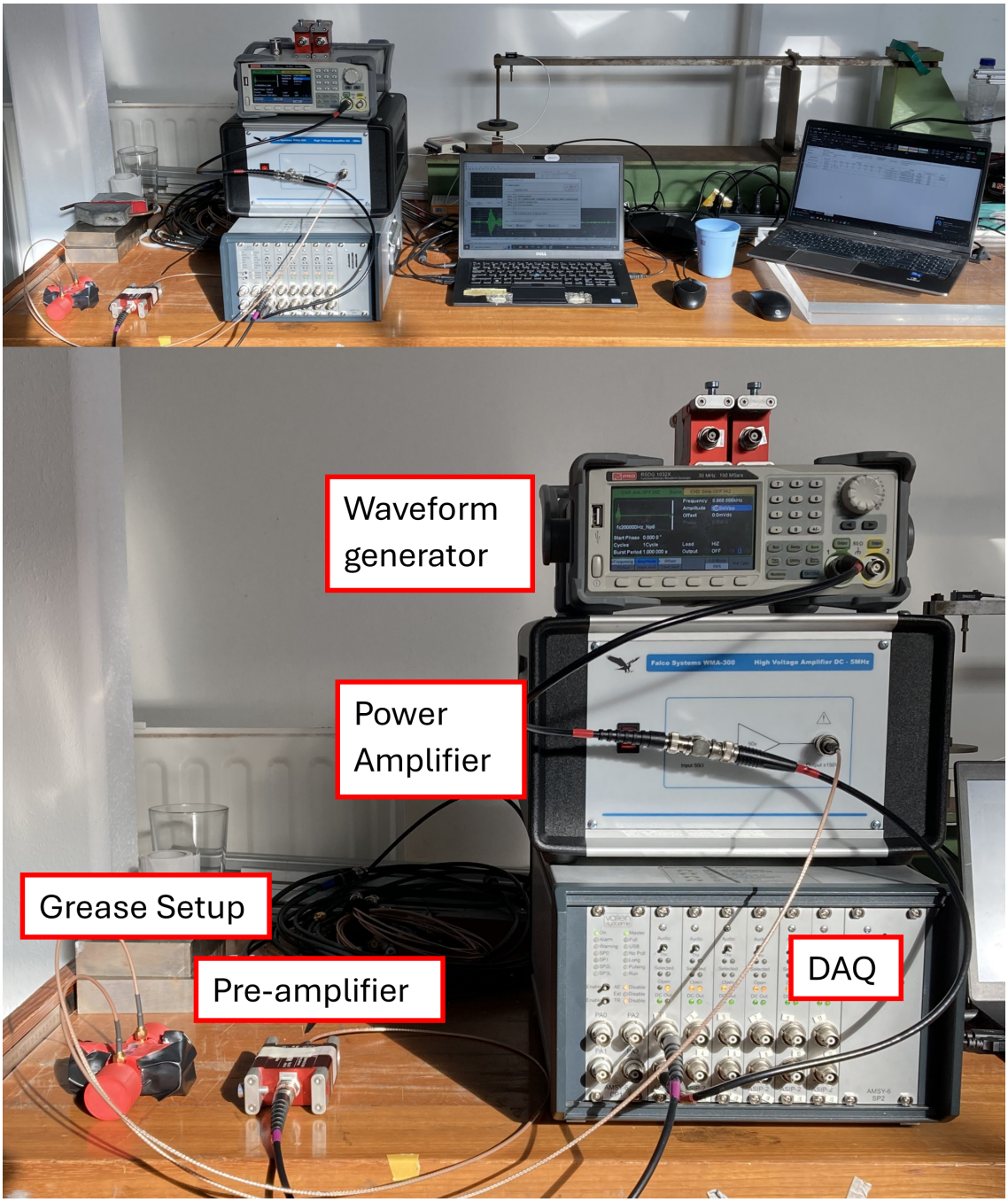

Figure 3.7: Equipment setup used in the laboratory.

3.4. Methodology of Experiments

In this section, the comprehensive methodology employed to conduct the series of laboratory experiments is presented. Initially, a detailed step-by-step procedure is delineated, illustrating the sequential stages undertaken during the experimental phase. Subsequently, the specific methodologies adopted for each individual experiment have been highlighted, providing a focused overview of the procedures and techniques employed to address the research objectives. First, the step-by-step procedure that has been followed during every laboratory experiment is listed. This includes the four preparation steps and the two signal detection steps. In the various experiments, the measurement steps might be repeated several times, every time changing a single variable. This will be further discussed in the methodologies of every laboratory experiment.

Preparation Stage 1: Preparing the Test Setup

1. Choose the right test setup from Figure 3.6a or Figure 3.6b.
2. Place the Mistras WSα sensors within the chosen test setup.
3. Connect the RS PRO splitter to the input of the Falco Systems power amplifier.
4. Connect the output of the RS PRO waveform generator to one open end of the RS PRO splitter using a RG58 coaxial cable.
5. Connect the other end of the RS PRO splitter to channel 2 of the AMSY-6 DAQ using a RG58 coaxial cable.
6. Connect the output of the Falco Systems power amplifier to the transmitting WSα sensor using a RG316 coaxial cable.
7. Connect the receiving WSα sensor to the AEP5H pre-amplifier using a RG316 coaxial cable.
8. Connect the AEP5H pre-amplifier to channel 1 of the AMSY-6 DAQ using a RG58 coaxial cable.

Preparation Stage 2: Preparing the Grease Sample

1. Choose the type of grease necessary for the experiment.
2. Weigh the desired amount of grease using the digital scale.
3. Choose the type of contamination necessary for the experiment.
4. Weigh the desired amount of grease using the digital scale.
5. Stir the contamination into the grease sample using any type of stirring stick.
6. Wait a desired amount of time to let the grease sample 'rest'.

Preparation Stage 3: Loading Test Setup With Grease

1. Fill the test setup from end one with grease until the pipe overflows on end two.
2. Close end two of the test setup.
3. Apply small bits of pressure onto the grease on end one to push out air bubbles.
4. Close end one of the test setup.
5. Wait a desired amount of time to let the grease sample 'rest'.

Preparation Stage 4: Setting Equipment Settings

1. In Vallen Acquisition, set the threshold on the transmitted signal to a desired amplitude.
2. In Vallen Acquisition, set the threshold on the received signal to a desired amplitude.
3. In Vallen Acquisition, apply bypass filters on both channels.
4. In the waveform generator, specify the desired output voltage.
5. In the waveform generator, specify the desired burst period.

Signal Detection Stage 1: Forward Measurement

1. Using the waveform generator, generate a 200kHz pulse with 6 periods (np=6).
2. Transmit this burst ten times.
3. Repeat step 1 and 2 for 300kHz, 400kHz, 500kHz, 600kHz, 700kHz, 800kHz and 900kHz.

Signal Detection Stage 2: Backward Measurement

1. Change the orientation of the sensors by reversely connecting the cables: The transmitting sensor becomes the receiving sensor and vice versa.
2. Repeat the steps of Signal Detection Stage 1: Forward Measurement.

3.4.1. Experiment 1: Influence of Distance Between Sensors

This first experiment aims to identify the effect of the influence of the distance between the transmitting sensor and the receiving sensor, as discussed in section 3.1. The objective of this first experiment was to ascertain the optimal distance between the transmitting sensor and the receiving sensor. This was achieved by systematically varying the separation distance and assessing the resulting outcomes. To facilitate this investigation, a modular setup was designed. The emphasis in this design was placed on ensuring the simplicity of adjusting the distance between the sensors, while simultaneously minimizing alterations to the sensor holders. This modular approach not only allowed for the efficient exploration of diverse distances but also ensured the stability and consistency of the sensor arrangement throughout the experiments.

To enable the functionality of a modular setup, a test configuration has been devised, incorporating PVC sensor caps designed to firmly secure the transmitting and receiving sensors. These sensors are affixed inside the sensor caps using putty or kneadable rubber. The sensor caps can then be securely attached to sections of PVC pipes of varying lengths, allowing for the systematic exploration of the impact of different pipe lengths. Importantly, these pipes are loaded with the grease sample, forming an integral part of the experimental setup aimed at investigating the effects under consideration. For the purposes of this experiment, the decision was initially made to assess pipes with lengths of 50 mm, 100 mm, 150 mm, and 200 mm. The six images in Figure 3.8 depict the construction of the sensor setup, providing a clear visual representation of the steps involved in securing the sensors into the caps and subsequently affixing the caps onto the pipes.

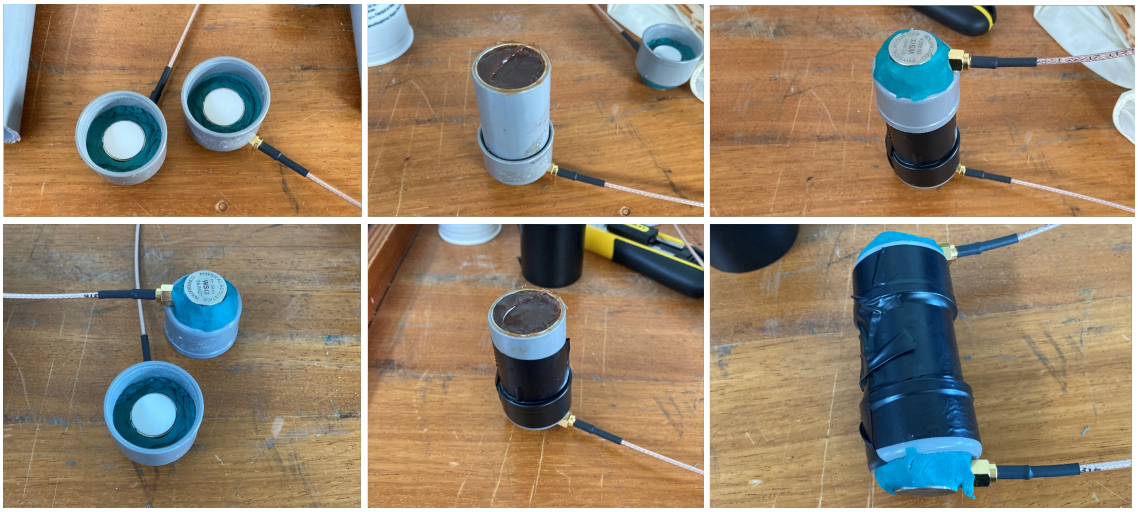

Figure 3.8: Construction of experimental setup used in experiment 1.

For this experiment, the Shell Gadus S2 V220 2 grease was used due to its availability, as well as due to the fact that the application temperatures and kinematic viscosities of this grease closely represent the average values of the researched greases shown in Appendix B. Additionally, it was decided to conduct these experiments by only varying the pipe length, and therefore not use any contaminants to contaminate the clean grease. The threshold on the transmitted signals was set to 70dB, the threshold on the received signals was set to 30dB, the output voltage was set to 6Vpp and the burst period was set to 1 second.

The transmitted and received signals have all been recorded using the Vallen Acquisition and Vallen VisualAE software. Following the Signal Detection Stages 1 and 2, a total of sixteen measurements per pipe length have been conducted. The goal of this experiment was to determine how well the ultrasound would propagate through the grease when the propagation length increases. Therefore, the key performance indicator for this experiment is the amount of signals that manage to propagate through the grease sample when transmitting ten pulses per frequency per pipe length.

3.4.2. Experiment 2: Influence of Noise

As discussed in section 3.1, there are various ways in which noise can be introduced into the signal. Surrounding noise can easily be accounted for by applying the right thresholds and filters. Noise signals due to propagation through the test-setup material instead of the grease need to be investigated and excluded. A new test-setup was designed and 3D-printed, incorporating the findings from the previous experiment to select improved dimensions and structures. In this second experiment, the propagation of the ultrasound through this test setup has been investigated by observing the propagation of ultrasound waves through a test setup devoid of grease, as well as observing the propagation through the air excluding the use of the 3D printed setup. The assumption in this experiment is that the ultrasound propagation through air is sufficiently bad that if the sensors are not connected by any structure, the signal should not reach the receiving sensor.

In this new, 3D-printed sensor setup, the distance between the two sensor surface plates is precisely maintained at 22 mm, secured by the screw cap affixed to the sensor holders. This design ensures a standardized environment for conducting experiments with precision. An overview of this new setup is depicted in Figure 3.9a, where the (white) sensor surface plate is visible in the right image.

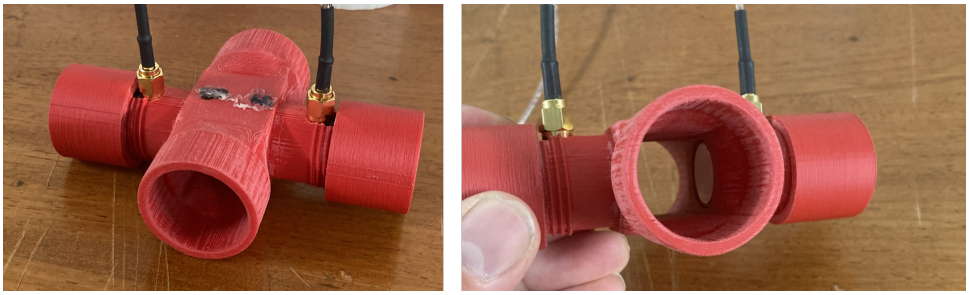

(a) 3D-printed experimental setup used in experiment 2.

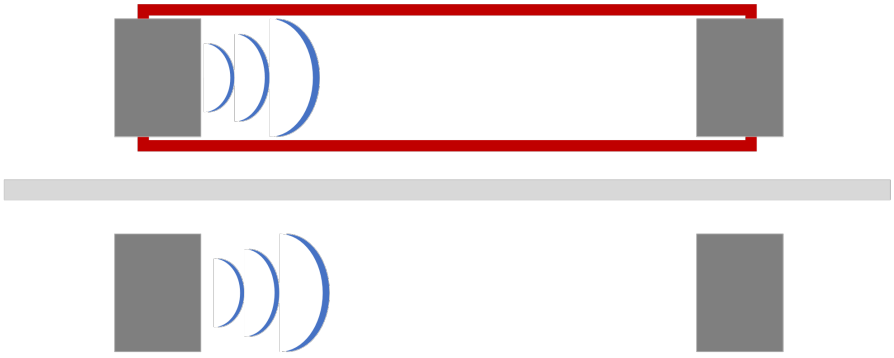

(b) Comparison between sensors with sensor setup and without sensor setup.

Figure 3.9: Construction of experimental setup used in experiment 2.

For this experiment, neither grease nor contamination were used, as the primary objective was to assess ultrasound propagation through the 3D-printed plastics. Consequently, the 3D-printed setup was solely filled with air. To evaluate propagation through this setup, it was compared with propagation through air using two unconnected sensors positioned by hand at a 22 millimetre distance. As depicted in Figure 3.9b, one set of sensors is linked by the (red) sensor setup, while the other remains unconnected. The transmitted signal threshold was set to 70dB, while the received signal thresholds differed: 30dB for the 3D-printed setup and 40dB for the handheld test, adjusted due to increased noise levels when holding the sensors by hand. Output voltage was initially set to 6Vpp and later adjusted to 0.06Vpp for both experiments, and a burst period of 1 second was applied.

The objective of this experiment is to ascertain whether ultrasound waves would propagate through the 3D-printed setup as opposed to through the air. Consequently, the focus of this experiment lies in assessing the quantity of received responses when transmitting ten pulses per frequency per setup per output voltage.

3.4.3. Experiment 3: Influence of Air Bubble and Temperature Fluctuations

The aim of this third experiments was to examine the influence of air bubble concentration and temperature fluctuations on the propagation of ultrasound waves through grease samples. The air bubbles are introduced into the grease sample during grease handling processes such as mixing, stirring or loading of the test setup, and the bubbles are expected to gradually dissipate from the grease sample over time. Hence, this experiment partly focuses on investigating the temporal influence of bubble dissipation on the propagation of ultrasound. A validation measurement has been conducted in which air bubbles were deliberately introduced in the grease sample between the sensors. Meanwhile, grease temperature variations are introduced when the laboratory temperature fluctuates. This second part of this experiment focuses on the identification of the effect of temperature on the propagation of the ultrasound. All steps in this experiment utilized the 3D-printed setup described in the preceding section and depicted in Figure 3.9a. Clean Mobilux EP2 was used for all experiments.

Influence of Air Bubble Concentration Fluctuations

The introduction of air bubbles into the grease sample during the laboratory procedures such as mixing is almost insurmountable. Because these air bubbles are expected to influence the propagation of the ultrasound, an experiment has been devised to investigate and negate this influence.

Because it is expected that the air bubbles will dissipate out of the grease sample over time, the influence of time on this dissipation rate, and subsequently on the propagation of the ultrasound has been investigated. A series of experiments have been conducted, in which the only changing variable was the dissipation time. In this research, dissipation time means, the time that the grease sample has been idly sitting inside the grease test-setup, in other words, the time since the grease test-setup has been loaded with grease until the time of conducting measurements. This means that all the other variables, including temperature, were kept constant. The contribution of air bubble dissipation has been investigated by conducting ultrasonic spectroscopy measurements in a clean grease sample after 0 hours, 1.5 hours, 2.5 hours, 4.0 hours and 22 hours after loading the test setup. The threshold on the transmitted signal was set to 70dB. The threshold on the received signal started out at 50dB, however, as the propagation of the ultrasound through the grease improved with time, the noise level increased and therefore the threshold was later increased to 55dB. The output voltage was set to 60mVpp.

Influence of Temperature Fluctuations

Temperature fluctuations of the grease sample are introduced when the laboratory or offshore environment experiences temperature fluctuations. This is expected to have an influence on the propagation of the ultrasound through the grease sample. In order to investigate this effect, the previous air bubble experiments have been repeated, but this time with grease samples at a higher temperature. The first session of air bubble measurements (0h, 1.5h, 2.5h, 4.0h, 22.0h) was conducted at $17°C \pm 0.5°C$. Following this, the grease test-setup has been emptied and cleaned before filling it up with the warmer grease sample. This was mainly done to ensure similar loading conditions for both experiment sessions. The second session of measurements (0h, 1.5h, 2.5h, 4.0h) was conducted at $23°C \pm 1.0°C$. Due to time constraints, the 22 hour measurement has been omitted from the second series of measurements.

Again, the threshold on the transmitted signal was set to 70dB. The threshold on the received signal started out at 55dB, however, as the propagation of the ultrasound through the grease improved with time, the noise level increased and therefore the threshold was later increased to 62dB. The output voltage was set to 60mVpp.

The objective of these experiments was to ascertain the influence of air bubble concentration and temperature fluctuations on the propagation of the ultrasound through the grease sample. Therefore, both the attenuation and the velocity spectroscopy methods have been applied here. During these experiments, clean grease samples are used, and only one variable at the time is changed. Therefore, for the air bubble fluctuation measurements, it is safe to assume that an increase in received signal amplitude signifies a decrease in attenuation and thus a decrease in air bubble concentration. An increase in speed of sound signifies the removal of air bubbles because the bulk speed of sound increases. For the temperature fluctuation measurements, an increase in received signal amplitude signifies an increase in particle energy, which can be translated to an increase in temperature, whereas

an increase in speed of sound signifies a decrease in medium density caused by the particle movement, caused by the increase in temperature.

3.4.4. Experiment 4: Influence of Contamination

This fourth and final laboratory experiment was aimed at determining the effect of contamination on the propagation of ultrasound through the contaminated grease sample. As was discussed in subsection 2.1.5, grease can be contaminated through various sources, either inside the bearing, or outside. To investigate this effect, various types and concentrations of contamination have been purposely inserted into grease samples. Additionally, the findings of the previous experiments have been implemented in the experimental procedure, meaning that a constant distance, test-setup, dissipation time and temperature have been used for these experiments.

This experiment was threefold. First of all, the scalability of the transmitted signal amplitude had to be investigated. The introduced contamination caused a problem with the signal propagation through the grease, causing the need for stronger transmitted signals. Secondly, clean grease samples were deliberately contaminated using various concentrations of tap water or iron particles. Thirdly, an experiment was done aimed at scrutinizing the propagation of ultrasound through grease that had been used in real offshore roller bearings. In this case, the contaminated sample was extracted from a Huisman linear bearing that was taken out of its housing because it had reached 100% of its calculated lifetime.

Scalability

Initial tests were conducted using an output voltage of 60mVpp. It turned out however, that this output voltage was not strong enough to produce an ultrasound wave that would propagate all the way through a severely contaminated sample. Therefore, the output voltage of some of the transmitted signals had to be increased. Based on Equation 3.2 it was hypothesised that physically increasing this output voltage, and later on electronically decreasing this peak to peak voltage again, would not affect the received signal. If the noise would again be neglected, and the grease sample and sensors stay constant, this equation can be rewritten to:

$$P_{cont} = D_r W_{cont} D_t S + N_{cont} \quad \rightarrow \quad P_{cont} = CS \tag{3.4}$$

Herein, C denotes a constant. This would mean that if the source signal is doubled, the recorded response would also be doubled, thus making it possible for the source signal to be increased in order to create an ultrasound wave that is able to propagate through the contaminated sample, and making sure that the electronically received signal can later on be scaled back to represent a received signal that can be compared to other measurements that were conducted at different output voltages. In order to prove this hypothesis, a signal has been sent through a clean grease sample at 60mVpp and at 480mVpp, a scaling factor of 8. Next, the received electronic signal of the 480mVpp measurement was than scaled back 8 times. Lastly, a comparison was made between the electronic signal of the 60mVpp waveform and the scaled back 480mVpp waveform.

Known Contamination

For this second part of this fourth experiment, contamination samples were deliberately mixed into clean grease samples in order to investigate the influence of these contaminants on the propagation of the ultrasound. The ultrasound performance in the deliberately contaminated grease samples were compared to the ultrasound performance in a clean baseline sample of the same grease type. Based on the literature review and the data presented in Table 2.1, tap water and iron particle contamination were selected as the contaminants for this experiment. The previously investigated influences were kept constant during these measurements. This means that all deliberate contamination measurements were conducted at $25.5°C \pm 0.6°C$ and after 1.5 hours of dissipation time in the test setup. It is however noteworthy that extra air bubbles are introduced into the grease samples because the contaminants need to be stirred and mixed into the grease. Because of this, all the samples, contaminated or not, were prepared and stirred the day before the testing, approximately 18 hours before conducting the experiments, in order for the stirring effects to dissipate similarly in every sample. Additionally, these deliberate contamination measurements were conducted using Mobilux EP2, because that grease type corresponds to the grease type used in the linear bearing experiment.

The influence of water contamination has been investigated by mixing tap water into the grease sample at 1wt%, 5wt% and 10wt% of the grease weight. These measurements have subsequently been compared to a baseline measurement using a clean grease sample. The 3D-printed setup can hold approximately 40 grams of clean grease, which results in either 0 grams, 0.4 grams, 2.0 grams or 4.0 grams of tap water added to a clean sample. These experiments have been conducted at a constant temperature of $25.5°C \pm 0.6°C$ and a constant air bubble dissipation time of 1.5 hours. A decreasing amplitude and bulk speed of sound is expected with an increase in water concentration.

The influence of iron particle contamination has been investigated by mixing iron particles into the grease sample at 1wt%, 5wt% and 10wt% of the grease weight. These measurements have subsequently been compared to a baseline measurement using a clean grease sample. The 3D-printed setup can hold approximately 40 grams of clean grease, which results in either 0 grams, 0.4 grams, 2.0 grams or 4.0 grams of iron particles added to a clean sample. These experiments have been conducted at a constant temperature of $25.5°C \pm 0.6°C$ and a constant air bubble dissipation time of 1.5 hours. A decreasing amplitude and bulk speed of sound is expected with an increase in iron particle concentration.

Initially, the output voltage of the measurements was set to 60mVpp, however, in the more severely contaminated samples, the propagation of the ultrasound through the grease was obstructed too much, resulting in no discernible signals between the noise. Because of this, it was decided to increase the output voltage of the transmitted signals in order to try to get the signal to propagate through the contaminated sample. For the 5% and 10% water contaminated samples, the output voltage was increased to 3840mVpp and for the 5% and 10% iron contaminated samples, the output voltage was increased to 960mVpp. The scaled back signal amplitudes, and the signal arrival times, for all frequencies and all contamination concentrations have been presented and compared.

Unknown Contamination

In this last experiment, an attempt was made to compare the amplitude and arrival time of ultrasound through three different mediums; Shell Gadus S2, Mobilux EP2 clean and Mobilux EP2 contaminated by the linear bearing at 100% of its lifetime. The measurements to substantiate this comparison were however conducted before the conclusions of the air bubble concentration fluctuation and the temperature fluctuation measurements had been drawn. Because of this, the findings presented in the air bubble concentration fluctuation and the temperature fluctuation measurements were not taken into account for this experiment. This means, that unfortunately, no record has been kept about the temperature behaviour of the grease, or the dissipation time of the experimental procedure. Apart from that, the data collection of this experiment has commenced similarly compared to that of the known contamination experiments.

3.5. Results and Discussion

In this section, the results of the previously introduced laboratory experiments shall be presented. For each experiment, a short recap of the relevant performance indicators shall be provided. This is followed by a presentation of the relevant results, as well as a discussion of the implications of these results.

3.5.1. Experiment 1: Influence of Distance Between Sensors

In conducting this experiment, a crucial aspect was to ascertain the transmission of signals from the transmitting sensor, through the grease and their subsequent recording by the sensor on the opposite side of the test setup. To achieve this, an analysis was undertaken to determine the quantity of signals received following the transmission of ten bursts per frequency. The detailed results of this analysis are presented in Table 3.1.

Pipe Length	Measurement Direction	Frequency [kHz]							
		200	300	400	500	600	700	800	900
50 mm	Forward	10	10	10	10	10*	10	10	10
	Backward	10	10	10	10	10*	10	10	10
100 mm	Forward	0	0	0	10	10**	10**	0	0
	Backward	0	0	0	10	10	10	10**	0
150 mm	Forward	0	0	0	0	0	0	0	0
	Backward	0	0	0	0	0	0	0	0
200 mm	Forward	-	-	-	-	-	-	-	-
	Backward	-	-	-	-	-	-	-	-

Table 3.1: The amount of pulses recorded per frequency per pipe lengths.
* sensor exceeded 95% of input range, ** received signal is close to the 30dB threshold.

The data presented in Table 3.1 shows the amount of responses obtained from transmitting 10 bursts at an output voltage of 6Vpp. This output voltage was chosen because it represents the maximum allowable output voltage of the waveform generator and therefore indicates an upper limit for conducting measurements. The results presented in the table suggest that an ultrasound wave can travel at least 50 millimetres through a clean grease sample when pulsed at an output voltage of 6Vpp, however, at 100 millimetres, only the 500kHz, 600kHz, 700kHz and 800kHz pulses are getting through. The tests conducted at a transmission length of 150 millimetres did not yield any response, and because of that, the test at 200 millimetres was cancelled.

It was hypothesised that an increase in propagation distance would cause a decrease in received signal amplitude, and thus a decrease in received signals that cross a certain predefined threshold. It is however important to note that not every frequency presented in Table 3.1 portrays the same results. The 600kHz results presented for the 50mm experiment for example, show clipping behaviour, meaning that the received sensor input exceeded 95% of the allowed input range, whereas the other frequencies in that same 50mm experiment did not show such behaviour. Another outlier can be observed in the 100mm experiment, where only the 500kHz to 800kHz show any measurable results, and most of these results are close to the threshold value. A reason for this difference of ultrasound behaviour between different frequencies might have something to do with the frequency response of the Mistras WSα sensors, as can be observed in Figure 3.5d. In this graph, it can be observed that the frequency response of the sensor differs per frequency. Especially the frequencies below 400kHz and above 700kHz show a lower sensor amplitude response. This would be consistent with the results presented here.

The presented results suggest that a transmission length of 100 millimetres or longer proves to be excessive, leading to an incomplete registration of all waveforms, even when the employed output voltage is at its maximum. It can therefore be concluded that when considering the propagation through grease, a shorter propagation distance causes less attenuation of the ultrasound wave and therefore yields more response. Therefore the propagation length should be minimized. Additionally, it should be noted that it is always possible to generate signals at a lower output voltage, in order to prevent the

response to be close to the clipping range, as is the case for the 600kHz pulses at 50 millimetres of propagation length. Last but not least, it should be noted that this analysis does not take into account any noise measurements or analysis of the wave path, meaning that propagation in this test is not guaranteed to travel through the grease, but might instead travel through the test setup material or the air. These effects have been further studied in experiment 2.

3.5.2. Experiment 2: Influence of Noise

In conducting this second experiment, a crucial aspect was to ascertain the transmission of signals through the plastic of the 3D-printed test setup, because these signals have to be interpreted as noise signals. By evaluating the quantity of signals that propagate through the empty test setup and comparing them to the quantity of signals that propagate through 22 millimetres of air without test setup, an estimation can be made of the propagation of the signals through the plastic as opposed to through the grease in a normally filled test setup. The underlying rationale for conducting these measurements lies in the fundamental principle that ultrasound waves exhibit relatively poor propagation through air, while demonstrating significantly improved propagation through grease.

		Frequency [kHz]								**Vpp**
		200	300	400	500	600	700	800	900	
3D printed	Forward	10	10	10	10	10	10	10	10	6
	Backward	10	10	10	10	10	10	10	10	
	Forward	10**	0	0	0	0	0	0	0	0.06
	Backward	10**	0	0	2	0	0	0	0	
Sensor in hand	Forward	10	10	10	10	10	10	10	10	6
	Backward	10	10	10	10	10	10	10	10	
	Forward	0	0	0	0	0	0	0	0	0.06
	Backward	0	0	0	0	0	0	0	0	

Table 3.2: The amount of pulses recorded per frequency per amplitude for the two experimental procedures, ** received signal is close to the 30dB threshold.

The data depicted in Table 3.2 shows the quantity of responses resulting from transmitting 10 bursts at output voltages of 6Vpp and 0.06Vpp across diverse frequencies. This analysis encompasses both the 3D-printed setup and the scenario where the sensors are held 22 millimetres apart in the air. Again, a forward and a backward measurement has been conducted for the sake of reciprocity.

The comparison between the propagation through the empty 3D setup and the propagation through air (sensors held in hands) aims to highlight the limited propagation values through the 3D-printed plastic. The observations from the sensor-in-hand measurements reveal that, at an output voltage of 6Vpp with a 22 millimetre separation, the signal effectively propagates through the air from the transmitting sensor to the receiving sensor. In contrast, at an output voltage of 0.06Vpp with the same 22 millimetre separation, the signal fails to propagate purely through the air from the transmitting sensor to the receiving sensor.

The measurements conducted with the 3D-printed setup exhibit similar trends to those performed without the 3D-printed setup, both at 6Vpp and 0.06Vpp output voltages with a 22 millimetre separation. This consistency leads to the conclusion that, as long as the signal strength remains at an output voltage of 0.06Vpp and the sensors are positioned with a minimum separation of 22 millimetres, the wave propagation through the 3D-printed setup does not introduce significant noise to the received signal. These findings affirm the stability and reliability of the 3D-printed setup under the specified conditions.

3.5.3. Experiment 3: Influence of Air Bubble and Temperature Fluctuations

The objectives of this third experiment were to ascertain the effects of the air bubbles introduced to the sample during the loading procedure, and the effects of grease temperature fluctuations on the propagation of ultrasound through the grease sample. The attenuation and velocity results are presented in Figure 3.10

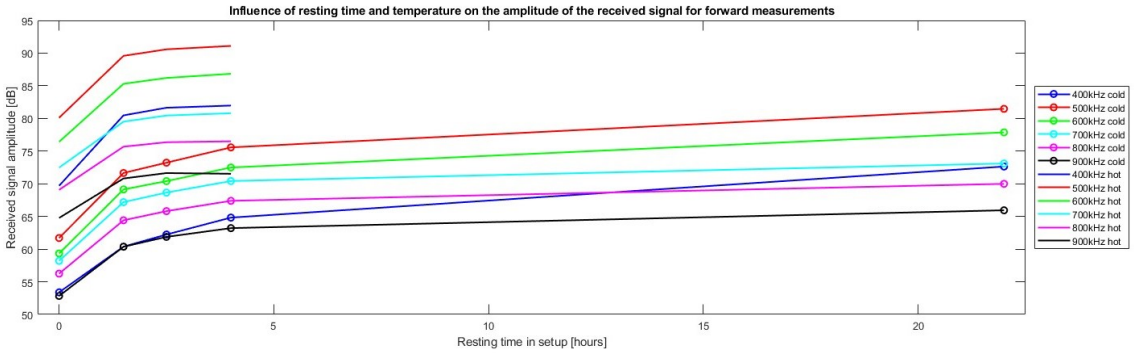

(a) Influence of dissipation time and temperature on the amplitude of the received signal for forward measurements

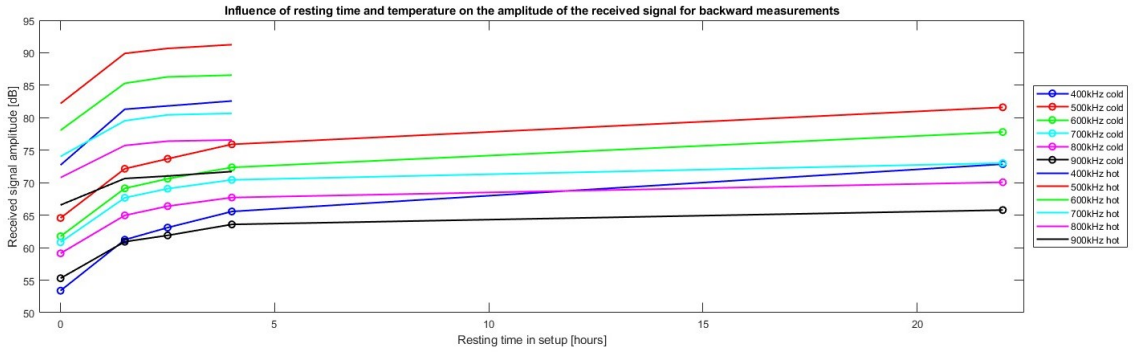

(b) Influence of dissipation time and temperature on the amplitude of the received signal for backward measurements

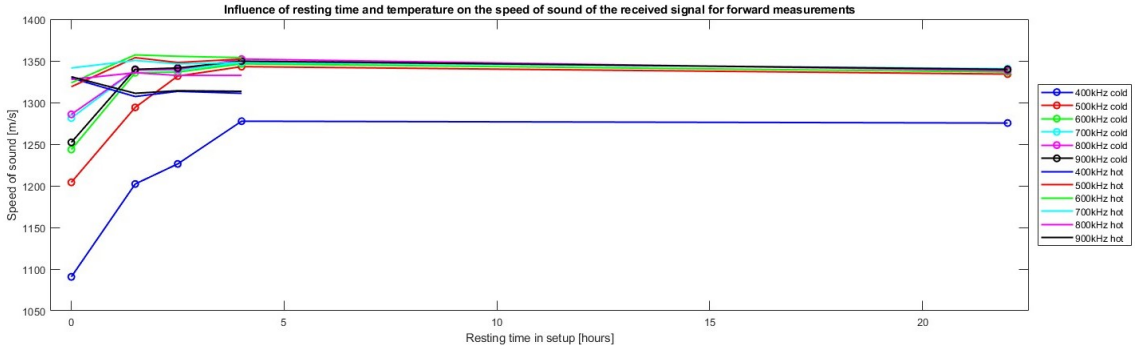

(c) Influence of dissipation time and temperature on the speed of sound of the received signal for forward measurements

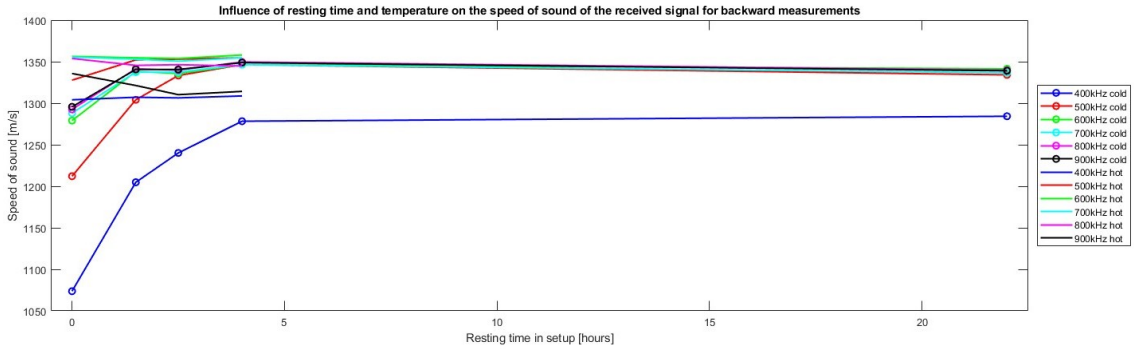

(d) Influence of dissipation time and temperature on the speed of sound of the received signal for backward measurements

Figure 3.10: The influence of dissipation time and temperature on the amplitude and speed of sound.

The attenuation results for the influence of dissipation time and temperature fluctuations have been plotted in Figure 3.10a (forward) and Figure 3.10b (backward). The speed of sound results for the influence of dissipation time and temperature influence have been plotted in Figure 3.10c (forward) and Figure 3.10d (backward). The first thing to note is that although all measurements were conducted

for frequencies ranging from 200kHz to 900kHz, the 200kHz and 300kHz results were omitted from these graphs due to the high contribution of noise on these signals, causing an indeterminable received signal.

Influence of Air Bubble Concentration Fluctuations

The presented amplitude measurements in Figure 3.10 show a clear increase in signal amplitude as the dissipation time of the grease sample within the grease setup increases, both for the cold and the warm grease samples. Although the strongest increase in amplitude can be observed during the first 1.5 hours of resting time, the trends suggest that none of the samples have reached a steady state with respect to air bubble dissipation within the studied time frame. It is noteworthy that regardless of the frequency or temperature, the amplitude levels seem to follow the same diminishing rate of increase. An exception to this is the 400kHz pulse in the cold grease sample, of which the amplitude undergoes a slightly stronger increase than the other frequencies. The increase in received signal amplitude is supposedly due to the dissipation of the air bubbles out of the grease sample over time. The increase in signal amplitude would signify a decrease in attenuation, and therefore in this case a decrease in boundaries caused by air bubbles. Additionally, the trend that the amplitude graph is following seems to indicate that eventually, a steady state received signal amplitude will be reached, meaning that almost all of the air must have dissipated out of the grease sample.

The presented speed of sound measurements in Figure 3.10 show an increasing speed of sound for the ultrasound signals with an increasing dissipation time. Again, the first 1.5 hours of dissipation time show the steepest increase. The results suggest, that over time, the speed of sound of the ultrasound signal settles towards a steady state value. The increase in speed of sound is supposedly due to the dissipation of the air bubbles out of the grease sample over time. The measured increase in speed of sound would signify an increase in the overall bulk speed of sound. Seeing as the speed of sound in air is much lower than that of grease, the presence of air bubbles would decrease the overall bulk speed of sound of the sample. Therefore the dissipation of the air bubbles would cause the bulk speed of sound to increase which is confirmed by these measurements.

Influence of Temperature Fluctuations

The presented amplitude measurements in Figure 3.10, clearly show an increase in signal amplitude, as the temperature of the grease sample is increased, for all measured frequencies and all measured dissipation time steps. What also can be observed from these graphs, is that the difference between the cold and the warm sample stays relatively constant for every frequency and every resting period up to 4.0 hours. It can however be observed that the warm samples seem to settle towards a steady state slightly faster than the cold samples do, because the line segments between 2 and 4 hours are a little more horizontal as opposed to the cold sample measurements. The increase in received signal amplitude is supposedly due to the increased grease particle energy caused by the increase in temperature. Because the grease particles have more energy, they take away less energy from the ultrasound wave through attenuation.

The presented speed of sound measurements in Figure 3.10 show a slightly increasing speed of sound for the ultrasound signals with an increasing temperature. From the graphs, it can be observed that most warm measurements result in a slightly higher speed of sound as compared to the cold measurements. This difference is however not very big, due to the fact that the applied temperature difference is not very big. The increase in speed of sound is supposedly caused by the fact that at higher temperatures, the density of a medium decreases due to the vibration of the particles of the medium. A lower density results in a higher speed of sound, based on Equation 2.3. This effect is confirmed by the conducted measurements.

The influences of air bubble concentration and temperature fluctuations, illustrated in this experiment, imply that ultrasound propagation is heavily influenced by these two phenomena. This means that for all of the future measurements, some procedure must be devised to ensure comparable measurement circumstances. This can be done in two ways. Either, all experiments that must be compared to one another must be conducted using similar air bubble concentrations and temperatures, or a method must be devised to account for the amplitude and speed of sound difference caused by these two influences.

3.5.4. Experiment 4: Influence of Contamination

The objective of this fourth experiment was to ascertain the influence of contamination on the attenuation and velocity of the ultrasound waves. Firstly, an experiment has been conducted to verify the scalability of the output voltage with retention of the amplitude of the received waveforms. Secondly, an experiment has been conducted in which various concentrations of tap water and iron particle contamination have been mixed into clean Mobilux EP2 grease samples. For this experiment, the findings of the air bubble and temperature fluctuations experiment have been adopted. Lastly, an experiment has been conducted to examine original linear bearing grease, originating from a bearing at 100% of its lifetime, and an attempt is made to estimate the contamination levels of this grease.

Scalability

In some cases, it was necessary to scale the transmitted output voltage to a higher level in order to receive signals that propagated through the sample. However, this demands some research into the scalability of this voltage and the effect of scaling this voltage on the amplitude of the received signals. A clean sample was investigated both using a 60mVpp and a 480mVpp output voltage. The waveforms that were received during the 480Vpp tests were scaled back by dividing their amplitudes by the scaling factor 8. After this, the output voltages were converted to dB, and these results can be observed in Table 3.3.

		Frequency [kHz]				
		500	600	700	800	900
60 mVpp	Forward	64.56	64.3	58.49	55.42	51.82
480 mVpp	Forward	64.56	64.23	58.46	55.44	52.1
60 mVpp	Backward	64.86	64.35	58.99	55.71	52.26
480 mVpp	Backward	64.89	64.38	58.86	55.76	52.39

Table 3.3: The corrected amplitudes in [dB] of two clean grease experiments with differing output voltages.

As can be observed from Table 3.3, only a very minimal difference between the amplitudes that have been recorded for the various responses can be distinguished. Firstly, the differences between the forward and the backward amplitude measurements can be neglected because these are due to the sensor irregularities. Secondly, the difference between the measured amplitudes ranges from 0dB to 0.28dB, with an average difference of 0.077dB. Additionally, the time-domain waveforms have an overall comparable shape, with the main difference being in the noise level. The 60mVpp pulsed signals have a higher background noise level with respect to the signal as compared to the 480mVpp signals. This can be observed in Figure 3.11.

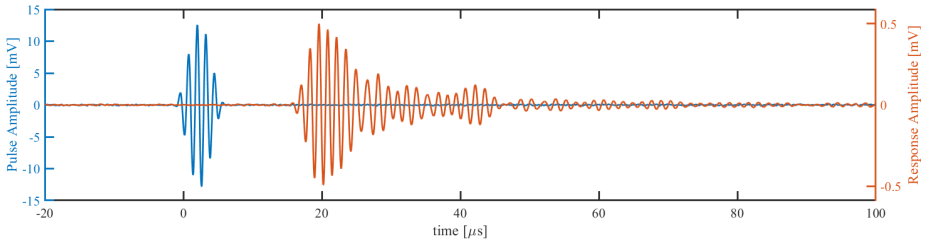

(a) 800kHz pulse and response, at 60mVpp, forward measurement.

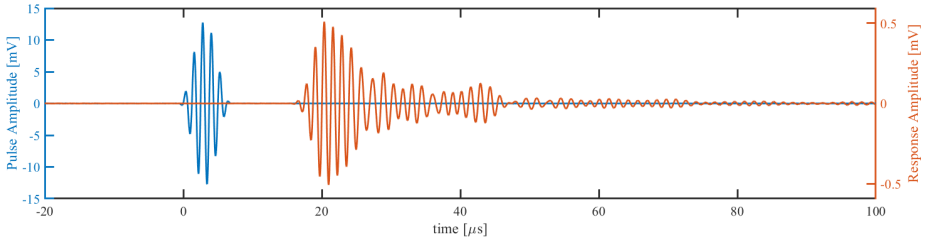

(b) 800kHz pulse and response, at 480mVpp and scaled back, forward measurement.

Figure 3.11: Similarities between a non-scaled pulse and response and a scaled pulse and response.

It is safe to say that using a higher output voltage for the transmitted signal, and afterwards scaling back the pulsed and received signal to correspond to the non-scaled level, has a negligible effect on the amplitude and the shape of the waveform. It is however important to note that pulsing with a stronger signal might have an effect on the propagation of the signal through the 3D setup, and the subsequent generation of noise, as was discussed in experiment 2.

Known Contamination

The influence of contamination on the propagation of ultrasound through the grease sample has been investigated using the attenuation spectroscopy as well as the velocity spectroscopy. The objective was to ascertain a trend in the change of amplitude of the received signal and in the change of speed of sound of the received signal as a function of the percentage of contamination. This has been done both for tap water contamination, as well as iron particle contamination, separately. Again, all frequencies have been tested, however, the 200kHz, 300kHz and 400kHz signals could not be resolved due to excessive noise, and were therefore omitted.

First, the experiments conducted with the tap water contamination samples have been presented. These can be observed in Figure 3.12. In Figure 3.12a and Figure 3.12b, it can clearly be observed that the amplitude of the received signal undergoes a decrease due to an increase in tap water concentration. Additionally, it can be observed that the trend of the amplitude drop graph seems to settle towards a steady state. Moreover, it can be observed that this trend is consistent for all of the studied frequencies, as well as for the forward and backward measurements. Lastly, it can be observed that the most severe drop in received signal amplitude presents itself in the first percentile of contamination concentration. This amplitude drop is presumably caused by the increase in attenuation phenomena that are introduced to the grease sample by the increase of tap water contamination. An increase in tap water contamination concentration seems to increase the amount of signal attenuation in the grease sample, causing the amplitude drop between the clean baseline measurement and the contamination measurement to increase.

In Figure 3.12c and Figure 3.12d, it can clearly be observed that the speed of sound of the received signal undergoes a decrease due to an increase in tap water concentration. Similar to the amplitude drop graph, the speed of sound drop graph also seems to settle towards a steady state. Again, it can be observed that the presented trends are consistent for the various frequencies, as well as the forward and backward measurements. And lastly, the most severe drop in speed of sound can be observed in the first percentile of tap water contamination concentration. The decrease of speed of sound due to the increase of tap water contamination is supposedly due to the fact that tap water has a higher density than grease. The increase in density due to the increase in tap water concentration causes a decrease in bulk speed of sound according to Equation 2.3.

It has been noted that the most severe drops in amplitude and speed of sound are located within the first percentile of contamination concentration. In offshore bearing condition monitoring, this first percentile is the most important one. After one percent of grease contamination, the grease will most likely be flushed and replaced. Because of this, the fact that this ultrasonic method shows the highest sensitivity to this first percentile, shows great promise for the implementation of this method in offshore applications. However, although these results already look promising for the detection of tap water contamination in grease samples, it must be said that these experiments were conducted after a dissipation time of 1.5 hours. According to the results presented in subsection 3.5.3, a longer dissipation time would remove more of the air bubbles, and would potentially increase the measured difference between a clean baseline sample and a contaminated sample.

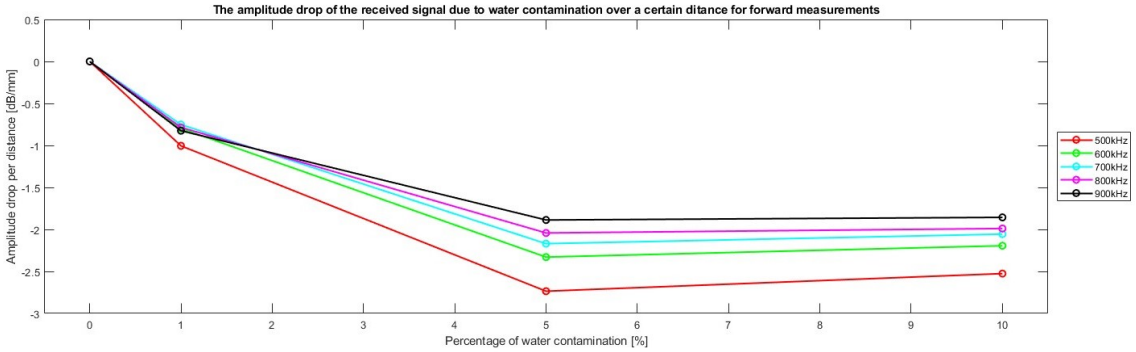

(a) Amplitude drop of the received signal due to water contamination over a certain distance (forward).

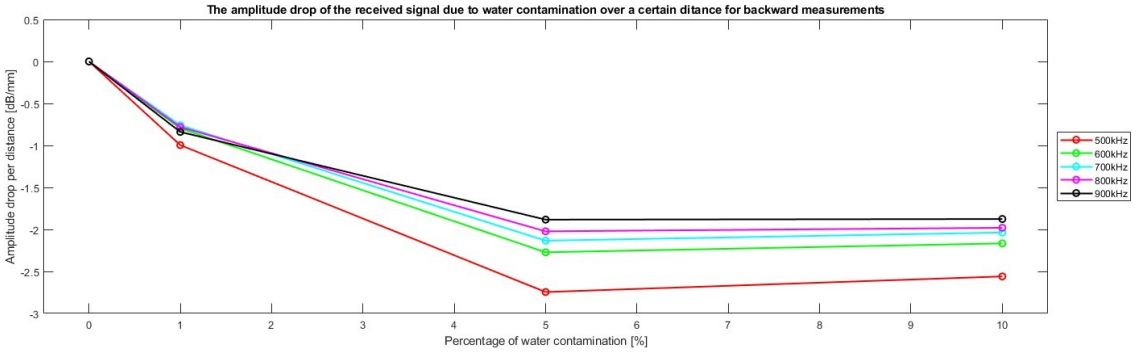

(b) Amplitude drop of the received signal due to water contamination over a certain distance (backwarc).

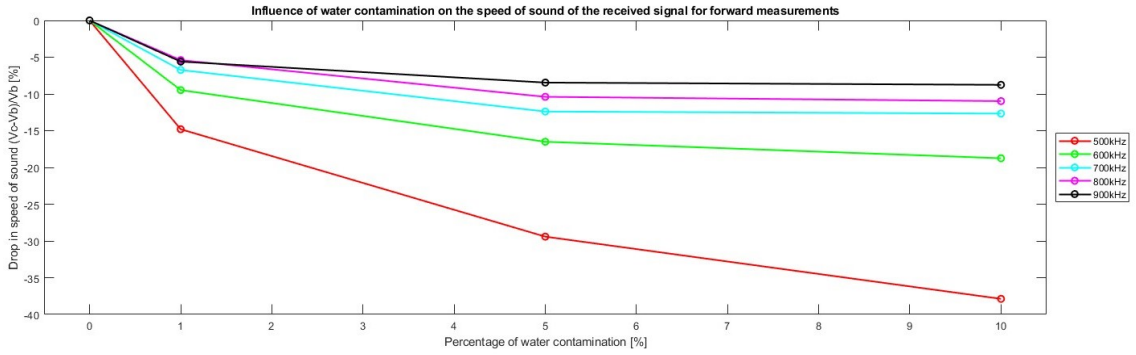

(c) Speed of sound drop of the received signal due to water contamination over a certain distance (forward).

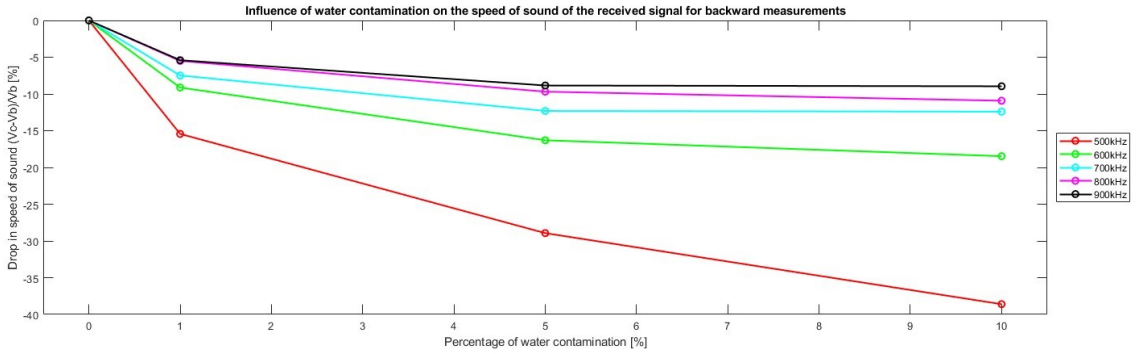

(d) Speed of sound drop of the received signal due to water contamination over a certain distance (backward).

Figure 3.12: Influence of water contamination on signal amplitude and speed of sound.

Second, the results of the experiment with the iron particle contamination has been presented. These can be observed in Figure 3.13. In Figure 3.13a and Figure 3.13b, it can be clearly observed that the amplitude of the received signal undergoes a decrease due to an increase in iron particle contamination concentration. Additionally, it can be observed that the trend of the amplitude drop graph seems to settle towards a steady state. Moreover, it can be observed that this trend is consistent for all of the studied frequencies, as well as for the forward and backward measurements. Next, it can be observed that the most severe drop in received signal amplitude presents itself in the first percentile of contamination concentration. Lastly, it can be observed that the at 10% iron particle contamination, the amplitude drop seems to be a little less than at 5%.

The initial amplitude drop is presumably caused by the increase of attenuation phenomena that are introduced into the grease sample by the increase of iron particle contamination. An increase in iron particle contamination seems to increase the amount of signal attenuation in the grease sample, subsequently causing the amplitude drop between the clean baseline measurement and the contamination measurement to increase. The final decrease in amplitude drop at 10% can be caused by two things. The first explanation is that when more metal particles get into the grease sample, these particles might clump together to form somewhat larger 'particles'. Recall that scattering happens when the particle size in a medium is much smaller than the wavelength of the ultrasound wave. An increase in particle size would therefore cause the particle size to be closer to the wavelength of the wave than before. This would in turn mean that some scattering attenuation changes to diffraction attenuation. Also recall that diffraction does not consume wave energy, whereas scattering does, resulting in a larger portion of the wave energy propagation through the contaminated grease. Another explanation could simply be the loading procedure that has been followed in these experiments. Every contamination level presented in Figure 3.13 is the result of one single loading procedure. This means that the data points for a single contamination percentage are the result of measurements conducted on a sample that has been loaded into the setup once. Because the upwards trend for the 10% sample seems to be universal, except for the 500kHz sample, it could simply be the result of a loading error and therefore more air bubbles in the sample.

In Figure 3.13c and Figure 3.13d, it can clearly be observed that the speed of sound of the received signal undergoes a decrease due to an increase in iron particle concentration. Similar to the amplitude drop graph, the speed of sound drop graph also seems to settle towards a steady state. Again, it can be observed that the presented trends are consistent for the various frequencies, as well as the forward and backward measurements. And lastly, the most severe drop in speed of sound can be observed in the first percentile of iron particle contamination concentration. The speed of sound drop is presumably caused by the lengthening of the wave path due to the increase of scattering attenuation. When more small particles are introduced into a grease sample, more scattering attenuation occurs. This forces the ultrasound wave to propagate through the grease not in a straight line and thus lengthening the wave path and therefore the time it takes to travel the 22mm between the transmitting and receiving sensor.

Again, the fact that the most severe amplitude and speed of sound drop can be observed in the first percentile of contamination concentration means that this technique shows promise to be applied in offshore bearings. But again, improving the dissipation time of the measurements might improve the results even more. Moreover, a comparison of its performance for water contamination and iron particle contamination, as shown in Figure 3.14, shows that it is very difficult to differentiate between tap water contamination and iron particle contamination, in the first percentile of contamination. This can be concluded from the fact that for every frequency, the first line-elements in these graphs are almost parallel for water and iron contamination.

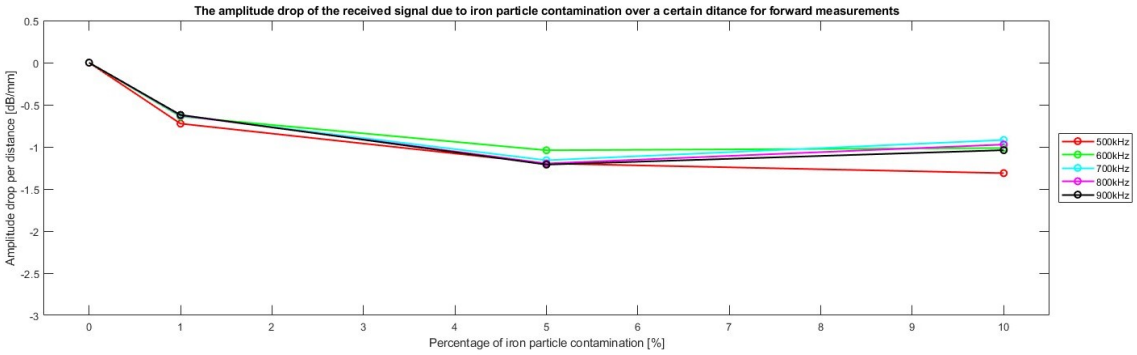

(a) Amplitude drop of the received signal due to iron contamination over a certain distance (forward).

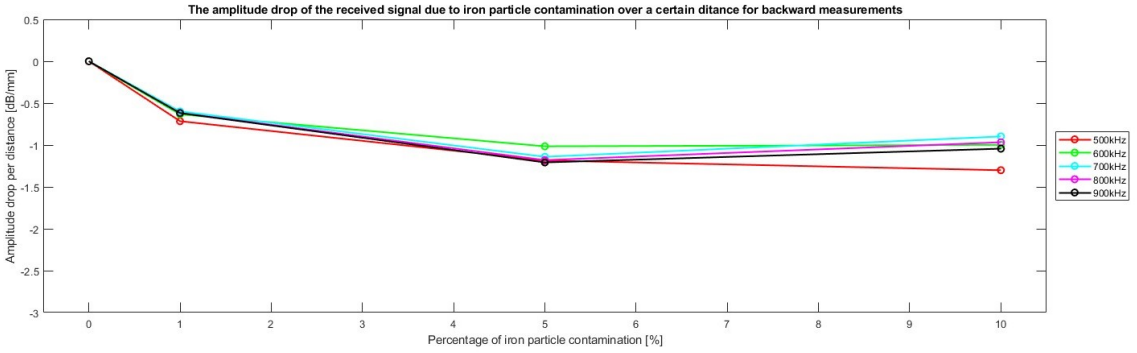

(b) Amplitude drop of the received signal due to iron contamination over a certain distance (backward).

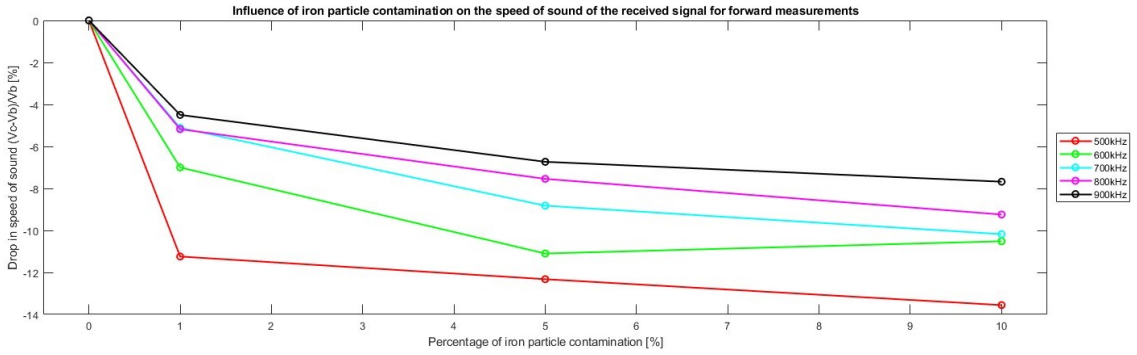

(c) Speed of sound drop of the received signal due to iron contamination over a certain distance (forward).

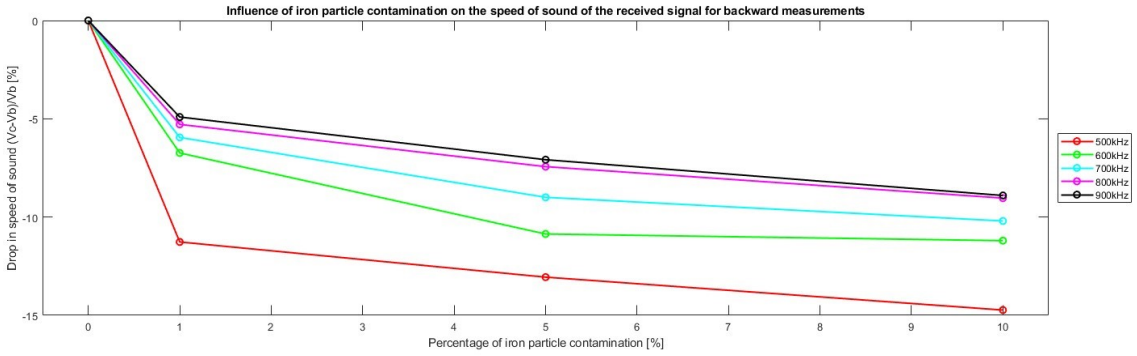

(d) Speed of sound drop of the received signal due to iron contamination over a certain distance (backward).

Figure 3.13: Influence of iron particle contamination on signal amplitude and speed of sound.

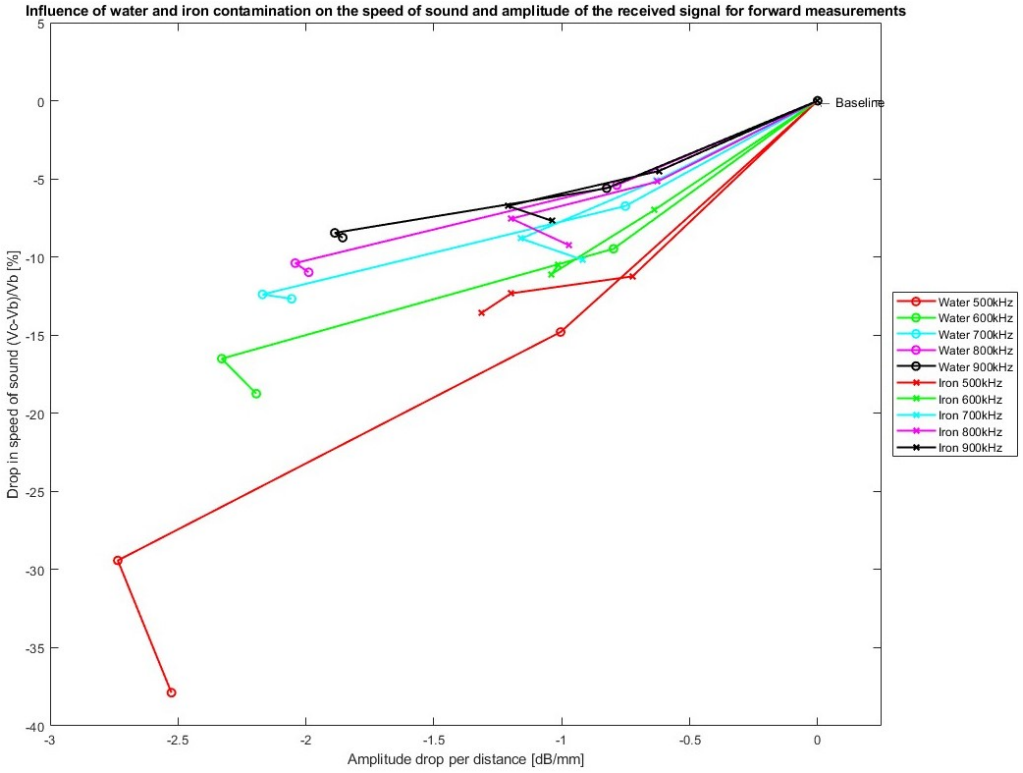

(a) Amplitude drop vs. speed of sound drop (forward)

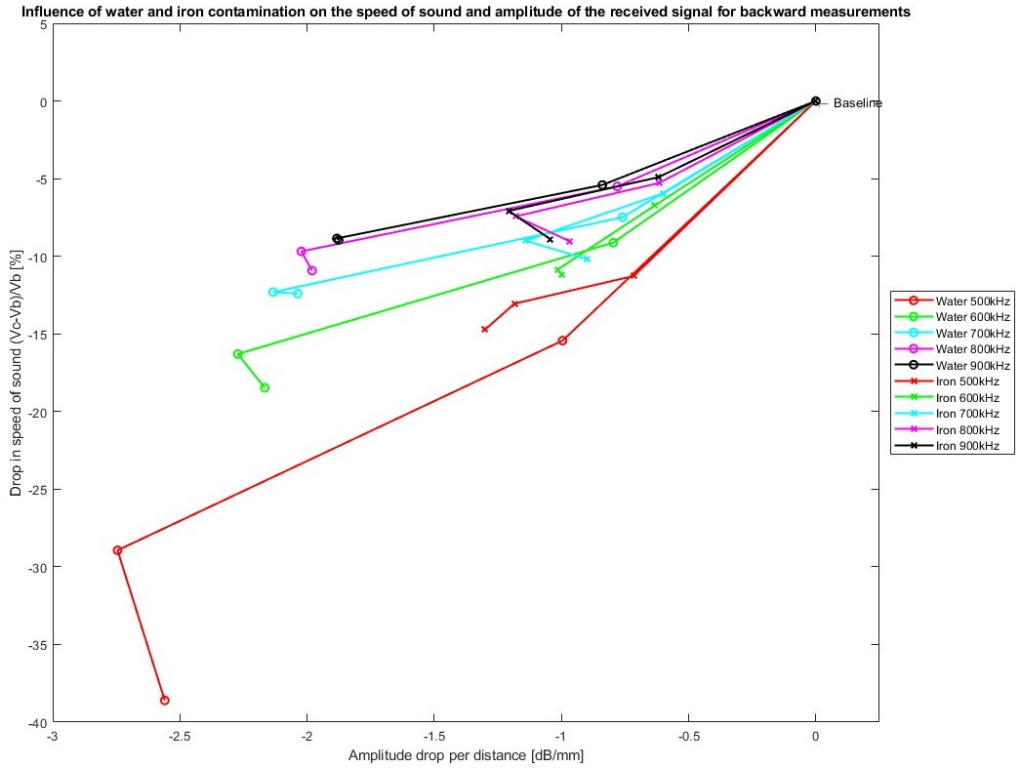

(b) Amplitude drop vs. speed of sound drop (backward)

Figure 3.14: Amplitude drop vs. speed of sound drop for water and iron particle contamination.

Unknown Contamination

In this last experiment, an attempt was made to compare the amplitude and the speed of sound of ultrasound through three different mediums, two types of clean grease and one type of contaminated grease with unknown contamination levels. Unfortunately, these measurements were conducted before experiments 3 and 4 had been conducted, and because of that, no considerable effort had gone into maintaining constant temperature or loading procedure. Due to time constraints on the course of this thesis, a repetition of these measurements was not possible.

The results of the measurements have been presented in Table 3.4 and Table 3.5. When looking at the signal amplitudes, it can be noted that the amplitudes of the contaminated sample are in most cases lower than the amplitudes of the uncontaminated samples. When looking at the arrival times, however, something peculiar can be noted. The measured arrival times for the contaminated samples seem to be shorter than the clean samples.

The previously presented results, might be caused due to the fact that the temperature and the loading procedure were not kept strictly constant for these measurements. Unfortunately, no useful conclusions can therefore be drawn from these measurements, and a repetition of these experiments is warranted, this time accounting for the effects deduced in experiment 3.

		Frequency [kHz]							
		200	300	400	500	600	700	800	900
Shell Gadus S2 V220 2	Forward	78.55	74.42	84.76	93.46	88.67	84.06	80.02	75.88
	Backward	78.36	75.45	85.33	93.8	88.78	84.34	80.74	75.82
Mobilux EP2 Clean	Forward	77.22	76.44	79.22	92.54	88.94	85.78	82.67	77.84
	Backward	78.01	77.29	80.41	93.12	89.32	86.29	83.14	78.11
Mobilux EP2 Contaminated	Forward	69.63	71.22	77.37	88.34	85.23	80.69	78.3	74.2
	Backward	74.12	75.46	81.53	90.93	87.55	82.68	80.03	75.64

Table 3.4: amplitudes of the received signals for various mediums, pulsed at 60mVpp.

		Frequency [kHz]							
		200	300	400	500	600	700	800	900
Shell Gadus S2 V220 2	Forward	22.53	20.86	16.6	16.45	16.49	16.52	16.96	17.02
	Backward	22.37	20.06	16.4	16.33	16.37	16.37	16.71	16.92
Mobilux EP2 Clean	Forward	22.61	19.08	16.9	16.32	16.32	16.36	16.5	16.87
	Backward	22.25	19.03	16.46	16.31	16.33	16.38	16.39	16.9
Mobilux EP2 Contaminated	Forward	24.15	18.92	16.31	16.12	16.12	16.1	16.17	16.58
	Backward	20.93	17.38	16.08	16.11	16.11	16.15	16.13	16.17

Table 3.5: Arrival time of the received signals for various mediums, pulsed at 60mVpp.

3.6. Conclusions and Recommendations

The results of the laboratory experiments, presented in the previous section, provide the basis for a number of insights on which the development of the in-line ultrasound condition monitoring setup can be continued. In this section, we consolidate the key outcomes derived from the laboratory experiments and offer actionable recommendations based on these findings. By revisiting the research objectives and reflecting on the data collected, the aim is to draw meaningful conclusions that contribute to the understanding of the research problem and its implications. Additionally, practical recommendations for future research directions and potential applications have been provided, with the goal of informing decision-making and guiding further scientific inquiry in this field.

During these laboratory experiments, a couple of factors have been investigated. These are the influence of the distance between the sensors, the noise introduced through the test-setup material, the air bubble concentration fluctuations, the temperature fluctuations, the scalability of the output voltage, and influences of tap water contamination and iron particle contamination.

From the results of the distance experiments, it can be concluded that when pulsing at an output voltage of 6Vpp, the maximum output voltage of the waveform generator, the distance between the transmitting and receiving sensors should definitely be shorter than 100 millimetres. The findings indicate that shorter transmission distances are more effective. Clipping should be taken into account when minimizing the propagation distance between the sensors, but seeing as the output voltage can always be adjusted to a lower value, a short distance should not pose a problem. Moreover, the signal-to-noise ratio should be taken into account when minimizing the distance, because noise from the surroundings does not diminish in amplitude. Therefore, when minimizing the distance, and lowering the value of the output voltage, a careful examination of the noise is warranted.

From the presented results, it seems plausible to exclude waveform propagation through the 3D-printed setup when the output voltage of the transmitted pulse is set to 60mVpp. The material of the setup does not seem to influence the waveform propagation, which means that the possible noise introduced to the received signal through the 3D-printed material is negligible. When the need arises to pulse at a higher output voltage, a new examination of this phenomenon must however be conducted. Additionally, any new grease setup should be evaluated with respect to signal propagation through its material in order to exclude these effects from the received signals.

The effect of air bubble concentration fluctuations has been studied, and the presented results suggest that both the amplitude of the received signal, as well as the speed of sound of the received signal improve when implementing a longer resting time. Resting time, provides the possibility for air bubbles to dissipate out of the grease sample, improving the overall propagation of the ultrasound through the grease. For future work, as well as for the inline setup, it might be interesting to examine ways to speed up this dissipation process. This could for example be done with the help of a vibrating table, however, an effort should be made to investigate the effect of a vibrating table on the mix of grease and contamination. That is to say, if a vibration table causes the mix of grease, particles, and water to separate, it might have wanted or unwanted implications for the ultrasound measurements.

The effect of temperature fluctuations, meaning the temperature of the room and subsequently the temperature of the sample, has been studied, and the presented results suggest that both the amplitude of the received signal, as well as the speed of sound of the received signal improve when implementing a higher sample temperature. For future work, as well as for the inline setup, measurements that have to be compared to one another on the basis of attenuation or speed of sound, should be conducted at the same temperature. Sufficient temperature control is necessary to ensure comparable and reproducible results.

Using a higher output voltage does not seem to pose any scalability problems. Based on the presented results, a 60mVpp pulse yields a sufficiently similar response as a scaled back 480mVpp pulse. There is even something to say for the fact that when using a higher output voltage, and subsequently scaling the received signal back to represent the original output voltage, the noise is also scaled back, resulting in a better signal-to-noise ratio for the received signal. However, as was said before, it should

be kept in mind that pulsing at a stronger output voltage might introduce unwanted noise and vibrations through the test setup as opposed to through the grease.

The tap water contamination measurements reveal distinct trends in amplitude drop and speed of sound drop. Both the amplitude and the speed of sound, show a clear drop with an increase of tap water contamination concentration. The amplitude drop is presumably caused by the increase in attenuation phenomena due to the increase in water contamination. The speed of sound drop is presumably caused by the increase in density of the bulk. The biggest drop can be observed in the first percentile of contamination. For future work, longer dissipation times and improved temperature control are recommended for enhanced measurements.

The iron particle contamination analysis reveals consistent trends in received signal amplitude and speed of sound. The amplitude drop is presumably caused by the in-crease in attenuation phenomena due to the increase of iron particle contamination. The speed of sound drop is presumably caused by the lengthening of the wave path due to the increase of scattering attenuation. Initially, signal amplitude decreases with rising contamination concentration, but a slight increase is observed between 5% and 10%. This anomaly may be attributed to iron particle clumping, leading to changes in attenuation mechanisms from scattering to diffraction. Another plausible explanation could be variations in the loading procedure, potentially introducing more air bubbles in the sample. It's noteworthy that each contamination level represents a single loading procedure, implying that data points for a specific contamination percentage are derived from measurements on a single loaded sample. Thus, the observed upward trend in the 10% sample may be influenced by loading errors. For future work, it might be valuable to repeat the loading procedure and subsequent measurements multiple times with the same contamination level, to see if repeatability exists within these results. Additionally, longer resting times and improved temperature control can also improve these measurements.

The results of the attenuation spectroscopy and the velocity spectroscopy for the tap water contamination experiments and the iron particle contamination experiments have been compared with the aim of trying to differentiate between these two different types of contamination. Unfortunately, it is difficult to differentiate between the two contamination types. To overcome this hurdle, it is proposed for further research to investigate the time and frequency domain information of the measured data, to see if the type of contamination has an effect on the waveform itself, as opposed to its amplitude and velocity properties.

Results of the unknown contamination experiments indicate lower signal amplitudes for contaminated samples compared to uncontaminated ones. However, arrival times for contaminated samples appear shorter, suggesting potential inconsistencies due to temperature and loading procedure variations. Consequently, meaningful conclusions cannot be drawn from the unknown contamination results, warranting a repeat of this particular experiment while implementing a longer resting time and improved temperature control for all samples. Additionally, valuable insights could be drawn from determining the actual contamination levels through grease sampling. These results can then be compared to the unknown contamination results from the ultrasound spectroscopy method, providing valuable insights into its efficacy.

To conclude, the active ultrasound spectroscopy methods pursued and investigated in this chapter pose a viable option for the detection of tap water contamination and iron particle contamination in offshore bearing grease samples. The ultrasound waves show the highest sensitivity to the first percentile of contamination concentration. This one percent is also the threshold value that is used in most offshore applications to signify that a flush of the bearing grease is warranted. On the other hand, more research must be invested in the pursuit of differentiating between the various types of contamination in offshore bearing grease.

4

In-line Grease Monitoring Setup

This chapter delves into the process of conceptualizing, designing, and testing an in-line grease monitoring setup for offshore bearings. The emphasis lies on outlining the design of the setup and its integration into operational bearings. The purpose and hypotheses guiding this setup and subsequent experimentation are discussed, along with detailed examination of design intricacies for both the in-line setup and the experimental setup with the operational bearing. Additionally, the materials, equipment, and methodology employed in conducting this experiment are highlighted, followed by a thorough analysis of results. The last section delves into the drawn conclusions, and recommendations are proposed for future endeavours.

4.1. Purpose and Hypotheses

The main purpose of designing an in-line grease monitoring setup is to facilitate the demand for new, in-line condition monitoring methods. The workings of ultrasound spectroscopy have been evaluated and illustrated in the previous chapter, demonstrating the possibility of a bearing grease condition monitoring setup driven by ultrasound spectroscopy. The purpose of experimenting with such an in-line grease condition monitoring setup for offshore bearings, is to get an understanding of the various obstacles in the implementation of a new method to an already existing product. Based on review of the relevant literature, as well as the findings of chapter 3, it is expected that the implementation of an in-line grease monitoring setup needs to overcome the following obstacles:

1. *Spatial constraints:* the condition monitoring setup shall be placed on an operational bearing. Great care must be taken to ensure that the monitoring setup does not impact or influence the operation of this bearing, or of the surrounding components. Additional spatial constraints are imposed by the dimensions of the peripheral equipment, such as the sensors, waveform generator, and data acquisition system. It is expected that the setup can be implemented in the already exiting grease ports. By keeping the in-line setup as small as possible, it might be possible to occupy the same amount of space as the lubrication system is doing now.
2. *Location on bearing:* the placement of the condition monitoring setup on a specific location on the bearing has its implications for the measured grease contamination. Initially, the experiments are conducted with one set of in-line condition monitoring equipment, but it is expected that by placing multiple setups on a bearing, an improved bearing failure localisation can be realised, comparable to that of the existing grease sampling method, but faster.
3. *Flowability of grease:* bearing grease is in itself not a free flowing fluid, and therefore the flowability of the grease within the bearing and into the condition monitoring setup needs to be evaluated. It is expected that motion of the bearing exerts a pressure on the grease, causing it to flow freely into the in-line condition monitoring setup.
4. *Surrounding noise:* an operational, offshore bearing is often applied in locations with a lot of noise. These noise sources can either originate in surrounding components, or in the bearing itself. The impact of this noise on the recorded signals must be evaluated. It is expected that by implementing the right thresholds and filters, this noise can be sufficiently counteracted.

4.2. Design of In-Line Monitoring Setup

The envisioned design of the in-line monitoring setup has to have six components to facilitate in-line grease monitoring. Firstly, it needs to be possible to connect the setup to the operational bearing. Secondly, there should be an inlet to allow the grease to flow into the setup. Thirdly, the setup should have a compartment where the grease can flow into in order to be examined. Fourthly, there should be positions for the sensors to be located and secured. Fifthly, there should be an outlet, to let the grease drain out of the setup, and lastly, there should be an air outlet to let the air that is initially in the setup escape. Additional to the above-mentioned demands, the in-line setup should also overcome the first and third obstacle listed in the previous section.

As a starting point for this design, the test setup from the laboratory experiments, shown in Figure 3.9a, was taken. The screw caps used to secure the sensors at 22 millimetres apart were a great success, and therefore a similar, plus-shaped structure was used for the body of the in-line setup. Implementing the plus-shaped design would however take too much space in the horizontal direction next to the bearing. Therefore, a 90°angle was placed on one of the open ends of the plus-shape. At the end of this bend, a hollow thread was designed, with the same thread as the grease nipples inside the bearing. By doing so, the plus-shape is now positioned vertically along the bearing wall instead of horizontally, minimizing the occupied space. Additionally, the hollow thread also facilitates a way for the grease to enter the in-line setup. The open bottom end was altered to fit yet another screw cap onto, which can function as the grease outlet. Lastly, a hole was positioned in the side of the 90°bend, through which the air can escape out of the setup. Additionally, a pin was designed with the aim of closing up this hole once the grease setup was fully filled. An overview of the designed in-line setup can be found in Figure 4.1. Due to its shape and its application, this in-line monitoring setup was named the Grease Eagle, or Greagle.

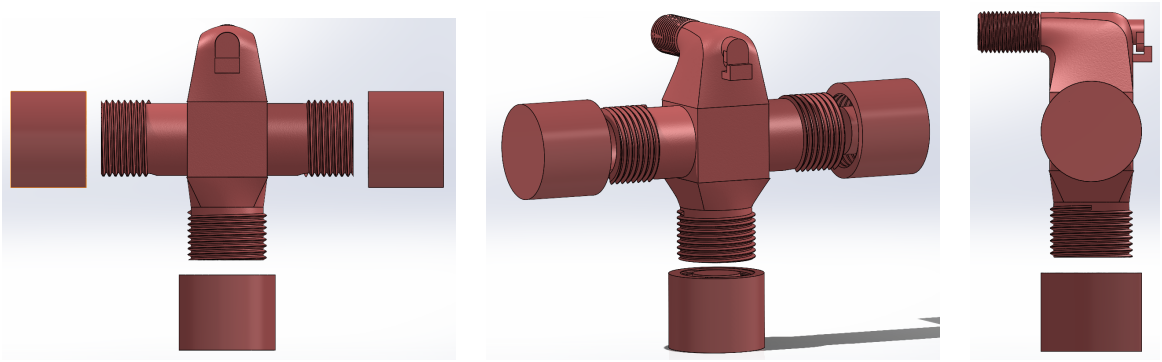

Figure 4.1: Design of the in-line condition monitoring setup: the Greagle.

4.3. Design of Experimental Setup

Throughout the experimental implementation of the in-line grease condition monitoring setup to the bearing, the aim was to determine whether the grease would flow into the in-line setup, and whether it would be possible to filter out possible surrounding noise. In order to do so, the in-line monitoring setup is connected to the Huisman linear bearing inside the Huisman TriboIII test setup. This test setup is specifically designed to test linear bearings under a load while moving.

The in-line monitoring setup is screwed into one of the existing grease ports of the bearing using its hollow threaded inlet. A waveform generator is employed to generate the desired waveform. This waveform is then sent both through a power amplifier to the transmitting sensor, and directly to the Data Acquisition System (DAQ). The transmitting sensor converts the electrical signal to an ultrasound waveform, which propagates through the grease sample and is captured by the receiving sensor. The receiving sensor converts the received ultrasound waveform back into an electrical signal, which is sent through a pre-amplifier to the DAQ. The DAQ converts the electrical signal into a format suitable for processing using specific software. All the collected data is then stored on a laptop, where it can undergo processing. The processed data can be interpreted to give insights into the condition of the

grease and, consequently, the condition of the bearing. An illustration of the experimental setup can be found in Figure 4.2.

In order to get an idea of the grease flowing into the in-line setup, as well as an idea of the noise over a period of time, it is necessary to conduct this experiment in one go. Because of that, it is not possible to transmit various frequencies and a single frequency must be selected. Based on its relatively stable results in chapter 3, a 800kHz pulse of 6 periods was selected for this experiment. This pulse was transmitted every second for a period of 6 minutes.

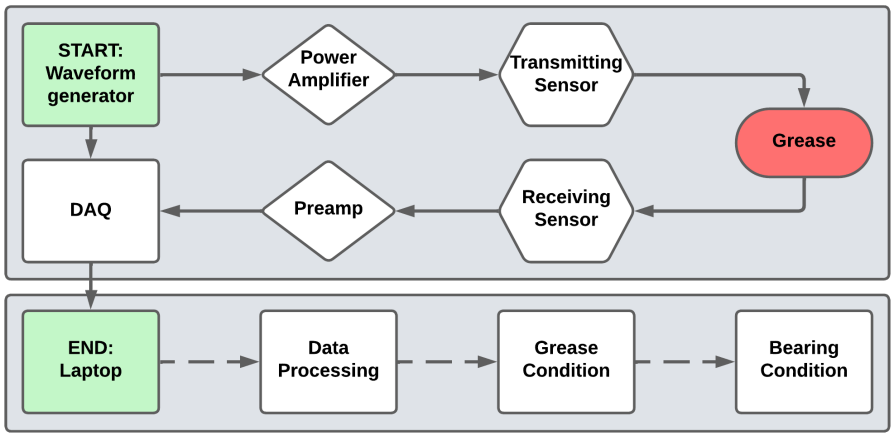

Figure 4.2: Design of the experimental setup used for the in-line experiment.

4.4. Materials and Equipment

In this section, a comprehensive overview of all the materials and equipment used in conducting this in-line experiment has been provided. It serves to shed light on the resources necessary for the accurate data collection and analysis. It also serves to facilitate a list of the necessary resources for the reproducibility of the experimental results.

4.4.1. Materials

For this experiment, the extracted sample of grease that has flowed into the test setup is Mobilux EP2, with unknown levels of contamination. This is due to the fact that during the collection of this grease inside the in-line setup, new grease and old grease have mixed. This was by design, and seeing as the objective of this experiment is to ascertain the flowability of the grease, possible levels of contamination do not pose a problem.

4.4.2. Equipment

An overview of all the equipment used to execute the various laboratory experiments has been provided below. An extensive overview of the various available sensors can be found in Appendix B. An overview of the equipment setup is depicted in Figure 4.3.

Electrical Components

- *Waveform generator:* RS PRO RSDG 1032X 30MHz 150MSa/s [62].
- *Data Acquisition System:* Vallen Systeme AMSY-6 [63].
- *Laptop:* any laptop with Vallen Acquisition, Vallen VisualAE and MATLAB installed.

Amplification Components

- *Power Amplifier:* Falco Systems WMA-300 [64].
- *Pre-Amplifier:* Vallen Systeme AEP5H - 40dB [65].

Ultrasonic Sensors

- *Transmitting Sensor:* Mistras WSα Sensor, frequency range: 100kHz to 1MHz [66].
- *Receiving Sensor:* Mistras WSα Sensor, frequency range: 100kHz to 1MHz [66].

Cables

- *BNC to BNC:* RG58C/U Coaxial Cable
- *BNC to SMA:* RG316 Coaxial Cable
- *BNC to BNC splitter:* RS PRO Tee, three-way splitter

Physical Grease Setup

The physical in-line grease condition monitoring setup as discussed in section 4.2 was used to contain the sensors and the grease sample.

Figure 4.3: The equipment setup used in the in-line condition monitoring experiment.

4.5. Methodology of Experiment

In this section, the comprehensive methodology employed to conduct the in-line experiment is presented. A detailed step-by-step procedure is delineated, illustrating the sequential stages undertaken during the experimental phase.

Preparation Stage 1: Preparing the Test Setup

1. Place the Mistras WSα sensors within the in-line test setup.
2. Screw the in-line test setup into the available grease port.
3. Connect the RS PRO splitter to the input of the Falco Systems power amplifier.
4. Connect the output of the RS PRO waveform generator to one open end of the RS PRO splitter using a RG58C/U coaxial cable.
5. Connect the other end of the RS PRO splitter to channel 2 of the AMSY-6 DAQ using a RG58C/U coaxial cable.
6. Connect the output of the Falco Systems power amplifier to the transmitting WSα sensor using a RG316 coaxial cable.
7. Connect the receiving WSα sensor to the AEP5H pre-amplifier using a RG316 coaxial cable.
8. Connect the AEP5H pre-amplifier to channel 1 of the AMSY-6 DAQ using a RG58 coaxial cable.
9. Make sure all the cables are out of the moving path of the various moving components of the TriboIII test setup.

Preparation Stage 2: Setting Equipment Settings

1. In Vallen Acquisition, set the threshold on the transmitted signal to 70dB.
2. In Vallen Acquisition, set the threshold on the received signal to 35dB.
3. In Vallen Acquisition, apply a bypass filter to the transmitting channel.
4. In Vallen Acquisition, apply a 520kHz-960kHz filter to the receiving channel.

5. In the waveform generator, specify the peak-to-peak voltage at 60mVpp.
6. In the waveform generator, specify the desired burst period at 1.0s.

Signal Detection Stage 1: Continuous Pulsing

1. Using the waveform generator, generate an 800kHz pulse with 6 periods (np=6).
2. Transmit this burst continuously.

4.6. Results and Discussion

In conducting this experiment, crucial aspects were to ascertain data on the flowability of the grease when implementing the in-line grease setup, and data on the noise levels in and around an operational bearing. In order to gain these insights, a continuous 800kHz pulse was transmitted and the corresponding received signal and the noise were recorded. The results of these measurements are presented in Figure 4.4.

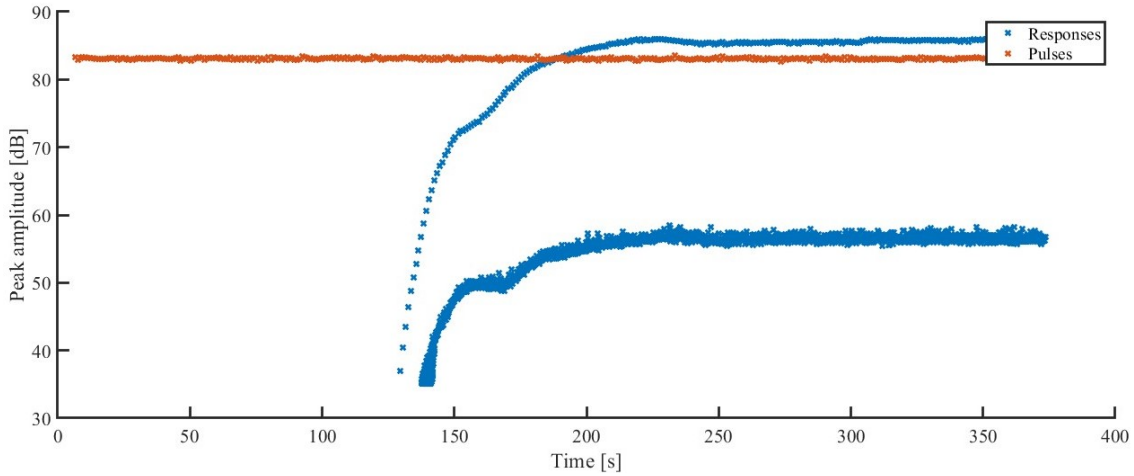

Figure 4.4: Results of the in-line condition monitoring experiment.

In this graph, the orange dots represent the continuous 800kHz transmitted signal. The blue dots represent the recorded signals. In this graph, a clear distinction can be made between the recorded response, which is the upper blue band of dots, and the recorded noise, which is the lower blue band of dots. Additionally, a clear diminishing increase in recorded signals can be observed, which ends in a steady state response.

Firstly, it is necessary to evaluate the flowability of the grease. The gradual increase in signal propagation can be interpreted as an increase of the amount of grease inside the in-line setup. Over time, the in-line setup seems to fill itself up. The settling of the amplitude of the response, on the other hand, can be interpreted as a sign that the in-line grease setup has been filled. Secondly, the noise levels can be evaluated. As can be seen from the graph, the amplitude of the surrounding noise is settling at a much lower value than the amplitude of the received signal. Because of this, the surrounding noise can easily be filtered from the readings by implementing a higher threshold on the received signals.

4.7. Conclusions and Recommendations

The results of the in-line experiment, presented in the previous section, provide the basis for a number of insights on which the development of an overall condition monitoring strategy can be continued. In this section, the key conclusions of the in-line experiment have been presented and recommendations based on these findings shall be offered.

From the presented results, it can be concluded that for this specific case, the problems posed by the spatial constraints, the flowability of the grease and the surrounding noise have been negated.

The obstacle of location on the bearing has not been further researched, but it is assumed that an overall condition monitoring setup can be implemented on every single grease port in the bearing. This means that this method at least has the same coverage as the nowadays implemented grease sampling method, only the developed in-line ultrasound setup would provide earlier results.

The spatial constraints imposed on the design by the bearing arrangement and the surrounding equipment might differ for every situation and therefore, it is recommended to evaluate the spatial applicability of this setup per situation. If other spatial constraints exits, adaptations can be made to the design of the in-line setup without altering its basic working principles. However, as the in-line grease monitoring setup does not take up more space than the lubrication system that is already present in most offshore bearings, it is expected that this will not be a problem.

The flowability of the grease does not seem to be a problem, since the results clearly show that the in-line grease setup is being filled with grease. This can also be observed from Figure 4.3, the left bottom picture, where the in-line grease monitoring setup is clearly overflowing. It is however recommended to develop a more efficient grease outlet.

The surrounding noise does not seem to be a problem because it is clearly distinguishable from the recorded signals. Because of that, this noise can easily be removed by increasing the threshold of the received signal. Additionally, it would be possible to insulate the outside of the in-line grease monitoring setup with some sort of sound insulation, in order to ward off some recorded noise.

Last but not least, the influences studied in Chapter 3 must be accounted for. Because this in-line grease monitoring setup does not obstruct the regular bearing operations, it is possible to fill the grease monitoring setup, and leave it alone for a certain amount of hours. By doing so, the air bubbles get the chance to dissipate out of the grease sample. The temperature fluctuations of an offshore environment on the other hand might pose a bigger problem. Most bearing applications are not suitable for a heating element, and therefore other ways of dealing with these fluctuations must be devised. This shall be addressed in Chapter 5.

5

Overall Condition Monitoring Strategy

In this chapter, an analysis of the performance of the in-line ultrasonic grease condition monitoring setup, as designed throughout chapter 3 and chapter 4, is provided. This analysis is meant as the basis for an improved in-line condition monitoring setup. The functionality of this improved in-line setup is then evaluated and compared to the other condition monitoring techniques as presented in section 2.2. A combination of the relevant condition monitoring techniques is made, and subsequently, a preliminary design for an overall condition monitoring strategy is created.

5.1. Suggested Improvements to In-Line Setup

In order to identify the possible locations for improvement, the various hypotheses presented in section 3.1 and section 4.1 have been reevaluated. This reevaluation serves as a way to scrutinize the designed in-line ultrasound setup. The findings of this reevaluation can then be interpreted to form possible improvements. Ways to evaluate the recommended improvements have also been suggested.

5.1.1. Influence of Signal Type

In order to eliminate the influence of signal type, the various laboratory experiments were conducted with a large range of frequencies, ranging from 200kHz to 900kHz. It is recommended to invest extra time into the determination of the frequency that has the highest sensitivity to the contamination types. By limiting the amount of selected frequencies, more specialized transducers can be implemented, meaning an improved registration of responses. Additionally, a limited amount of frequencies would also mean a more efficient data collection and processing structure, which in turn improves the speed of detection, the ease of implementation, and the perfection of the data processing. For now, it is proposed to invest more time into the frequencies above 500kHz, because these are the frequencies that are consistently following the same trends.

5.1.2. Influence of Sensor Type

The Mistras WSα sensor type, used for the laboratory and the in-line experiments, was selected due to its broad frequency spectrum. The improvement suggested before, to limit the frequency spectrum of testing, would results in a more specialized sensor type. Additionally, for these experiments, the decision was made to opt for a commercially available sensor. Improvements could be made by designing a new, more specialised, bare, piezoelectric element transducer. By doing so, the sensor itself can be more specialised in terms of signal generation and reception. Additionally, the sensor can be much smaller, subsequently resulting in a smaller overall test setup.

5.1.3. Influence of Grease Type

Most of the experiments, presented in this thesis, were conducted using Mobilux EP2 grease. Keeping the grease type consistent was done on purpose to maintain comparable results throughout the various experiments. This is however not the only grease type that is being used in the lubrication of offshore bearings. This means that in situations where a different lubrication grease is used, a new baseline measurement must be conducted. This can be done either in a laboratory using a laboratory

setup with similar settings and proceedings, or this could be done using an improved version of the in-line monitoring setup. This second option can again be divided into two options. Firstly, the baseline measurement can be conducted once, at the beginning of the implementation of the in-line setup. Secondly, the baseline measurement could be conducted continuously by placing an extra set of sensors with a grease compartment close to the original in-line setup. This secondary compartment is filled with clean grease and a baseline measurement can be conducted every time a regular measurement is conducted. Such an arrangement can be seen in Figure 5.1. Off course, it is not necessary for the baseline measurement to be directly next to the in-line measurement, as long as the experimental procedure and environment for both samples is identical. This could mean that the baseline measurement is placed somewhere else on the surface of the bearing, as opposed to directly next to the in-line setup.

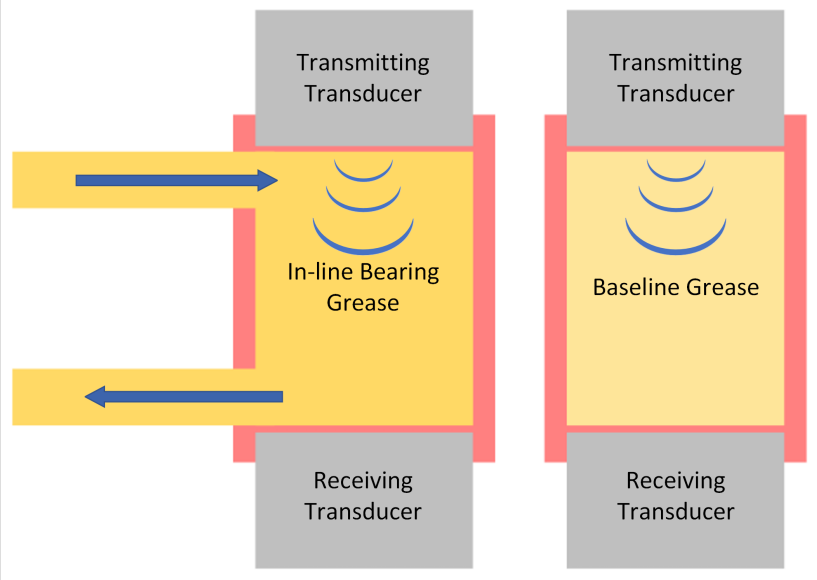

Figure 5.1: An in-line grease setup combined with a baseline grease setup.

5.1.4. Influence of Distance between Sensors

As has been concluded in chapter 3, in order for sufficient signals to propagate through the grease, the distance between the sensors must be minimized, while also lowering the peak-to-peak voltage of the transmitted signal and keeping an eye on the signal-to-noise ratio. The 22 millimetres between the sensors that was applied in the laboratory setup and the in-line setup was mainly based on structural constraints imposed by the sensors. If, as discussed before, the commercially available sensors are replaced by novel, bare piezoelectric element transducers, these spatial constraints are removed. An optimization study of the distance between the sensors and a varying peak-to-peak voltage can then be conducted, with the signal-to-noise ratio as a key performance indicator.

5.1.5. Influence of Noise

It is expected that when minimizing the distance between the transducers, and maximizing the transmitted peak-to-peak voltage, the contribution of noise signals through the test setup material will increase. Therefore, this should be taken into account when conducting the optimization study discussed in the previous section. It is however safe to say that the optimal distance and peak-to-peak voltage will be dependent on the selected signal type, the selected sensor type, the filter settings and the threshold settings.

5.1.6. Influence of Air Bubble Concentration Fluctuations

As was illustrated in the results of the laboratory experiments, the air bubbles inside the grease sample cause an effect both on the amplitude of the received signal, as well as on its speed of sound. Additionally, it was demonstrated that these air bubbles will dissipate out of the grease sample over

time. In order to minimize the amount of air introduced into the sample during loading, as well as to increase the rate of dissipation after loading, a couple of improvements can be implemented. The most straightforward improvement is based on the resting time principle. The longer the grease stays in the test setup, the more air is dissipated out of this sample. Just leaving the grease in the test setup for an extended period of time improves the received results of the measurement. However, this is a time-consuming and somewhat unpredictable process. The second option is to improve the loading procedure by conducting grease flow analyses. By designing a hole in the right location for the air to seep out, the amount of air that is trapped within the grease chamber with the grease is minimized. Last but not least, it is hypothesised that vibrations will help the air dissipate out of the grease sample. More research is needed to corroborate this hypothesis, and great care must be applied in investigating the effect of vibrations on the mix of grease and contamination. An unwanted effect of the vibration would be to separate the particles from the grease sample and have them either float or sink to one end of the sample. If vibration turns out to be a viable option, this could either be done with some sort of vibration platform, or by using specific types of transducers.

5.1.7. Influence of Temperature Fluctuations

The effect of temperature on the amplitude and speed of sound of the received signals has been illustrated. However, the influence of temperature can be overcome in two different ways. Firstly, it is possible to maintain a relatively constant temperature for all the grease samples by implementing some sort of heating element into the setup. The heating element would heat up the grease sample to a desired and constant temperature, ensuring the comparability of the results. A heating element is however not possible for every application, since some offshore bearing applications are subjected to a lot of strict regulations regarding heat sources due to flammability. The second option, is to implement the baseline setup next to the in-line setup, as was shown in Figure 5.1. By implementing the baseline measurement close to the in-line measurement, and conducting a baseline measurement every time the in-line measurement is conducted, the temperature conditions for both measurement are assumed to be similar.

5.1.8. Influence of Contamination

A couple of useful conclusions with respect to the behaviour of ultrasound when subjected to contamination have been drawn from the conducted experiments. It is however still quite difficult to distinguish between water contamination and iron particle contamination. In order to solve that, it is proposed to invest more time into researching the ultrasound behaviour in the time and frequency spectra of the response. On top of that, during the laboratory experiment, both forward and backward measurements have been conducted, to ensure reciprocity of the results. However, changing the sensor orientations around is a laborious job and therefore not applicable to in-line setups. Because of that, it is proposed to improve the setup by implementing a second set of ultrasound transducers, perpendicular to the first. The active sensor set would then alternate between the two sensor sets. An additional advantage to this approach would be that the results of the two sensor sets can be compared. These should at all times give comparable results. If this is not the case, the test setup might not be fully loaded, and air bubbles might be present somewhere in the sample. This approach would increase the reciprocity of the results and the homogeneity of the sample, which would improve the overall results of the measurement with respect to contamination. An example of such a setup is presented in Figure 5.2. Last but not least, a couple of grease

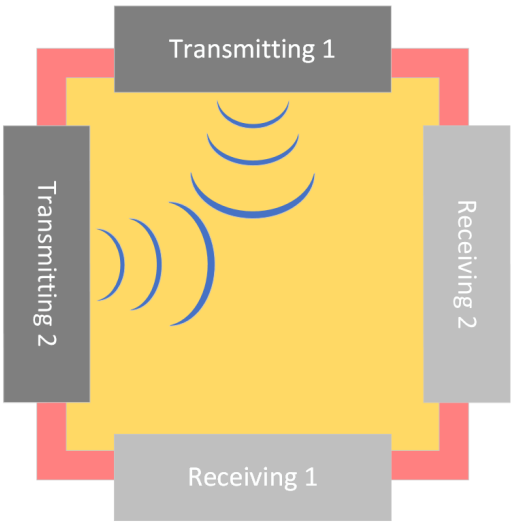

Figure 5.2: Improved version of the in-line setup with respect to reciprocity.

samples could be sent to a laboratory, to do a particle analysis and to 'train' the in-line monitoring setup data analysis.

5.1.9. Spatial Constraints

The spatial constraints imposed by the bearing and its surroundings will differ per situation. Therefore, the aim is to make this in-line monitoring setup as small as possible. Certain steps to achieve this have already been discussed, such as creating a new type of bare, piezoelectric sensor, and optimizing the propagation distance and peak-to-peak voltage. It is however necessary for the in-line condition monitoring system to be attached to, or close to the bearing, to ensure the most reliable contamination results.

5.1.10. Location on Bearings

The location of the in-line test setup on the bearing has implications for the resulting grease condition and subsequent bearing condition. If only one in-line measurement setup is implemented on a large offshore bearing, the possibility of that location being the most contaminated location, and therefore getting valuable results, is quite small. It is therefore suggested to implement multiple in-line condition monitoring setups, preferably on every grease sampling or lubrication location. When contamination is located in one or more of these in-line measurement setups, it would provide insights into the origin of the damage particles. Additionally, more sampling setups mean more data, and a higher chance of registering a problem when it occurs.

5.1.11. Flowability of Grease

The flowability of the grease has been illustrated in the experiment conducted in chapter 4. In the used in-line setup, however, not much thought had gone into incorporating a lubrication mechanism or an in-line outlet mechanism. Because the in-line grease monitoring setup is screwed into the existing grease nipple locations, less lubrication nipples are available for the lubrication of the bearing. This is unacceptable and therefore this should be improved. As can be seen from Figure 5.3, a possible solution for this problem is to implement a switching system, as well as placing a grease nipple through which the grease can be inserted into the bearing. When closing this switch, the bearing will push the grease into the in-line test setup. Off course, it should be kept in mind that there is a piece of pipe from the bearing to the in-line setup, that is going to be filled with new, unused grease from the previous filling time. This amount of grease must be allowed to pass the sensors, without being measured, in order for the contaminated grease that is coming out of the bearing to fill up the examination area.

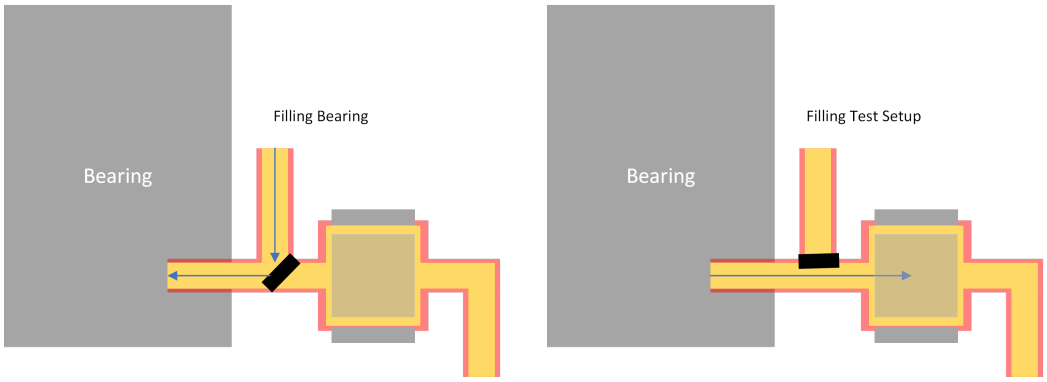

Figure 5.3: Proposed improved inlet and outlet mechanism for the in-line grease monitoring setup.

5.1.12. Surrounding Noise

In the conducted measurements, the surrounding noise does not seem to pose a problem for distinguishing the relevant signals from the noise signals. If this does pose a problem, a couple of solutions can be implemented. Firstly, the thresholds and filters can be adjusted to improve the measurements. And secondly, the outside of the grease monitoring setup could be insulated using some sort of ultrasound sound insulation. This would help to minimize the registered noise levels.

5.2. Comparison to Other Condition Monitoring Techniques

Based on the conducted literature review, the various existing condition monitoring methods have been graded on a couple of criteria. These criteria are, the ability to detect defects of the roller elements, the ability to detect defects of the bearing raceways, the ability to detect defects of the sealing arrangements, the ability to locate wear damage and the ability to locate fatigue damage. The designed in-line grease monitoring method shall now be graded on these same criteria.

- *The ability to detect defects of the roller elements,* is based on the ability to detect metal particles of a certain type, size and hardness, originating from the roller elements. Based on the presented results, it may be assumed that the in-line ultrasound grease condition monitoring setup will be able to detect particle contamination. It is however too soon to say whether the employed ultrasound method will be able to differentiate between different types of particle contamination.
- *The ability to detect defects of the bearing raceways,* is based on the ability to detect metal particles of a certain type, size and hardness, originating from the raceways. Again, it is too soon to say whether the developed technique will be able to differentiate between the different particle types.
- *The ability to detect defects of the sealing arrangement,* is based on the ability to detect water, salt and/or silica contamination. It has been illustrated that the in-line monitoring setup will be able to detect water contamination, it is however still difficult to differentiate between water contamination and iron particle contamination.
- *The ability to locate wear damage,* is based on the ability to detect wear particles, close enough to the particle source. The detection of wear particles, as illustrated, is possible using the in-line ultrasound method, however, because this method is limited to a fixed amount of grease nipple locations for its measurements, it is difficult to precisely pinpoint the wear debris origin.
- *The ability to locate fatigue damage,* is based on the ability to detect structural changes in the material of the bearing. The developed method is not capable to detect such changes.

Method	Rollers	Raceway	Seals	Wear	Fatigue
Temperature	No	No	No	Yes	No
Disassembly	Yes	Yes	Yes	Yes	Yes
Hatches	Maybe	Maybe	Maybe	Maybe	No
Mechanical	No	No	No	Yes	No
Vibration	No	No	No	No	No
Acoustic Emission	Yes	Yes	No	Yes	Yes
Guided Wave	No	Maybe	No	No	Yes
Electrostatic	No	Yes	No	Yes	Yes
Online Oil	No	No	No	No	No
Offline Grease	Yes	Yes	Yes	Maybe	No
In-line Grease	Maybe	Maybe	Maybe	Maybe	No

Table 5.1: Detection of defects by condition monitoring methods.

5.3. Overall Condition Monitoring Strategy

The results of the comparison of the various condition monitoring setups have been presented in Table 5.1. Future research might turn the roller and raceway column entries into a yes, this is however not certain, so for the construction of the overall condition monitoring setup, it is assumed that the in-line method can definitely detect the particle contamination of the rollers and the bearings, but it cannot differentiate between these two particle contamination sources.

In order for an overall bearing condition monitoring strategy to be successful, all five of the presented criteria must be met with a definitive yes. As can be seen from Table 5.1, the disassembly of the bearing is the only condition monitoring method that meets these demands. However, as was discussed before, this method is very time-consuming and causes a lot of equipment downtime, and

therefore a lot of monetary losses. A different strategy that could be adapted is to implement various condition monitoring methods alongside one another. Two combinations can be made to satisfy all five criteria simultaneously, while only implementing two condition monitoring methods. The first combination is to combine acoustic emission condition monitoring with the offline grease sampling method. And the second option is to combine the acoustic emission monitoring method with the developed in-line ultrasound spectroscopy method. Although, the offline grease monitoring method is definitely able to distinguish between roller and raceway debris contamination, this method is a lot more time-consuming, and therefore, a long delay is introduced between the moment of conducting the grease extraction and the moment that the results of the measurements are known. The in-line grease monitoring setup has great promise to determine the grease contamination concentrations much quicker than the offline grease method. Because of that, it is proposed to implement both the acoustic emission measurements as well as the developed in-line ultrasound grease condition monitoring method.

6

Conclusions and Recommendations

The conclusions drawn from the results of the laboratory experiments presented in Chapter 3 provide valuable insights for the development of an in-line grease monitoring setup for offshore bearings, as presented in Chapter 4. Through an analysis of various factors such as distance between sensors, test-setup material, air bubble concentration and temperature fluctuations, scalability of peak-to-peak voltage, water contamination and iron particle contamination, several key findings have emerged. In this chapter, the key findings from this thesis shall be summarized in order to answer the sub-questions and research question provided in Chapter 1. Next, the subsequent research and design recommendations have been listed.

6.1. Conclusions

To answer the first sub-question: ”How can active ultrasound spectroscopy be used to monitor the condition of bearing grease?”, a number of laboratory experiments have been conducted. The results of these experiments show that the ultrasound exhibits sensitivity of signal amplitude and speed of sound to various contamination types and concentrations, as well as to temperature and air bubble concentration fluctuations, in the frequency range of 500kHz to 900kHz.

Firstly, **air bubble concentration fluctuations cause amplitude and speed of sound fluctuations.** Longer dissipation times allow the air bubbles to dissipate out of the grease sample, subsequently causing an improvement of the amplitude and speed of sound of the received signals. A clean grease sample has been subjected to various dissipation times in order to see if an increase in amplitude and speed of sound would be measured. This was case, signifying that the air bubbles indeed dissipate out of the grease sample over time.

Secondly, **temperature fluctuations cause amplitude and speed of sound fluctuations**. This has been investigated by conducting the same measurement multiple times, at different temperatures. By doing so, the increase in temperature showed an increase in received signal amplitude and an increase in received signal speed of sound.

Thirdly, the water contamination measurements exhibit clear patterns in both signal amplitude and speed of sound, **illustrating the ability to detect (tap) water contamination in a grease sample**. Initially, signal amplitude decreases before stabilizing at higher contamination levels, while speed of sound follows a diminishing increase trajectory, also stabilizing eventually. These trends are influenced by attenuation principles affected by water content, temperature variations, and air bubbles. This influence has been investigated by repeating the same experiments while increasing the tap water contamination concentration.

Similarly, the analysis of iron particle contamination shows consistent trends in signal amplitude and speed of sound, **illustrating the ability to detect iron particle contamination in a grease sample**. Initially, signal amplitude decreases with higher contamination concentrations, but a slight increase is

observed between 5% and 10%. This anomaly may be due to iron particle clumping, leading to changes in attenuation mechanisms. Variations in the loading procedure could also introduce more air bubbles, influencing the results. The influence of iron particle contamination has been investigated by repeating the same experiments while increasing the iron particle contamination concentration. It has also been observed that **it is still difficult to differentiate between tap water and iron particle contamination** using only the attenuation spectroscopy and the velocity spectroscopy.

Additionally, it is observed that **shorter propagation distances yield more effective results**. This has been investigated by employing a modular test setup, focused on the ease of exchanging the propagation distance. By examining various propagation distances, it was confirmed that 100mm would be the maximum allowable distance between the sensors for the available equipment, but minimizing this distance would be more beneficial.

Moreover, it has been found that the material of the setup does not significantly influence wave propagation in the considered frequency range, indicating that **noise introduced through 3D-printed material is negligible**. This has been investigated by transmitting an ultrasound waveform through the 3D-printed setup without any grease in it, and comparing this to a measurement in which the two sensors are not physically connected to one another through the 3D-printed grease setup. By doing so, the propagation through the plastic material and through air could be compared.

Lastly, **scalability of peak-to-peak voltage does not pose significant issues with the representation of the received waveforms**, with higher voltages potentially improving signal-to-noise ratios. This has been investigated by conducting the same measurement at two different peak-to-peak voltages. Subsequently, one of the two signals is afterwards electronically scaled back to represent the signal strength of the other measurement. The results have then been compared and no significant differences have been observed.

To answer the second sub-question: ”How can the condition of bearing grease be monitored using an in-line monitoring setup?”, an in-line grease monitoring setup has been designed and experimentally evaluated. The results of the in-line experiment offer valuable insights for the development of an overall condition monitoring setup. It is concluded that **spatial constraints, grease flowability, and surrounding noise pose minimal challenges** in this specific case. The method shows potential for implementation on every grease port in a bearing, offering coverage comparable to traditional grease sampling methods. However, the spatial constraints imposed by bearing arrangement and equipment may vary, necessitating evaluation of spatial applicability on a case-by-case basis. **Overall, the in-line grease monitoring setup shows promise for effective condition monitoring in offshore bearings**.

To answer the third sub-question: ”What are the limitations of using an in-line active ultrasound spectroscopy monitoring setup for bearing condition monitoring?”, the initially designed in-line monitoring setup has been evaluated and improved. Subsequently, the improved version has been evaluated, and complementing condition monitoring techniques have been selected to construct an overall condition monitoring strategy. **Combining acoustic emission monitoring with the developed in-line ultrasound grease condition monitoring method offers a promising outlook for comprehensive bearing condition monitoring.** This approach addresses the limitations of individual methods while providing timely and accurate results for effective maintenance decision-making.

6.2. Recommendations

Throughout this thesis, a number of recommendations have been listed, either for further research or for the next design steps for the realisation of an operational in-line bearing grease condition monitoring set.

- First of all, while minimizing propagation distance is important, consideration must be given to clipping and noise levels, necessitating careful adjustment of peak-to-peak voltage and propagation distance.
- Second, further examination of 3D-print material induced noise sources must be further examined, particularly when pulsing at higher peak-to-peak voltages. The propagation of noise through the 3D printed test setup must be evaluated for every peak-to-peak voltage and every grease setup.
- Third, future research could explore methods to expedite the air bubble dissipation process through the incorporation of vibrational methods for example, though caution is advised to assess potential impacts on grease composition and contamination separation.
- Fourth, maintaining constant temperature control is crucial for comparable and reproducible results in ultrasound measurements. Sufficient temperature control ensures consistency in signal amplitude and speed of sound measurements. Therefore, more effort must be invested in designing a way to account for temperature fluctuations, either through a heating element, or through a baseline sample that undergoes the same temperature fluctuations.
- Fifth, concerning the contamination experiments, repeating the loading procedure and measurements multiple times with the same contamination level could provide valuable insights into repeatability of the experiments. Additionally, longer resting times and improved temperature control are recommended for enhancing the accuracy of these measurements in future studies.
- Sixth, concerning the differentiation between tap water contamination and iron particle contamination, more time should be invested in determining differences in the time domain and frequency domain of the individual waveforms. It is possible that discernible differences are observable within these domains, that could not be uncovered using the attenuation spectroscopy and the velocity spectroscopy.
- Lastly, adaptations to the design can be made to accommodate specific spatial constraints without altering basic working principles. While grease flowability appears sufficient based on the experiment results, it is recommended to develop a more efficient grease outlet for improved performance. Furthermore, surrounding noise is distinguishable from recorded signals and can be effectively managed by adjusting signal thresholds or implementing sound insulation.

References

[1] United Nations. “Renewable energy – powering a safer future.” (n.d.), [Online]. Available: https://www.un.org/en/climatechange/raising-ambition/renewable-energy (visited on 07/03/2023).

[2] Vattenfall. “Windenergie: Essentieel voor de energietransitie.” (n.d.), [Online]. Available: https://www.vattenfall.nl/fossielvrij-leven-binnen-een-generatie/windenergie/ (visited on 07/03/2023).

[3] G. Constanzo, G. Brindley, and P. Cole, “Wind energy in europe, 2022 statistics and the outlook for 2023-2027,” 2023.

[4] H. D. Azevedo, A. Araújo, and N. Bouchonneau, “A review of wind turbine bearing condition monitoring: State of the art and challenges,” *Renewable and Sustainable Energy Reviews*, vol. 56, pp. 368–379, Apr. 2016, ISSN: 13640321. DOI: 10.1016/j.rser.2015.11.032.

[5] HiTeAM. “Programme.” (2023), [Online]. Available: https://hiteam.tudelft.nl/?page_id=61 (visited on 07/11/2023).

[6] Emerson Bearing. “Roller bearings.” (2023), [Online]. Available: https://www.emersonbearing.com/products/roller-bearings/ (visited on 08/16/2023).

[7] SKF, “Rolling bearings,” SKF Group, Tech. Rep., 2018.

[8] NSK Motion and Control. “What is a bearing?” (2023), [Online]. Available: https://www.nskamericas.com/en/services/what-s-a-bearing.html (visited on 08/16/2023).

[9] M. Forsthoffer, *Forsthoffer’s Component Condition Monitoring*. Butterworth-Heinemann, 2019, ISBN: 978-0-12-809599-7.

[10] N. Thakoerdajal, “Damage assessment of highly-loaded low-speed roller bearings with acoustic emission monitoring,” TU Delft, 2022.

[11] Q. Wang and Y. Chung, *Encyclopedia of Tribology*. Springer, 2013, ISBN: 978-0-387-92897-5.

[12] F. Wang, C. Liu, W. Su, Z. Xue, H. Li, and Q. Han, “Condition monitoring and fault diagnosis methods for low-speed and heavy-load slewing bearings: a literature review,” *Journal of Vibroengineering*, vol. 19, no. 5, pp. 3429–3444, 2017. DOI: 10.21595/jve.2017.18454.

[13] L. Kania, M. Krynke, and E. Mazanek, “A catalogue capacity of slewing bearings,” *Mechanism and Machine Theory*, vol. 58, pp. 29–45, 2012. DOI: 10.1016/j.mechmachtheory.2012.07.012.

[14] SKF, “Slewing bearings,” SKF Group, Tech. Rep., 2019.

[15] SKF. “51101 single direction thrust ball bearing.” (n.d.), [Online]. Available: https://www.skf.com/sg/products/rolling-bearings/ball-bearings/thrust-ball-bearings/productid-51101 (visited on 08/17/2023).

[16] H. Ohta and E. Hayashi, “Vibration of linear guideway type recirculating linear ball bearings,” *Journal of Sound and Vibration*, vol. 235, no. 5, 2000. DOI: 10.1006/jsvi.2000.2950.

[17] J. Hung, Y. Lai, C. Lin, and T. Lo, “Modeling the machining stability of a vertical milling machine under the influence of the preloaded linear guide,” *International Journal of Machine Tools and Manufacture*, vol. 51, 2011. DOI: 10.1016/j.ijmachtools.2011.05.002.

[18] H. T. Corporation, “Hiwin linear guideway technical information,” Hiwin Technologies Corporation, Tech. Rep., 2022.

[19] M. Berlin. “What makes grease different from oil?” (2023), [Online]. Available: https://www.cenex.com/about/cenex-information/cenexperts-blog-page/agriculture-and-farming/grease-vs-oil (visited on 08/24/2023).

[20] M. Santora. “Bearing Lubrication: Oil vs. Grease - Bearing Tips.” (2015), [Online]. Available: https://www.bearingtips.com/bearing-lubrication-oil-vs-grease/ (visited on 08/24/2023).

[21] SKF. “Selecting grease or oil.” (), [Online]. Available: https://www.skf.com/in/products/rolling-bearings/principles-of-rolling-bearing-selection/bearing-selection-process/lubrication/selecting-grease-or-oil (visited on 08/24/2023).

[22] H. Allmaier, “Increase service life for rail wheel bearings—a review of grease lubrication for this application,” *Lubricants*, vol. 10, no. 36, 2022. DOI: 10.3390/lubricants10030036.

[23] P. Lugt, “A review on grease lubrication in rolling bearings,” *Tribology transactions*, vol. 52, no. 4, pp. 470–480, 2009. DOI: 10.1080/10402000802687940.

[24] SKF, “Skf maintenance and lubrication products,” SKF Group, Tech. Rep., 2022.

[25] B. Peng, Y. Bi, B. Xue, M. Zhang, and S. Wan, “A survey on fault diagnosis of rolling bearings,” *Algorithms*, vol. 15, 2022. DOI: 10.3390/a15100347.

[26] SKF, “Bearing damage and failure analysis,” SKF Group, Tech. Rep., 2017.

[27] R. Upadhyay, L. Kumaraswamidhas, and M. S. Azam, “Rolling element bearing failure analysis: A case study,” *Case Studies in Engineering Failure Analysis*, vol. 1, pp. 15–17, 2013. DOI: 10.1016/j.csefa.2012.11.003.

[28] N. Moundekar and B. Deshmukh, “Study of failure modes of rolling bearings: A review,” *International Journal of Modern Engineering Research (IJMER)*, vol. 4, no. 1, pp. 139–145, 2014.

[29] J. Halme and P. Andersson, “Rolling contact fatigue and wear fundamentals for rolling bearing diagnostics - state of the art,” *Proceedings of the Institution of Mechanical Engineers, Part J: Journal of Engineering Tribology*, vol. 224, 2009. DOI: 10.1243/13506501JET656.

[30] BearingNews. “How to minimise the lubrication contamination?” (2022), [Online]. Available: https://www.bearing-news.com/how-to-minimize-the-lubrication-contamination (visited on 01/30/2024).

[31] D. Koulocheris, A. Stathis, T. Costopoulos, and D. Tsantiotis, “Experimental study of the impact of grease particle contaminants on wear and fatigue life of ball bearings,” *Engineering Failure Analysis*, vol. 39, pp. 164–180, 2014.

[32] M. Tomimoto, “Experimental verification of a particle induced friction model in journal bearings,” *Wear*, vol. 254, pp. 749–762, 2003. DOI: 10.1016/S0043-1648(03)00250-3.

[33] J. Miettinen and P. Andersson, “Acoustic emission of rolling bearings lubricated with contaminated grease,” *Tribology International*, vol. 33, pp. 777–787, 2000. DOI: 10.1016/S0301-679X(00)00124-9.

[34] N. Tandon, K. Ramakrishna, and G. Yadava, “Condition monitoring of electric motor ball bearings for the detection of grease contaminants,” *Tribology International*, vol. 40, pp. 29–36, 2007. DOI: 10.1016/j.triboint.2006.01.024.

[35] V. Hariharan and P. Srinivasan, “Condition monitoring studies on ball bearings considering solid contaminants in the lubricant,” *Journal of Mechanical Engineering Science*, vol. 224, pp. 1727–1748, 2010. DOI: 10.1243/09544062JMES1885.

[36] J. Horng, T. Ta, R. Jheng, M. Huang, and K. Zhang, “Effect of liquid contaminants on tribological performance of greases,” *Wear*, vol. 530-531, 2023. DOI: 10.1016/j.wear.2023.205054.

[37] A. Soni and V. Patel, “Review and study of effect of water contaminants in lubrication in ball bearing through vibration analyses,” *Materials Today: Proceedings*, vol. 4, pp. 2717–2722, 2017. DOI: 10.1016/j.matpr.2017.02.148.

[38] N. Dittes, “Condition monitoring of water contamination in lubricating grease for tribological contacts,” Lulea University of Technology, 2016.

[39] B. Scheeren, “On acoustic emission condition monitoring of highly-loaded low-speed roller bearings,” Ph.D. dissertation, TU Delft, 2023.

[40] H. Zhang, C. Zhang, C. Wang, and F. Xie, “A survey of non-destructive techniques used for inspection of bearing steel balls,” *Measurement*, vol. 159, 2020. DOI: 10.1016/j.measurement.2020.107773.

[41] J. Worth. “Axial play vs radial play: What’s the difference?” (2023), [Online]. Available: https://toolbox.igus.com/motion-plastics-blog/axial-play-vs-radial-play-a-comprehensive-guide (visited on 01/30/2024).

[42] R. Bogue, “Sensors for condition monitoring: A review of technologies and applications,” *Sensor Review*, vol. 33, no. 4, 2013. DOI: 10.1108/SR-05-2013-675.

[43] Y. Kim, A. Tan, J. Mathew, and B. Yang, “Condition monitoring of low speed bearings: A comparative study of the ultrasound technique versus vibration measurements,” *Engineering Asset Management*, pp. 182–191, 2006. DOI: 10.1007/978-1-84628-814-2_21.

[44] L. Yu and Z. Tian, “Guided wave phased array beamforming and imaging in composite plates,” *Ultrasonics*, vol. 68, pp. 43–53, 2016. DOI: 10.1016/j.ultras.2016.02.001.

[45] J. Sha, M. Fan, B. Cao, and B. Liu, “Noncontact and nondestructive evaluation of heat-treated bearing rings using pulsed eddy current testing,” *Journal of Magnetism and Magnetic Materials*, vol. 521, 2021. DOI: 10.1016/j.jmmm.2020.167516.

[46] J. Fan and F. Wang, “Review of ultrasonic measurement methods for two-phase flow,” *Review of Scientific Instruments*, vol. 92, 2021. DOI: 10.1063/5.0049046.

[47] J. Krautkrämer and H. Krautkrämer, *Ultrasonic Testing of Materials*, 4th ed. Berlin: Springer, 1990. DOI: 10.1007/978-3-662-10680-8.

[48] G. Nicholas, “Development of novel ultrasonic monitoring techniques for improving the reliability of wind turbine gearboxes,” Ph.D. dissertation, The University of Sheffield, 2021.

[49] A. Carreira-Casais *et al.*, “Benefits and drawbacks of ultrasound-assisted extraction for the recovery of bioactive compounds from marine algae,” *International Journal of Environmental Research and Public Health*, vol. 18, 2021. DOI: 10.3390/ijerph18179153.

[50] Iowa State University. “Physics of nondestructive evaluation.” (2020), [Online]. Available: https://www.nde-ed.org/Physics/index.xhtml (visited on 02/09/2024).

[51] LibreTexts PHYSICS. “University physics.” (n.d.), [Online]. Available: https://phys.libretexts.org/Bookshelves/University_Physics/University_Physics_(OpenStax) (visited on 02/09/2024).

[52] A. Horwood and N. Chockalingam, *Clinical Biomechanics in Human Locomotion*. Elsevier, 2023. DOI: 10.1016/B978-0-323-85212-8.00002-X.

[53] T. Rossing, *Springer handbook of acoustics*. Springer, 2007, ISBN: 978-0-387-30446-5.

[54] F. Priego-Capote and M. L. D. Castro, “Analytical uses of ultrasound,” *Trends in Analytical Chemistry*, vol. 23, 2004. DOI: 10.1016/j.trac.2004.07.013.

[55] V. Bucking, B. O’Driscoll, C. Smyth, A. Alting, and R. Visschers, “Ultrasonic waves and material analysis: Recent advances and future trends,” *Lab Plus International*, vol. 16, no. 3, pp. 17–21, 2002.

[56] K. Sujana, P. Rani.A, B. Sandhya.P, Rajeesha.S, and Mounika.G, “Ultrasonic spectroscopy,” *Journal of Biomedical Science and Research*, vol. 3, no. 3, pp. 414–423, 2011.

[57] C. Nemarich, H. Whitesel, and A. Sarkady, “On-line wear particle monitoring based on ultrasonic detection and discrimination,” David Taylor Research Center, Tech. Rep., 1989.

[58] Engineering Toolbox. “Water - speed of sound vs. temperature.” (2004), [Online]. Available: https://www.engineeringtoolbox.com/sound-speed-water-d_598.html (visited on 03/07/2024).

[59] B. Scheeren, M. Kaminski, and L. Pahlavan, “Acoustic emission monitoring of naturally developed damage in large-scale low-speed roller bearings,” *Structural Health Monitoring*, pp. 1–23, 2023. DOI: 10.1177/14759217231164912.

[60] A. Berkhout, *Seismic migration: Imaging of acoustic energy by wave field extrapolation (A. theoretical aspects)*. Amsterdam, the Netherlands: Else-vier Scientific Pub. Co., 1980.

[61] J. Achenbach, *Evaluation of Materials and Structures by Quantitative Ultrasonics*. Wien: Springer-Verlag, 1993. DOI: 10.1007/978-3-7091-4315-5.

[62] RS PRO. “Rs pro sdg1032x waveform generator, 30mhz max - rs calibrated.” (n.d.), [Online]. Available: https://uk.rs-online.com/web/p/arbitrary-waveform-generators/1882691 (visited on 02/06/2024).

[63] Vallen Systeme. “Amsy-6 system specification.” (2022), [Online]. Available: https://www.vallen.de/zdownload/pdf/AMSY-6_Spec.pdf (visited on 02/06/2024).

[64] Falco Systems. “Wma-300 high speed high voltage amplifier.” (2021), [Online]. Available: https://www.falco-systems.com/High_voltage_amplifier_WMA-300.html (visited on 02/06/2024).

[65] Vallen Systeme. “Ae–preamplifier data sheet.” (n.d.), [Online]. Available: https://www.vallen.de/zdownload/DataSheets/Preamp/Datasheet_AEP5.pdf (visited on 02/06/2024).

[66] Mistras. “Wsa sensor.” (2013), [Online]. Available: http://www.physicalacoustics.com/content/literature/sensors/Model_WSa.pdf (visited on 02/06/2024).

[67] ExxonMobil. “Mobilux ep2.” (2022), [Online]. Available: https://www.msds.exxonmobil.com/IntApps/psims/Download.aspx?ID=743087 (visited on 08/23/2023).

[68] ExxonMobil. “Mobilith shc 460.” (2021), [Online]. Available: https://www.bunkeroil.no/Userfiles/Upload/images/Modules/Products/Attachments/187_MOBILITH-SHC-460.pdf (visited on 08/23/2023).

[69] ExxonMobil. “Mobil dte 10 excel 32.” (2008), [Online]. Available: https://www.geobv.nl/data/en/DTE%2010%20Excel%2032.pdf (visited on 08/23/2023).

[70] ExxonMobil. “Mobil dte 10 excel 32.” (2024), [Online]. Available: https://www.mobil.com/nl-nl/industrial/pds/gl-xx-mobil-dte-10-excel-series (visited on 03/13/2024).

[71] Castrol. “Spheerol epl range.” (2018), [Online]. Available: https://msdspds.castrol.com/bpglis/FusionPDS.nsf/Files/6D06A98AEF990527802582A4000CF91B/$File/bpxe-a3q8bc.pdf (visited on 08/23/2023).

[72] OlieOnline. “Castrol spheerol epl 2.” (2015), [Online]. Available: https://www.olieonline.nl/castrol-spheerol-epl-2 (visited on 08/23/2023).

[73] Castrol. “Spheerol epl 2.” (2006), [Online]. Available: https://msdspds.castrol.com/bpglis/FusionPDS.nsf/Files/E8B4D1ABD34BD3298025779600303563/$File/Spheerol%20EPL%20%28USA%20Eng%29.pdf (visited on 08/23/2023).

[74] Castrol. “Alpha sp150 p.” (2015), [Online]. Available: https://msdspds.castrol.com/bpglis/FusionPDS.nsf/Files/CCE4872E81FA10B880257E180037DD2A/$File/BPXE-9V5HJ3.pdf (visited on 08/23/2023).

[75] Castrol. “Optigear synthetic x range.” (2020), [Online]. Available: https://msdspds.castrol.com/bpglis/FusionPDS.nsf/Files/FAD7D2E97F8C59E28025857400503504/$File/wepp-bpzse6.pdf (visited on 08/23/2023).

[76] Castroll. “Hyspin awh-m.” (2015), [Online]. Available: https://msdspds.castrol.com/bpglis/FusionPDS.nsf/Files/A3A82A5B03D92DC980257D2A0052E605/$File/BPXE-9MVDCB.pdf (visited on 08/23/2023).

[77] Interflon. “Interflon grease ls1/2.” (2022), [Online]. Available: https://interflon.com/assets/TDS2/8901_TDS_BE_nl_Interflon_Grease_LS1_2.pdf (visited on 08/23/2023).

[78] Interflon. “Interflon grease ls1/2.” (nd.), [Online]. Available: https://interflon.com/nl/producten/interflon-grease-ls1-2 (visited on 08/23/2023).

[79] Shell. “Shell gadus s2 v220 2.” (2018), [Online]. Available: https://www.oqvalue.nl/wp-content/uploads/Shell_Gadus_S2_V220_2_TDS-1.pdf (visited on 08/23/2023).

[80] Shell. “Shell gadus s2 v220 2.” (2020), [Online]. Available: https://industrialfluidsmfg.twinoils.com/Asset/Gadus%20S2%20V220%202%20SDS.PDF (visited on 08/23/2023).

[81] SKF. “Skf maintenance and lubrication products.” (2022), [Online]. Available: https://cdn.skfmediahub.skf.com/api/public/094fe398236d3d0a/pdf_preview_medium/094fe398236d3d0a_pdf_preview_medium.pdf (visited on 08/23/2023).

[82] Vallen Systeme. “Vs150-wic-v01.” (nd.), [Online]. Available: https://www.vallen.de/wp-content/uploads/2019/03/VS150-WIC-V01_1512.pdf (visited on 08/23/2023).

[83] Vallen Systeme. “Vs600-z2.” (nd.), [Online]. Available: https://www.vallen.de/zdownload/DataSheets/Sensors/VS600-Z2.pdf (visited on 08/23/2023).

[84] Mistras. “R3i-ast sensor.” (2011), [Online]. Available: https://www.physicalacoustics.com/content/literature/sensors/Model_R3I-AST.pdf (visited on 08/23/2023).

[85] Mistras. “R6i-ast sensor.” (2011), [Online]. Available: https://www.physicalacoustics.com/content/literature/sensors/Model_R6I-AST.pdf (visited on 08/23/2023).

[86] Mistras. “R15i-ast sensor.” (2015), [Online]. Available: https://www.physicalacoustics.com/content/literature/sensors/Model_R15I-AST.pdf (visited on 08/23/2023).

[87] Mistras. “Wdi-ast sensor.” (2011), [Online]. Available: https://www.physicalacoustics.com/content/literature/sensors/Model_WDI-AST.pdf (visited on 08/23/2023).

[88] Mistras. “R6a sensor.” (2011), [Online]. Available: https://www.physicalacoustics.com/content/literature/sensors/Model_R6a.pdf (visited on 08/23/2023).

[89] Mistras. “R15a sensor.” (2011), [Online]. Available: https://www.physicalacoustics.com/content/literature/sensors/Model_R15a.pdf (visited on 08/23/2023).

A

Paper

The paper has been provided as a separate document.

B

Informative Tables

On the following pages, a number of tables have been presented. These tables give an overview of the collected data throughout this thesis.

- Firstly, an overview of the various grease types that have been reviewed during the literature review has been presented.
- Secondly, an overview of the various sensor types that have been reviewed during the literature review has been presented.
- Next, an overview of the experimental conditions for the time and air bubble experiments has been presented
- And lastly, an overview of the experimental conditions for the contamination experiments has been presented.

Name	Dropping Point	Consistency NLGI	Thickener	Oil	Density	Application temp		Kinematic viscosity			Source
						Low LTL	High HTPL	40 C [mm2/s]	100 C [mm2/s]	index	
Mobilux EP2	190 C	2	Li		0.918 g/cm3 at 15C	-20 C	130 C	160.0 mm2/s	14.8 mm2/s	91	[67]
Mobilith SHC 460	265 C	1.5	Li	synthetic	0.862 g/cm3 at 15C	-30 C	150 C	460.0 mm2/s	55.6 mm2/s	188	[68]
Mobil DTE 10 Excel 32					0.845 g/cm3 at 15C			31.5 mm2/s	6.5 mm2/s	164	[69, 70]
Spheerol EPL 2	190 C	2	Li	Mineral oil	0.900 g/cm3 at 20C	-25 C	120 C	175.0 mm2/s			[71–73]
Castrol Alpha SP 150					0.887 g/cm3 at 15C			150.0 mm2/s	14.6 mm2/s	94	[74]
Optigear Synthetic X 220					0.850 g/cm3 at 15C			220.0 mm2/s	29.3 mm2/s	172	[75]
HYSPIN AWH-M32					0.880 g/cm3 at 15C			32.0 mm2/s	6.4 mm2/s	157	[76]
Interflon LS ½	180 C	1.5	Li-Ca	Mineral oil	0.930 g/cm3 at 20C	-20 C	120 C	550.0 mm2/s			[77, 78]
Shell Gadus S2 V220 2	180 C	2	Li	Mineral oil	1.000 g/cm3 at 15C	-20 C	130 C	220.0 mm2/s	19.0 mm2/s	97	[79, 80]
LGMT 2	180 C	2	Li	Mineral oil		-30 C	120 C	110.0 mm2/s	11.0 mm2/s	81	[81]
LGMT 3	180 C	3	Li	Mineral oil		-30 C	120 C	125.0 mm2/s	12.0 mm2/s	82	[81]
LGEP 2	180 C	2	Li	Mineral oil		-20 C	110 C	200.0 mm2/s	16.0 mm2/s	79	[81]
LGWA 2	250 C	2	Lix	Mineral oil		-30 C	140 C	185.0 mm2/s	15.0 mm2/s	76	[81]
LGGB 2	170 C	2	Li-Ca	Ester		-40 C	90 C	110.0 mm2/s	13.0 mm2/s	113	[81]
LGLT 2	180 C	2	Li	PAO		-50 C	110 C	18.0 mm2/s	4.5 mm2/s	175	[81]
LGWM 1	170 C	1	Li	Mineral oil		-30 C	110 C	200.0 mm2/s	16.0 mm2/s	79	[81]
LGEP 1	170 C	1	Li-Ca	Mineral oil		-20 C	130 C	400.0 mm2/s	25.0 mm2/s	81	[81]
LGWM 2	300 C	1 to 2	CaSx	PAO/min		-40 C	110 C	80.0 mm2/s	8.6 mm2/s	71	[81]
LGEM 2	180 C	2	Li-Ca	Mineral oil		-20 C	120 C	500.0 mm2/s	32.0 mm2/s	95	[81]
LGEV 2	180 C	2	Li-Ca	Mineral oil		-10 C	120 C	1020.0 mm2/s	58.0 mm2/s	111	[81]
LGHB 2	220 C	2	CaSx	Mineral oil		-20 C	150 C	425.0 mm2/s	26.5 mm2/s	84	[81]
LGHC 2	300 C	2	CaSx	Mineral oil		-20 C	140 C	450.0 mm2/s	31.0 mm2/s	99	[81]
LGHP 2	240 C	2 to 3	PU	Mineral oil		-40 C	150 C	96.0 mm2/s	10.5 mm2/s	90	[81]
LGHQ 2	260 C	2	PU	Mineral oil		-30 C	160 C	110.0 mm2/s	12.0 mm2/s	98	[81]
LGET 2	300 C	2	PTFE	PFPE		-40 C	260 C	400.0 mm2/s	38.0 mm2/s	142	[81]
LGFG 2	-	2	CaSx	Mineral oil		-30 C	140 C	150.0 mm2/s	16.0 mm2/s	111	[81]
LGFP 2	-	2	Alx	Mineral oil		-20 C	110 C	150.0 mm2/s	15.3 mm2/s	103	[81]
LGFQ 2	-	2	CaSx	PAO		-40 C	140 C	320.0 mm2/s	30.0 mm2/s	129	[81]
LGED 2	-	2	PTFE	PFPE		-30 C	240 C	460.0 mm2/s	42.0 mm2/s	142	[81]

Table B.1: An overview of the various grease types that have been researched during the literature review.

AE Sensor	Preamp		freq. range			operating temp.		size		Noise			Source
	int. preamp	dB gain	freq. resp. peak	low	high	low	high	diameter	height	µV	at kHz		
VS150-WIC-V01	yes	34 dB	150 kHz	100 kHz	450 kHz	-40 C	85 C	32.0 mm	48.0 mm	5.0 µV	95 kHz	300 kHz	[82]
VS600-Z2	no	-	600 kHz	400 kHz	800 kHz	-40 C	110 C	4.75 mm	5.3 mm	-	-	-	[83]
R3I-AST Sensor	yes	40 dB	31 kHz	10 kHz	40 kHz	-35 C	75 C	29.0 mm	39.0 mm	3.0 µV	unk.	unk.	[84]
R6I-AST Sensor	yes	40 dB	98 kHz	40 kHz	100 kHz	-35 C	75 C	29.0 mm	40.0 mm	3.0 µV	unk.	unk.	[85]
R15I-AST Sensor	yes	40 dB	150 kHz	50 kHz	400 kHz	-35 C	75 C	29.0 mm	31.0 mm	3.0 µV	unk.	unk.	[86]
WDI-AST Sensor	yes	40 dB	unk.	200 kHz	900 kHz	-35 C	75 C	29.0 mm	30.0 mm	3.0 µV	unk.	unk.	[87]
R6α Sensor	no	-	90 kHz	35 kHz	100 kHz	-65 C	175 C	19.0 mm	22.4 mm	-	-	-	[88]
R15α Sensor	no	-	150 kHz	50 kHz	400 kHz	-65 C	175 C	19.0 mm	22.4 mm	-	-	-	[89]
WSα Sensor	**no**	**-**	**650 kHz**	**100 kHz**	**1000 kHz**	**-65 C**	**175 C**	**19.0 mm**	**21.4 mm**	**-**	**-**	**-**	[66]

Table B.2: An overview of the various sensor types that have been researched during the literature review.

	3D printed setup	Date	Time		Grease amount	Rest time	Temperature	
			Setup in	Measurement			Sample	Room
Cold, not rested	Mobilux EP2 Clean time and temperature influence	11/01/2024 11/01/2024	11:35	11:35 11:45	40.0g	0.0 h	17.6 C	16.4 C
Cold, rested 1.5h	Mobilux EP2 Clean time and temperature influence	11/01/2024 11/01/2024	11:35	13:05 13:15	40.0 g	1.5 h	17.0 C	16.7 C
Cold, rested 2.5h	Mobilux EP2 Clean time and temperature influence	11/01/2024 11/01/2024	11:35	14:05 14:15	40.0 g	2.5 h	16.9 C	17.0 C
Cold, rested 4.0h	Mobilux EP2 Clean time and temperature influence	11/01/2024 11/01/2024	11:35	15:35 15:45	40.0 g	4.0 h	17.4 C	17.0 C
Cold, rested 22.0h	Mobilux EP2 Clean time and temperature influence	12/01/2024 12/01/2024	11:35	09:35 09:45	40.0 g	22.0 h	17.3 C	16.0 C
Warmer, not rested	Mobilux EP2 Clean time and temperature influence	12/01/2024 12/01/2024	10:50	10:50 11:00	40.0 g	0.0 h	22.0 C	16.1 C
Warmer, rested 1.5h	Mobilux EP2 Clean time and temperature influence	12/01/2024 12/01/2024	10:50	12:20 12:30	40.0 g	1.5 h	23.0 C	16.3 C
Warmer, rested 2.5h	Mobilux EP2 Clean time and temperature influence	12/01/2024 12/01/2024	10:50	13:20 13:30	40.0 g	2.5 h	22.6 C	16.8 C
Warmer, rested 4.0h	Mobilux EP2 Clean time and temperature influence	12/01/2024 12/01/2024	10:50	14:50 15:00	40.0 g	4.0 h	23.8 C	17.2 C

Table B.3: An overview of the various experimental conditions for the air bubble and temperature experiments.

	3D printed setup	Date	Time		Amount of		Sample prepared	Rest time	Temperature	
			Setup in	Experiment	Grease	Contamination			Sample	Room
Warm, rested 1.5 h	Mobilux EP2 Clean baseline 60mVpp	16/01/2024 16/01/2024	10:30	12:00 12:05	40.0 g	-	15/01/2024 15:00	1.5 h	26.0 C	17.4 C
Warm, rested 1.5 h	Mobilux EP2 and 1.0% water 60mVpp	16/01/2024 16/01/2024	12:30	14:00 14:05	40.0 g	0.4 g	15/01/2024 15:00	1.5 h	25.1 C	17.4 C
Warm, rested 1.5 h	Mobilux EP2 and 1.0% iron particles 60mVpp	16/01/2024 16/01/2024	14:30	16:00 16:05	40.0 g	0.4 g	15/01/2024 15:00	1.5 h	25.7 C	16.6 C
Warm, rested 1.5 h	Mobilux EP2 Clean baseline 60mVpp	17/01/2024 17/01/2024	10:00	11:30 11:35	40.0 g	-	16/01/2024 16:30	1.5 h	24.9 C	15.6 C
Warm, rested 1.5 h, transmitted 3840 mVpp	Mobilux EP2 and 5.0% water 3840mVpp	17/01/2024 17/01/2024	12:00	13:30 13:35	40.0 g	2.0 g	16/01/2024 16:30	1.5 h	25.0 C	16.0 C
Warm, rested 1.5, transmitted 960 mVpp	Mobilux EP2 and 5.0% iron particles 960mVpp	17/01/2024 17/01/2024	14:00	15:30 15:35	40.0 g	2.0 g	16/01/2024 16:30	1.5 h	25.6 C	16.6 C
Warm, rested 1.5 h	Mobilux EP2 Clean baseline 60mVpp	18/01/2024 18/01/2024	10:00	11:30 11:35	40.0 g	-	17/01/2024 16:00	1.5 h	24.9 C	17.0 C
Warm, rested 1.5 h	Mobilux EP2 Clean baseline 480 mVpp	18/01/2024 18/01/2024	10:00	11:30 11:35	40.0 g	-	17/01/2024 16:00	1.5 h	24.9 C	17.0 C
Warm, rested 1.5 h	Mobilux EP2 and 10.0% water 3840mVpp	18/01/2024 18/01/2024	12:00	13:30 13:35	40.0 g	4.0 g	17/01/2024 16:00	1.5 h	25.3 C	17.6 C
Warm, rested 1.5 h	Mobilux EP2 and 10.0% iron particles 960mVpp	18/01/2024 18/01/2024	14:00	15:30 15:35	40.0 g	4.0 g	17/01/2024 16:00	1.5 h	25.0 C	17.2 C

Table B.4: An overview of the various experimental conditions for the contamination experiments.